Libraries and Learning Services

University of Auckland Research Repository, ResearchSpace

Copyright Statement

The digital copy of this thesis is protected by the Copyright Act 1994 (New Zealand).

This thesis may be consulted by you, provided you comply with the provisions of the Act and the following conditions of use:

- Any use you make of these documents or images must be for research or private study purposes only, and you may not make them available to any other person.
- Authors control the copyright of their thesis. You will recognize the author's right to be identified as the author of this thesis, and due acknowledgement will be made to the author where appropriate.
- You will obtain the author's permission before publishing any material from their thesis.

General copyright and disclaimer

In addition to the above conditions, authors give their consent for the digital copy of their work to be used subject to the conditions specified on the Library Thesis Consent Form and Deposit Licence.

Application of Reinforcement Learning Controllers in Power Systems

Lv Zhou

This dissertation is presented as part of the requirements for the degree:

Doctor of Philosophy

The University of Auckland

Electrical, Computer and Software Engineering

April 2019

Abstract

With the increasing concerns about global energy crisis and the need for a clean renewable energy, wind energy has become one of the most competitive forms of renewable energy sources over the past few years. The increasing level of wind energy penetration into the conventional power grid requires new grid codes. One of the most important grid codes is referred to as low-voltage ride-through (LVRT) requirement. The goal of the present research is to achieve LVRT capability of hybrid power systems through the application of flexible alternating current transmission (FACTS) devices which are controlled by reinforcement learning controllers.

Initially, reinforcement learning (RL) controllers based on Q-learning and dynamic fuzzy Q-learning (DFQL) are designed to improve the transient stability of power systems consisting of only synchronous generators. Q-learning is one of the most popular reinforcement learning approaches and is able to provide optimal solution according to some learning strategy. The DFQL based controller combines Q-learning with the classical fuzzy controller and can effectively adjust fuzzy inference parameters with the help of Q-learning. The output of these controllers is being used to modify the value of a series compensator which is placed at various locations of the power system. The effectiveness of the controllers are demonstrated in both single and multi-machine power systems and their performances were compared with a bang-bang controller (BBC) whose parameters are optimized using particle swarm optimization (PSO).

Next, both Q-learning and DFQL based controllers are designed for rotor side converter of a doubly-fed induction generator (DFIG) based wind energy conversion system. The Q-learning based controller provides discrete control actions unlike the DFQL based controller which generates continuous control actions. The performances of these RL controllers are compared with a classical PID controller and a $\Sigma\Delta$ based PID controller. The controller using $\Sigma\Delta$ modulation is a single-bit controller and requires significantly less hardware re-

sources for its implementation. The comparative performance investigation of these controllers show that DFQL based controller and $\Delta\Sigma$ based PID controller perform better than other two controllers.

After designing RL controllers for traditional power system and WECS, the focus shifted to design these controllers for hybrid power system consisting of 2-synchronous generators and a wind generator. The objective of these controllers is to enhance the LVRT capability of this system through unified power flow controller (UPFC) which consists of a series and parallel branch; each equipped with a controllable voltage source and a series impedance. The proposed Q-learning and DFQL based controllers enable the UPFC to control the series and shunt compensation of the system. The performances of these RL controllers have been compared with classical PID controller. The results show that the DFQL based controller is the best in satisfying the LVRT grid codes in different countries.

Finally, RL controllers are designed to achieve LVRT requirements of different grid codes through convertible static compensator (CSC). The study considers four different configurations of CSC such as static synchronous series compensator (SSSC), one static synchronous compensator (STATCOM), two STATCOMs, unified power flow controller (UPFC) and three controllers which include both Q-learning, DFQL and a classical PID controller. The combination of CSC configuration and the controller which would give the best performance, from the perspective of LVRT enhancement is determined.

Acknowledgments

During the period of this research, I received great kindness and caring from many people which has made it easier for me to pursue my PhD.

I would like to express my sincere gratitude to my supervisor Prof. Akshya Swain. With his strong support, responsibility and professional guidance in academia, I could keep positive and confident in my research. I also wish to thank Dr. Ahbisek Ukil who has given me many research motivations from the perspective of power system in my research.

I would like to thank Prof. Nirmal-Kumar Nair, Dr. Prem Kethavath, Faizal hafiz and Chathura Wanigasekara for their contributions in this research. Some other individuals in the department deserve mention as well, such as Weiwei Ai, Dr. Liang Huang, Yuan Liu, Yuan Song, Liming Qiu and so on. Thanks to their friendship, I got through this research happily.

I also like to thank Rob and Sunita for offering me the work opportunity in the labs. This work helped me a lot financially in my last year so that I could concentrate on my research.

I am greatly thankful to the extended love and support from my sister-in-law, brother-in-law, parents-in-law, and little lovely nephew and niece.

Finally, I would like to dedicate this thesis to my dear parents and husband. Without their great support and love throughout my research, I could not have achieved this.

Contents

Abstract **iii**

List of Abbreviations **xvii**

List of Author's Publications **xix**

1 Introduction **1**

1.1 Motivation 1

1.2 Goal and Objectives 3

1.3 Thesis Structure 4

2 Control of Hybrid Power Systems with Wind Generators: Background Information **7**

2.1 Wind Energy Conversion System 8

2.1.1 Mechanical system 8

2.1.2 Electrical system 11

2.1.3 Control system 11

2.2 Wind turbines 12

2.2.1 Fixed-speed wind turbine 12

2.2.2 Limited-speed wind turbine 13

2.2.3 Variable-speed wind turbine 13

2.3 Wind generators 13

2.3.1 Asynchronous generator 13

2.3.2 Synchronous generator 16

2.3.3 Summary of configurations of wind turbines and wind generators 17

2.4 Low Voltage Ride Through Requirements 18

2.5 Different Methods to Achieve LVRT Requirements 18

2.5.1 Crowbar 20

2.5.2 Energy Storage System 22
2.5.3 Series dynamic resistor 23
2.5.4 Braking chopper 24
2.5.5 FACTS 25
2.5.6 Control Approaches 26

3 Improvement of Transient Stability of a Power System using Reinforcement Learning Controllers 27
3.1 Modelling of Synchronous Generator 28
3.1.1 Single machine infinite bus system with series compensator 28
3.1.2 Modelling of multi-machine power system 29
3.2 Controller design for series compensator 30
3.2.1 Q-learning based controller 30
3.2.2 Dynamic fuzzy Q-learning based controller 33
3.2.3 Bang-bang controller 37
3.3 Simulation Results 39
3.3.1 Results for SMIB 39
3.3.2 Results for a multi-machine system 42
3.4 Conclusion 45

4 Q-learning and Dynamic Fuzzy Q-learning Based Controllers for Rotor Side Control of Wind Energy Conversion System 47
4.1 Aggregated modelling of DFIG based WECS 48
4.1.1 Wind Turbine Modelling 49
4.1.2 Shaft System Modelling 49
4.1.3 Aggregated DFIG Modelling 50
4.2 Control of Rotor Side Converter 50
4.2.1 Technique of $\Delta\Sigma$ Based Control System 51
4.2.2 $\Delta\Sigma$ Based PID Controller 52
4.2.3 Q-learning based controller 55
4.2.4 DFQL based controller 55
4.2.5 Classical PID controller 56
4.3 Simulation results 56
4.4 Conclusion 58

5 Design of UPFC for LVRT Improvement in Hybrid Power System 65
5.1 Modelling of hybrid power system 67

5.1.1 Modelling of synchronous generators 67
5.1.2 Modelling of DFIG based wind farm 68
5.2 Modelling of UPFC 68
5.3 Low-voltage ride-through requirements 70
5.4 Controller design for UPFC 71
5.5 Simulation results 72
5.5.1 Simulated Hybrid Power System 72
5.5.2 Simulation Framework 73
5.5.3 Results 73
5.6 Conclusion 74

6 Design of CSC for LVRT Improvement in Hybrid Power System 77
6.1 Convertible static compensator 78
6.2 Controller design for CSC 79
6.3 Simulation results 80
6.3.1 Simulation 80
6.3.2 Results 81
6.4 Conclusion 87

7 Conclusions and Future Work 93
7.1 Conclusions 93
7.2 Future work 95

A Synchronous Generation Power System 97
A.1 Three-machine synchronous power system 97
A.2 Excitation system 97

Bibliography 97

List of Figures

1.1 Worldwide wind power capacity 1
1.2 Worldwide new installed wind power capacity 2
1.3 Global growth rate of wind power capacity 2

2.1 A typical wind energy conversion system 9
2.2 (a) Vertical axis wind turbine (b) Horizontal axis wind turbine . 10
2.3 Horizontal axis wind turbine based WECS 10
2.4 Pitch angle control system 12
2.5 Fixed-speed wind turbine equipped with an SCIG 14
2.6 Variable-speed wind turbine equipped with an SCIG 14
2.7 Limited-speed wind turbine equipped with WRIG 15
2.8 Limited-speed wind turbine equipped with DFIG 16
2.9 Variable-speed wind turbine equipped with PMSG 16
2.10 Variable-speed wind turbine equipped with WRSG (with full capacity power converter) 17
2.11 Variable-speed wind turbine equipped with WRSG (without full capacity power converter) 17
2.12 General limit curve for LVRT requirement. 20
2.13 LVRT improvement methods. 21
2.14 LVRT improvement using crowbar. 21
2.15 LVRT improvement using ESS in PMSG. 22
2.16 LVRT improvement using ESS in DFIG. 22
2.17 LVRT improvement using series dynamic resistor installed in series with stator 24
2.18 LVRT improvement using braking chopper 24

3.1 A single machine infinite bus system with series compensator . . 29
3.2 Interactions in Q-learning 31
3.3 Flowchart of designed Q-learning based controller 32

3.4 Flowchart of designed DFQL based controller 34
3.5 Control strategies of BBC 38
3.6 PSO Based Bang-Bang Controller 38
3.7 Framework of series compensator control using Q-learning based controller 39
3.8 Framework of series compensator control using DFQL based controller 40
3.9 Responses of Q-learning based controller in SMIB 40
3.10 Responses of DFQL based controller in SMIB 41
3.11 Responses of BBC in SMIB 41
3.12 A three-machine nine-bus synchronous power system 43
3.13 Responses of Q-learning based controllers in 3-machine power system 43
3.14 Responses of DFQL based controller in 3-machine power system 44
3.15 Responses of BBC in 3-machine power system 45
3.16 Convergence characteristic of PSO 45
3.17 Response of PSO based BBC in 3-machine power system 46

4.1 $\Delta\Sigma$-based encoder/decoder. (a). Encoder (b). Communication Channel (c). Decoder 52
4.2 Configuration of $\Delta\Sigma$ based control system. 53
4.3 $\Delta\Sigma$-based PID controller. 54
4.4 Control of RSC using Q-learning based controllers 55
4.5 Control for RSC using DFQL based controllers 56
4.6 Control for RSC using conventional PID controllers 57
4.7 DFIGs based WECS 57
4.8 Variations in rotor speed of DFIG with classical PID controllers 59
4.9 Variations in rotor speed of DFIG with $\Delta\Sigma$ based PID controllers 59
4.10 Variations in rotor speed of DFIG with Q-learning based controllers 60
4.11 Variations in rotor speed of DFIG with DFQL based controllers 60
4.12 Variations in torque of DFIG with classical PID controllers . . . 61
4.13 Variations in torque of DFIG with $\Delta\Sigma$ based PID controllers . . 61
4.14 Variations in torque of DFIG with Q-learning based controllers . 62
4.15 Variations in torque of DFIG with DFQL based controllers . . . 62
4.16 Variations in reactive power of DFIG with classical PID controllers 63
4.17 Variations in reactive power of DFIG with $\Delta\Sigma$ based PID controllers 63

4.18 Variations in reactive power of DFIG with Q-learning based controllers 64
4.19 Variations in reactive power of DFIG with DFQL based controllers 64

5.1 Equivalent circuit of an UPFC 69
5.2 Diagram of Controlling Shunt and Series Branch of UPFC. . . . 70
5.3 Diagram of current controllers in UPFC. 70
5.4 Limit curves for LVRT requirements in international grid codes. 71
5.5 A three machine hybrid power system. 72
5.6 LVRT capability of UPFC1 in Case 1 (Fault duration is 9.9 cycles, and the fault is cleared by removing line 6 - 9). 74
5.7 LVRT capability using UPFC2 in Case 2 (Fault duration is 15.1 cycles and cleared by removing line 8 - 9). 75

6.1 Schematic of CSC 78
6.2 Performance of PID controller in Case-I 82
6.3 Performance of Q-learning based controller in Case-I 83
6.4 Performance of DFQL based controller in Case-I 83
6.5 Performance of CSC configured as STATCOM-I in Case-I 84
6.6 Performance of CSC configured of two STATCOMs in Case-I . . 84
6.7 Performance of CSC configured of UPFC-I in Case-I 85
6.8 Performance of PID controller in Case-II 87
6.9 Performance of Q-learning based controller in Case-II 88
6.10 Performance of DFQL based controller in Case-II 88
6.11 Performance of CSC configured as STATCOM-II in Case-II . . . 89
6.12 Performance of CSC configured as two STATCOMs in Case-II . 89
6.13 Performance of CSC configured as UPFC-II in Case-II 90

A.1 IEEE-Type I excitation system 98

List of Tables

2.1 Summary of configurations of wind turbines and wind generators [1] 19

5.1 Characteristics of LVRT requirements in international grid codes 71

6.1 Possible configurations of CSC 79
6.2 Configurations of CSC considered in different scenarios 80
6.3 Performance of different combinations in Case-I in regard to LVRT requirement of Germany (E.ON) 85
6.4 Performance of different combinations in Case-I in regard to LVRT requirement of Canada(Hydro Quebec) 85
6.5 Performance of different combinations in Case-I in regard to LVRT requirement of New Zealand (North Island) 86
6.6 Critical recovering time in Case-I 86
6.7 Performance of different combinations in Case-II in regard to LVRT requirement of Germany (E.ON) 87
6.8 Performance of different combinations in Case-II in regard to LVRT requirement of Canada (Hydro Quebec) 90
6.9 Performance of different combinations in Case-II in regard to LVRT requirement of New Zealand (North Island) 90
6.10 Critical recovering time in Case-II 91

A.1 Synchronous machine data 97
A.2 Power flow results of 3-machine synchronous power system . . . 98
A.3 Exciter data 98

List of Abbreviations

$FACTS$ flexible alternating current transmission system
$DFQL$ dynamic fuzzy Q-learning
$LVRT$ low voltage ride through
$WECS$ wind energy conversion system
$DFIG$ doubly fed induction generator
$UPFC$ unified power flow controller
ESS energy storage system
RL reinforcement learning
$SMIB$ single machine infinite bus
BBC bang bang controller
PSO particle swarm optimization
RSC rotor side control
CSC convertible static compensator
$SSSC$ static synchronous series compensator
$STATCOM$ static synchronous compensator
$VAWT$ vertical axis wind turbine
$HAWT$ horizontal axis wind turbine
$SCIG$ squirrel-cage induction generator
$WRIG$ wound rotor induction generator
$PMSG$ permanent magnet synchronous generator
$WRSG$ wound rotor synchronous generator
$WRIG$ wound rotor induction generator
GSC grid side converter
PCC point of BESScommon coupling
$BESS$ battery energy storage system
$FESS$ flywheel energy storage system
$SMESS$ superconducting magnetic energy storage system
$EDLC$ electrical double-layer capacitor

SDR series dynamic resistor
SVC static VAR compensator
DVR dynamic voltage restorer
$TCSC$ thyristor controlled series capacitor
LQ linear quadratic
FIS fuzzy inference system
COI center of inertia
SEP stable equilibrium point
SNR signal-to-noise ratio
$FPGA$ field programmable gate array
BS bit stream
LTI linear time invariant
SBR series braking resistor
FRT fault ride through
$WSCC$ Western System Coordinating Council

List of Author's Publications

1. Lv Zhou, Akshya Swain and Abhisek Ukil, Reinforcement Learning Controllers for Enhancement of Low Voltage Ride Through Capability in Hybrid Power Systems, IEEE transactions on Industrial Informatics, (manuscript accepted November 15, 2019).

2. Lv Zhou, Akshya Swain and Abhisek Ukil, Q- and Dynamic Fuzzy Q-learning Based Controller for LVRT Capability of Mix Generation System, Applied Soft Computing, (manuscript submitted May 31, 2019).

3. Chathura Wanigasekara, Dhafer Almakhles, Lv Zhou, Akshya Swain, Umashankar Subramaniyan and Sanjeevikumar Padmanaban, Design of $\Delta\Sigma$ Based PID Controller for Wind Energy Systems, IEEE 3rd Industrial and Commercial Power System Europe, 19th International Conf. on Environment and Electrical Eng., June 10 - 14, 2019, Genova, Italy.

4. Lv Zhou, Akshya Swain and Abhisek Ukil, Q-learning and Dynamic Fuzzy Q-learning Based Intelligent Controllers for Wind Energy Conversion Systems, IEEE PES Innovative Smart Grid Technologies Asia (ISGT Asia) 2018, May 22 - 25, 2018, Singapore.

5. Lv Zhou, Akshya Swain, Prem K Naik, Faizal Hafiz and Nirmal-Kumar C Nair Optimum Design of Series Compensation to Improve Power System Transient Stability Using DFQL and PSO Based Controllers, 13th IEEE International Conference on Control and Automation, July 3-6 , 2017, Ohrid, Macedonia.

6. Lv Zhou, Akshya Swain, Prem K Naik and Nirmal-Kumar C Nair, A Dynamic Fuzzy Q-learning Controller to Improve the Transient Stability of a Power System, 2016 International Conference on Power Systems Technology, September 28 – October 1, 2016, Wollongong, Australia.

Chapter 1

Introduction

1.1 Motivation

In recent years, renewable energy such as wind, solar, hydro, geothermal, bio-energy etc is drawing increasing attention from researchers due to concerns about the environment of global warming and fossil fuels. Among different renewable energy sources, wind energy has been considered as one of the most feasible and competitive alternative energy sources in modern power system [1–3]. According to the World Wind Energy Associate, wind turbines capacity has experienced significant growth over the past decade. Fig. 1.1 - Fig. 1.3 show the installation of wind turbine capacity from 2011 to 2018 due to the great improvement of wind turbine technologies [4–11].

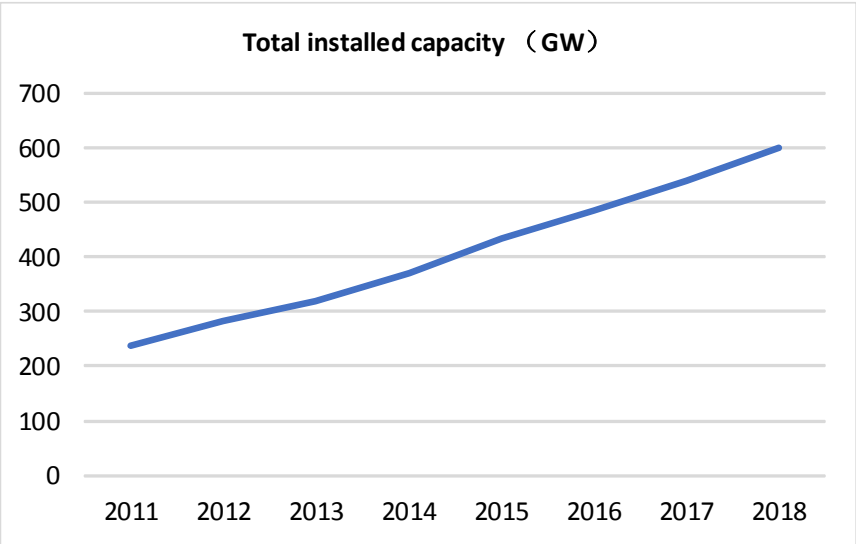

Figure 1.1: Worldwide wind power capacity

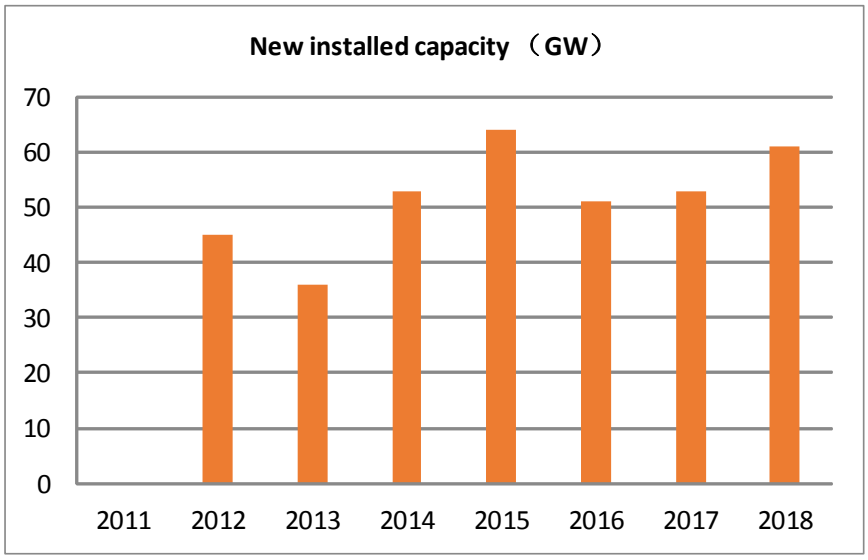

Figure 1.2: Worldwide new installed wind power capacity

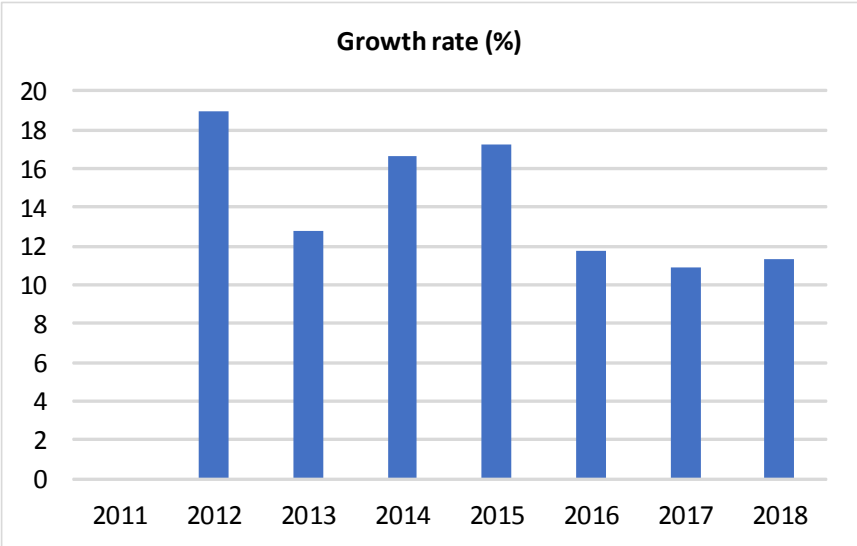

Figure 1.3: Global growth rate of wind power capacity

The impact of increasing penetration of wind energy systems into the existing grid is an important issue for power and control system researchers [12, 13]. It may cause some severe problems associated with power quality, transient instability, voltage instability and others.

These problems have been addressed by various researchers using flexible alternating current transmission system (FACTS) devices. FACTS can be operated and implemented with multi-functionality to solve those problems which arise due to integration of wind power. In [14], the researchers have shown how

these devices could contribute in improving the power quality in a wind energy conversion system. In [15–17], FACTS has been proposed to enhance the voltage stability in a power system with wind energy. In [18, 19], transient stability improvement of wind energy power system using FACTS has been studied. These FACTS devices have been controlled by different controllers, e.g., bang-bang modulation based controller [20], mixed H_2/H_∞ output-feedback controller [21], PID control [22] and so on.

An alternative control strategy which has been effectively used by researchers in recent years is Q-learning and dynamic fuzzy Q-learning (DFQL). Q-learning based controller is a model free controller and is based on the principle of reinforcement learning (unsupervised learning) which could successfully provide optimal control actions for systems, particularly for those with uncertainty [23]. Q-learning based controllers have successfully been used to solve some power system problems such as power system restoration [24], stability improvement of wide-area power system [25] and so on. However, the Q-learning based controller provides discrete control actions. An alternate reinforcement learning controller is the DFQL based controller which could handle continuous states and provide continuous actions. Combination of fuzzy logic control and reinforcement learning, especially Q-learning, has been considered of great significance for designing controllers for complex systems. Q-learning, with good learning ability, can be implemented in the rule-based fuzzy controller to improve the preciseness of fuzzy. As an extension of both Q-learning and fuzzy control, DFQL is a promising control method [26, 27].

1.2 Goal and Objectives

Motivated by the success of these controllers in various applications, the goal of this research is to investigate the effectiveness of reinforcement learning controllers to enhance low voltage ride through (LVRT) capability of a hybrid power system. In order to achieve this goal, this research sets the following main objectives:

- Design Q-learning and DFQL based controllers to improve the transient stability of classical power system (consisting of synchronous generators only) through dynamic series compensators.

- Design Q-learning and DFQL based controllers for the rotor side control of

wind energy conversion system (WECS) consisting of doubly fed induction generators (DFIGs).

- Design Q-learning and DFQL based controllers to enhance the low voltage ride through capability of a hybrid power system (consisting of both synchronous and wind generators) through unified power flow controller (UPFC).

- Design reinforcement learning controllers to achieve LVRT capability through convertible static compensator and establish the combination of controllers and CSC configurations which is optimum in LVRT enhancement of hybrid power system.

1.3 Thesis Structure

The rest of this study has been presented through six chapters which are structured as follows:

Chapter 2 reviews the basic background of this research. It starts with an introduction to the basic concepts of WECS and continues with different types of wind turbines, wind generators. The advantages and disadvantages of the combinations of these wind turbines and wind generators are highlighted. Among all these configurations of wind turbines and generators, variable-speed wind turbine, equipped with DFIG, is chosen for this study. Since the main objective revolves the integration of wind power into existing power grid, it is necessary to know the LVRT requirements in the grid codes of different countries. After that, various popular approaches to improve the LVRT capability are briefly described, including installation of external devices such as energy storage system (ESS), crowbar protection, FACTS devices, and improvement of internal controllers, such as fuzzy logic controller, reinforcement learning based controller and so on.

Chapter 3 proposes two controllers derived from the concept of reinforcement learning (RL): Q-learning and DFQL based controllers. Q-learning is one of the most popular algorithms in RL which could help the controller find the optimal solution by interacting with the system and does not require detailed mathematical model of the system. However, Q-learning based controller only gives discrete actions which could be further improved by the concept of DFQL. In DFQL based controller, it can effectively adjust fuzzy inference parameters

with the help of Q-learning and give continuous actions. In this chapter, the Q-learning based and DFQL based controllers are then designed to improve transient stability of both single machine infinite bus (SMIB) and multi-machine power systems (which consists of only synchronous generators) through dynamic series compensation. The effectiveness of designed RL based controllers are demonstrated and compared with bang bang controller (BBC) whose thresholds are optimized by particle swarm optimization (PSO) technique.

Chapter 4 investigates if the Q-learning based and DFQL based controllers are effective in controlling WECS. To achieve this objective, this chapter first establishes an aggregated dynamic model of a DFIG based wind farm, and then focuses on the rotor side control of wind generator. Next, Q-learning based and DFQL based controllers are designed for rotor side control (RSC), and their performance are compared with classical PID and Δ Σ based PID controllers .

Chapter 5 focus on designing Q-learning based and DFQL based controllers to improve LVRT capability of a three-machine hybrid power system through UPFC. This system consists of both synchronous generators and DFIGs based wind farm. The controller design follows similar procedures to previous chapters. The performance of designed controllers was compared with classical PID controller.

Chapter 6 is an extension of Chapter 5 where reinforcement learning strategy is used for controller design to improve the LVRT capability of a hybrid power system through convertible static compensator (CSC). The performance of different configurations of CSC such as static synchronous series compensator (SSSC), one static synchronous compensator (STATCOM), two STATCOMs, UPFC are investigated. The simulation was carried out progressively in 3 stages. First, for a given controller, such as PID, Q-learning and DFQL based controller, the performance of all the 4 different configurations of CSC are investigated. Next, for a a given configuration of the CSC, the performance of all the three controllers are studied . Finally,for a given LVRT grid code of a specific country, investigations are made to establish which combination of the controller and CSC configuration is better.

The main conclusions of this research and future work are summarised in Chapter 7.

Chapter 2

Control of Hybrid Power Systems with Wind Generators: Background Information

With the increasing concerns about a global energy crisis and the need for clean renewable energy resources, several renewable energies, such as hydro-power, bio-energy, geothermal power, solar and wind energy, have become cost-competitive when compared with fossil fuels and nuclear power over the past few years. Among them, wind power has been established as a mainstream. The cumulative installed wind power capacity over the world has increased to 600 GW by 2018 [4].

The level of wind power penetration into the power grid has correspondingly increased at a rapid rate due to the increasing accessibility and, development of wind energy conversion technologies, the growing demand for electricity, policy initiatives and so on [28]. All the capacity of installed wind turbines has approximately covered 6% of the global electricity demand by the end of 2018 [4].

The development of wind energy technologies is a driving force for the immediate application of a wind energy conversion system driven by wind to completely substitute fossil fuels. The development of wind energy system technology has been experienced in terms of mechanical sub-systems, electric subsystems, control subsystems and integration into a power grid. However, the integration of wind energy conversion systems into the traditional power system, consisting of synchronous generators, is a major challenging task [29, 30]. Because the grid codes defined for existing power system are no longer applicable with the penetration of wind power system. Thus, there is a need to modify the

grid codes to ensure their reliability and stability [31]. One of the most important considerations in the grid codes is the LVRT capability which will ensure continuous interconnection and fast response of wind turbines in the event of fault [1].

The goal of this study is to design and investigate the performance of two reinforcement learning controllers to enhance the LVRT capability of a hybrid power system consisting of both traditional synchronous generators and wind generators. These controllers will be used to control various FACTS devices placed at different locations. It is therefore appropriate to discuss briefly the wind energy conversion system, the concept of LVRT from the perspective of the hybrid power system and the important features of some of the most popular FACTS devices.

This chapter is therefore organized as follows: Section 2.1 discuss about the basic knowledge of wind energy conversion system. In Section 2.2, different types of wind turbines in current wind turbine systems are reviewed. Section 2.3 presents various types of wind generators driven in modern wind power systems. In Section 2.4, the general concept of LVRT requirement is given. Section 2.5 summarizes various LVRT compliance methods, including external devices based methods, such as crowbar, energy storage system, dynamic resistors, braking chopper, FACTS devices and so on, and internal controllers based methods.

2.1 Wind Energy Conversion System

The block diagram of a typical grid-connected WECS is shown in Fig. 2.1. This system mainly consists of mechanical, electrical and control systems. With this system, the kinetic energy of wind can be converted into stable and reliable electric energy into a power grid [1].

2.1.1 Mechanical system

The mechanical system in a WECS is essentially designed to capture the wind energy as much as possible and to convert the kinetic energy of wind into mechanical energy, which will be used to drive the electrical system of the WECS. It is mainly composed of blades, gearbox, wind turbine and so on.

According to the connection of their rotors with the shaft system, modern wind turbines could be categorized as two different types: vertical axis wind turbine (VAWT) (shown in Fig. 2.2a) and horizontal axis wind turbine (HAWT)

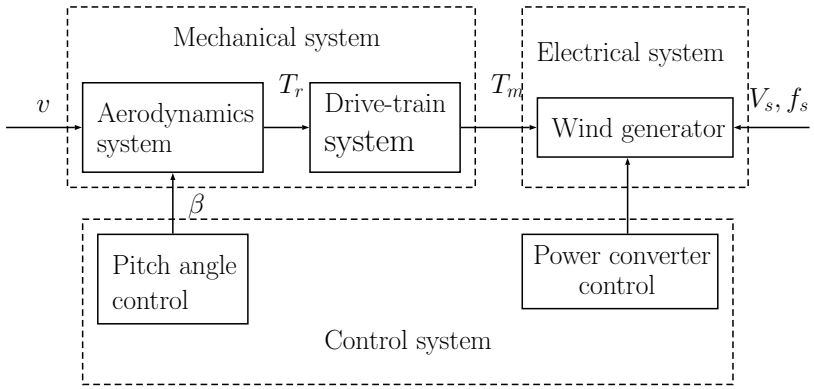

Figure 2.1: A typical wind energy conversion system

(shown in Fig. 2.2b). The most attractive feature of VAWT is that the gear box and wind generator are installed at the base of the tower, for which the maintenance is easy. Other advantages for VAWT include elimination of yawing mechanisms, and high rotational speeds that offer reduction in gear ratios [32]. However, HAWT dominates the commercial market due to its superiority to VAWT. For example, the power capacity and efficiency of VAWT is not as much as HAWT. Furthermore, a dynamic analysis of a VAWT based WECS is not easy due to the variable blades rotation of VAWT. Besides, VAWT also has several other disadvantages, such as tendency to stall under gusty wind conditions, sensitivity to off-design conditions, and the low installation height limiting operation to lower wind speed environments [32]. Therefore, HAWT based wind turbine system is considered in this study.

Fig. 2.3 shows a typical HAWT-based WECS, where the rotor blades, gear box and wind generator are connected with a horizontal shaft. As can be seen, the rotor is located at the top of a standing tower, and the gearbox and wind generator are assembled inside a nacelle.

In order to estimate the energy extracted from the wind, there are two different theories established for the aerodynamic models of the wind turbines: *actuator disc theory* [33] and *blade element theory* [34]. The former approach focuses on the energy extraction process and the energy conversion efficiency. The latter approach concentrates on the forces obtained by the wind on the blades. Because the wind power is only a driven power for the wind generators, in this study, without considering the wind conversion process, the blade element theory is used.

In the *blade element theory*, the power obtained by the turbine is expressed

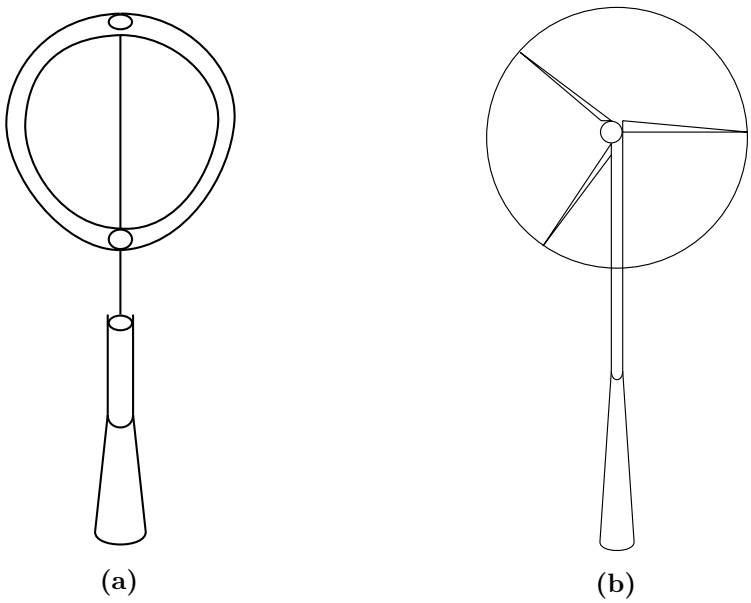

Figure 2.2: (a) Vertical axis wind turbine (b) Horizontal axis wind turbine

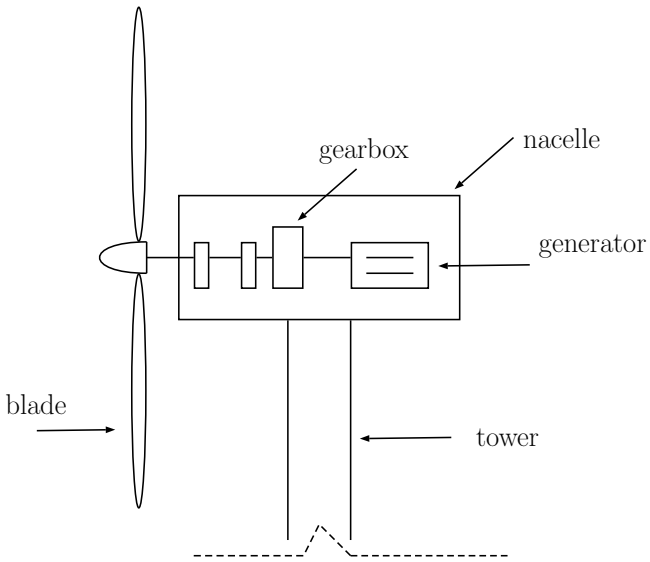

Figure 2.3: Horizontal axis wind turbine based WECS

as:

$$P_r = \frac{1}{2}\rho\pi C_P v^3 \tag{2.1}$$

where, C_P is the power coefficient; ρ (kg/m^3) is air density; R (m) represents the blade radius and v (m/s) denotes the wind speed.

The power coefficient C_P for wind turbine is usually given by wind turbine manufacturers as a function of the pitch angle β and tip-speed-ratio λ which is a predefined constant [35]. The tip-speed-ratio λ is a function of rotor speed ω_t and the wind speed v, which is expressed as :

$$\lambda = \frac{\omega_m R}{v} \tag{2.2}$$

where, ω_m(rad/s) is the rotational speed of wind turbine shaft system; and R(m) is the radius of the wind turbine.

2.1.2 Electrical system

The electrical system in a WECS essentially consists of a three-phase generator, which is driven by the wind turbine and converts the rotating mechanical energy into electric energy. Basically, the wind turbines could be equipped with any type of generators. During the past few decades, several types of generators have been developed in WECS, such as squirrel-cage induction generator (SCIG) [36, 37], DFIG [38–40], wound rotor induction generator (WRIG) [41, 42], permanent magnet synchronous generator (PMSG) [43, 44], wound rotor synchronous generator (WRSG) [45] and so on. In this study, DFIG has been considered in use.

2.1.3 Control system

Design of a proper controller for wind energy system is important as it is necessary to effectively control both the mechanical and electrical systems to achieve high performance of the wind turbine.

For example, in large-scale variable-speed wind turbine systems, the change of rotor speed is relatively slow due to large inertia. Therefore, this will easily result in high stress on the mechanical components. Pitch control system applied in these variable-speed wind turbine systems is an effective method to reduce the effect of this problem. Pitch control can essentially enable the angles of blades adjustable with respect to the wind speed variation and further achieve

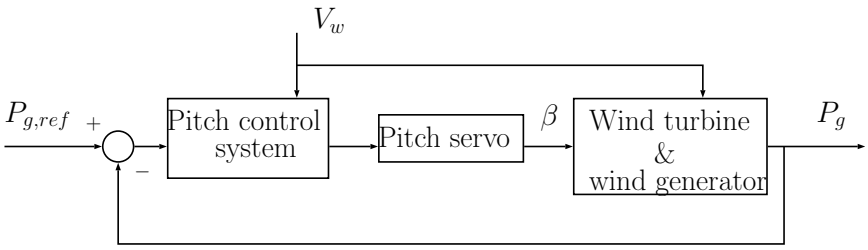

Figure 2.4: Pitch angle control system

maximum energy conversion efficiency [46]. A general pitch angle control system is shown in Fig. 2.4 [46, 47].

Another common control system used in a wind turbine system is the power converter control. This is used to control various variables of the electrical system, such as the active and reactive power generated by the wind generator, the currents flowing through the wind generator, to improve the dynamic and steady-state performance of the wind power system [1].

2.2 Wind turbines

Three types of wind turbines such as fixed-speed wind turbine, limited-speed wind turbine and variable-speed wind turbine are mainly used in the current wind energy systems. Their features are briefly discussed in the following:

2.2.1 Fixed-speed wind turbine

In the early years of the wind energy industry, wind turbines were usually operated at a fixed speed, where the rotor speed is fixed to some particular wind speed, and it is determined by the frequency of power supply grid and the gear ratio.

In a fixed-speed wind turbine based system, the wind turbine is usually equipped with an induction generator, which is directly connected with the power grid through a soft-starter and a capacitor bank for reactive power compensation [13].

Although the performances of fixed-speed wind turbines have been proven to be robust and reliable, they have some drawbacks. Due to fixed speed operation, these wind turbines are designed to achieve maximum efficiency at one particular wind speed and are unable to implement maximum-power-point-tracking. This implies that fixed-speed wind turbines have low wind energy conversion

efficiency. Furthermore, the power quality and voltage ride-through capability provided by fixed-speed wind turbines are poor, because they don't have reactive power compensation [48]. Another disadvantage of fixed-speed wind turbine is high mechanical stress caused by the fluctuations of wind [49].

2.2.2 Limited-speed wind turbine

In a limited-speed wind turbine system, the rotor speed could be adjusted to the wind gusts in a limited range, such as ±10%, ±30%. As the rotor speed is variable to some extent, the wind power captured by the system is increased compared with the fixed-speed wind turbine system. The wind energy conversion efficiency is higher than the fixed-speed wind turbine system. However, the rotor speed could only be adjustable in a limited range, and there could still be energy losses [1].

2.2.3 Variable-speed wind turbine

During the past decade, variable-speed wind turbines have dominated in newly installed wind turbines due to rapid development of power electronics.

Variable-speed wind turbines are designed to achieve maximum wind capture efficiency by operating at a wide range of wind speeds. The fluctuations of wind are absorbed by the variations in wind generator speed and, in turn, the rotational speed of the wind turbine could continuously be adjusted [50].

2.3 Wind generators

During the past decades, different types of generators have been developed for wind turbines [38, 39, 51–58]. They can be classified into asynchronous generators, synchronous generators and other types.

2.3.1 Asynchronous generator

Squirrel-cage induction generator

By far, over half of the present wind farms use SCIG based wind turbines connected to the grid [59]. SCIG could be connected with both fixed-speed wind turbines and variable-speed wind turbines in WECS.

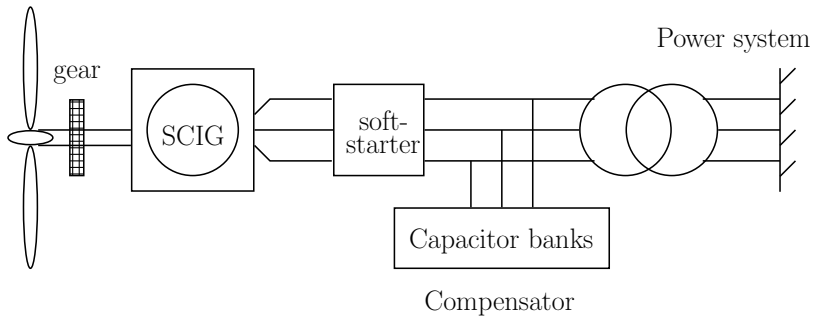

Figure 2.5: Fixed-speed wind turbine equipped with an SCIG

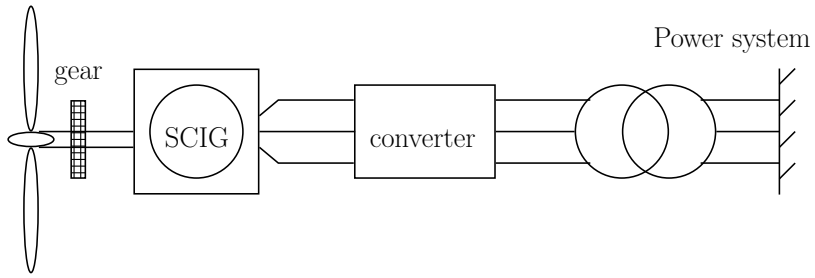

Figure 2.6: Variable-speed wind turbine equipped with an SCIG

Fig. 2.5 shows a fixed-speed wind turbine equipped with an SCIG and a gearbox. The SCIG is connected to the power grid directly through a transformer. In this system, the rotor speed of SCIG could only operate within a narrow range. Because the SCIG has high demand of reactive power from the power grid, a capacitor-based compensator is normally used to compensate for the inductive reactive power. The compensator is usually composed of capacitor banks which could be switched on or off to achieve different degrees of compensation according to the need of the generator. Furthermore, a soft-starter is also usually used in the system to help the start-up of the turbine and limit the inrush current in the generator windings.

Fig. 2.6 shows a variable-speed wind turbine equipped with an SCIG, a gearbox. The SCIG is connected to the power grid through power electronic converters. Compared with the fixed-speed SCIG system shown in Fig. 2.5, this variable-speed SCIG configuration is more flexible in power control, such as variable speed operation, reactive power compensation through the power converters. The disadvantage of SCIG is that it is not self-excited. Therefore, the magnetic field could not be regulated by the SCIG [60].

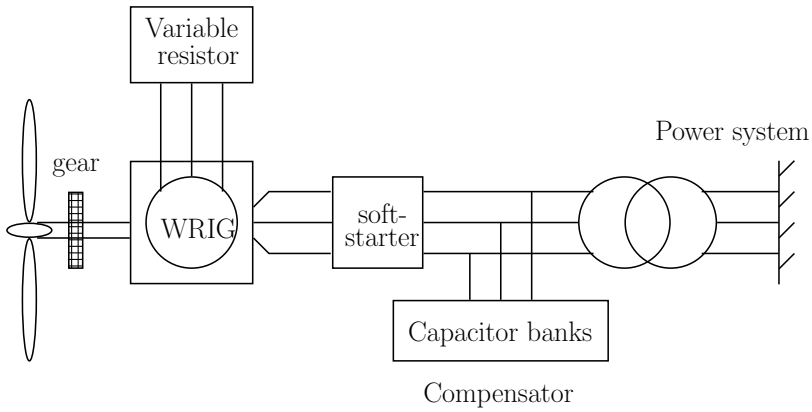

Figure 2.7: Limited-speed wind turbine equipped with WRIG

Wound rotor induction generator

The wound rotor induction generator (WRIG) is usually operated with a limited-speed wind turbine, of which the rotor speed is variable within a limited range (±10% of the rated speed) [61]. This concept is known as Optislip.

Fig. 2.7 shows the configuration of a limited-speed wind turbine equipped with a WRIG. In this configuration, the wind turbine could be operated within a certain speed range. The stator of WRIG is connected to the power grid through a soft-starter, which could reduce the inrush current of the generator windings. The rotor is equipped in series with an external variable resistor which is adjustable and controlled by a power converter. Compared with the fixed-speed wind turbine system, the energy conversion efficiency of the limited-speed wind turbine equipped with WRIG is increased.

Doubly-fed induction generator

DFIG is the trend of installed generators in modern WECS. A typical limited-speed wind turbine (±30% of the rated speed) equipped with a DFIG is shown in Fig. 2.8. As can be seen, the stator of the wind generator is directly connected with the power grid, whereas the rotor is connected with the grid through a back-to-back converter [62]. Because both the stator and rotor of the wind generator could transfer energy into the power grid, this is referred as a doubly-fed generator [39].

During the past few years, many research results on modelling and control of renewable energy systems including the DFIG have been reported [40,63–65]. Detailed modelling of both mechanical and electrical dynamics are presented in [66]. In DFIG control scheme, the controllers could either be applied to RSC

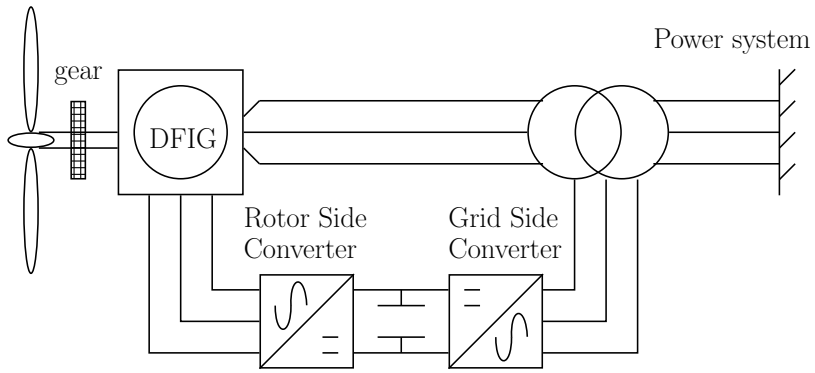

Figure 2.8: Limited-speed wind turbine equipped with DFIG

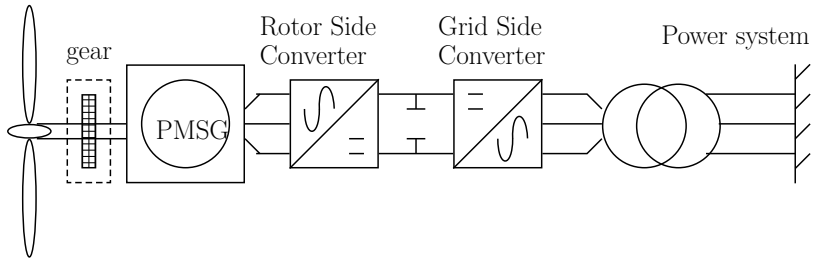

Figure 2.9: Variable-speed wind turbine equipped with PMSG

or to the grid side converter (GSC).

2.3.2 Synchronous generator

Compared with inductive generators, synchronous generators based wind energy conversion systems have more options for different configurations. The most common synchronous generators used in WECS are PMSG and WRSG.

Permanent magnet synchronous generator

PMSG is usually applied in variable-speed wind turbine based WECS. Fig. 2.9 shows the connection of a variable-speed wind turbine equipped with a PMSG. In this system, the PMSG is directly driven by the wind turbine without gearbox, and is connected to the power grid through a full-capacity power converter.

Wound rotor synchronous generator

WRSG could be installed with variable-speed wind turbine based WECS, and this configuration has two ways to be connected to the power grid.

In the first way, it is connected with the power grid through a set of full capacity frequency converters, as shown in Fig. 2.10. The full capacity converters

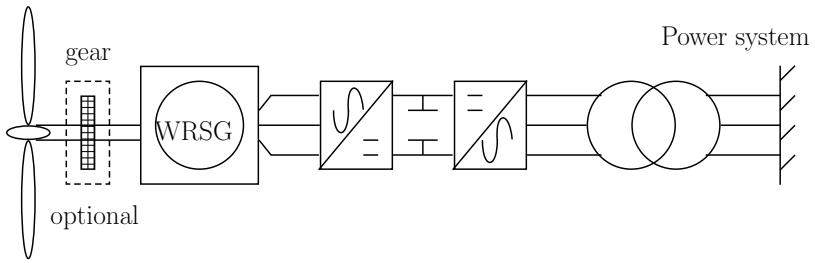

Figure 2.10: Variable-speed wind turbine equipped with WRSG (with full capacity power converter)

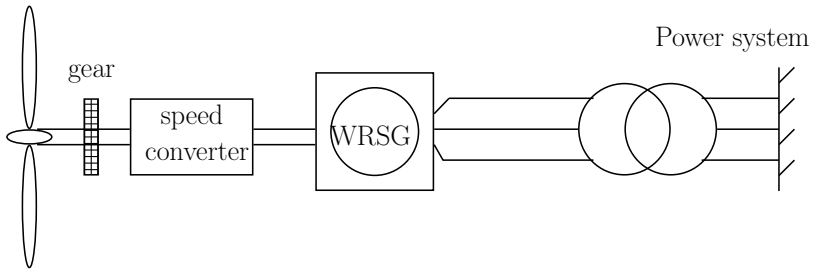

Figure 2.11: Variable-speed wind turbine equipped with WRSG (without full capacity power converter)

could enable the wind generator to be fully decoupled with the power grid and therefore could be operated in a variable speed mode.

The second connection is shown in Fig. 2.11. It can be observed from Fig. 2.11 that the wind generator is connected directly with the power grid. Therefore, it operates at a fixed speed. The variable speed of this configuration is achieved by the speed converter which is a mechanical converter rather than electrical converter [67].

In synchronous generator group, WRSG could be superior over PMSG in terms of the degrees of freedom of the control system. However, the robustness of PMSG is better than that of WRSG [45]. Further, WRSG is an old concept in modern wind power technology. Therefore it is only applied in some specific offshore wind energy power systems since it is cost-efficient.

2.3.3 Summary of configurations of wind turbines and wind generators

This section summarizes the features of all the common wind turbines and wind generators discussed in previous sections.

We have discussed several configurations of wind turbine and generator, such as fixed-speed wind turbine equipped with SCIG, variable-speed wind turbine

equipped with SCIG, limited-speed wind turbine equipped with WRIG, limited-speed wind turbine equipped with DFIG, variable-speed wind turbine equipped with PMSG and variable-speed wind turbine equipped with WRSG.

The features of these configurations of turbines and wind generators are given in Table 2.1 [1]. From this table, it can be seen that the limited-speed wind turbine, equipped with DFIG, is the most popular configuration in modern power systems. Therefore, in this study, this configuration is considered for investigation.

2.4 Low Voltage Ride Through Requirements

From a control perspective, wind farms have lower degree of controllablity. The integration of such systems into the existing power grid may introduce loss of generation for frequency support, voltage flicker, and instability etc [68].

In order to successfully integrate the WECS into the existing power grid, various countries have developed/modified their grid codes which indicate that the wind farms should contribute towards controlling the frequency and voltage of the grid by regulating their power output such that their operational characteristics are similar to the conventional power plants [68–70]. One of the most important requirements is LVRT capability, which states that, in the event of a disturbance, the wind farm must withstand voltage sag/dip to a certain percentage of the nominal voltage for a specified duration and stays connected to the power system. A general limit curve for LVRT requirement is illustrated in Fig. 2.12. This requires that the wind turbines must stay connected with the system if voltage profile is above the limit curve. According to Fig. 2.12, the WECS should be connected with the power grid when the voltage at the point of common coupling (PCC) drops to a low voltage level (as low as 0 p.u. in Fig. 2.12) during the fault period and should recover above the specified limit after the fault clearance.

2.5 Different Methods to Achieve LVRT Requirements

During the past decade, various researchers have proposed different methods to achieve LVRT requirement [70–73]. As shown in Fig. 2.13, these methods include installation of different types of external devices, such as crowbar, en-

Table 2.1: Summary of configurations of wind turbines and wind generators [1]

	SCIG		WRIG	DFIG	PMSG	WRSG	
	fixed-speed	variable-speed	limited-speed	limited-speed	variable-speed	variable-speed (with speed converter)	variable-speed (with power converter)
Power converter	No	Yes	Yes	Yes	Yes	No	Yes
Converter capacity	0%	100%	10%	30%	100%	100%	100%
Speed range	±1%	±100%	±10%	±30%	±100%	±100%	±100%
Softe starter	Required	Not required	Required	Not required	Not required	Required	Not required
Gear	required	required	required	required	optional	required	optional
External reactive compensation	needed	not needed	needed	not needed	not needed	not needed	not needed
FRT compliance	by external device	by external device or power converter	by external device	by external device or power converter	by external device or power converter	unknown	unknown
Current market penetration	few	few	few	> 50% share	2nd highest share	few	3rd highest share

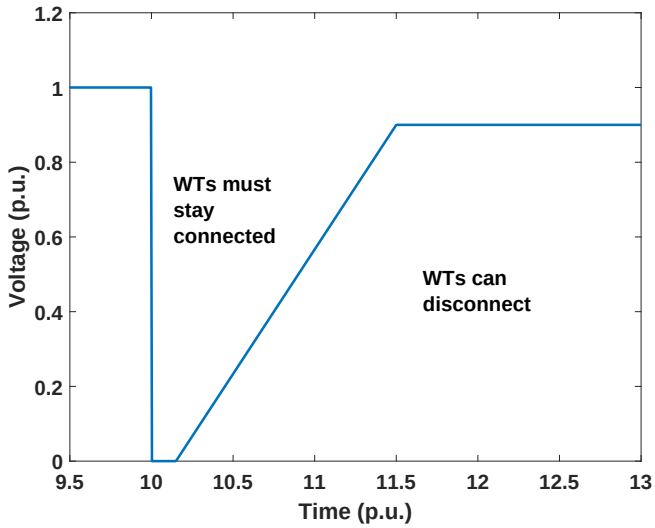

Figure 2.12: General limit curve for LVRT requirement.

ergy storage system, dynamic resistors, braking chopper, FACTS devices etc., and improvement of internal controllers approaches [74, 75]. These are briefly discussed in the following:

2.5.1 Crowbar

Due to grid faults, the voltage sag at PCC could cause over-voltages in rotor windings of DFIG and over-currents in rotor side power converters; it could even damage the mechanical components of the generators and wind turbines. In order to overcome these problems, crowbar is usually used to protect the rotor converter by short circuiting the rotor windings [76, 77]. A typical schematic of crowbar circuit installed with a DFIG based wind turbine is shown in Fig. 2.14.

Many researchers have worked on the enhancement of LVRT capability of DFIG based wind turbines using crowbar protection [78–82]. In [83], besides installed in series with rotor winding and RSC, a crowbar can also be connected with the dc-link capacitor of DFIG to cooperate with the rotor side crowbar and to support the DFIG based wind turbine to ride through the fault. In [84], a new advanced single phase crowbar, which is simpler and more cost-effective than classic three-phase dc crowbar, was proposed for DFIG and its effectiveness has been demonstrated in the cases with different types of faults to achieve the LVRT requirements. In [85], the crowbar protection is applied in a brush-less DFIG with coupled circuit model and its effectiveness to improve its LVRT capability was investigated.

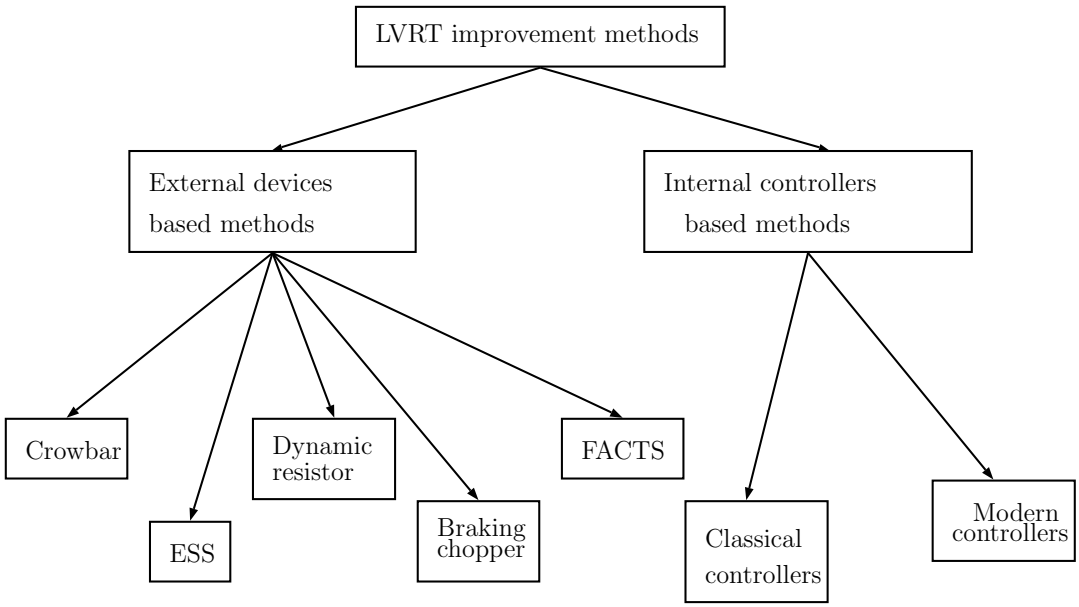

Figure 2.13: LVRT improvement methods.

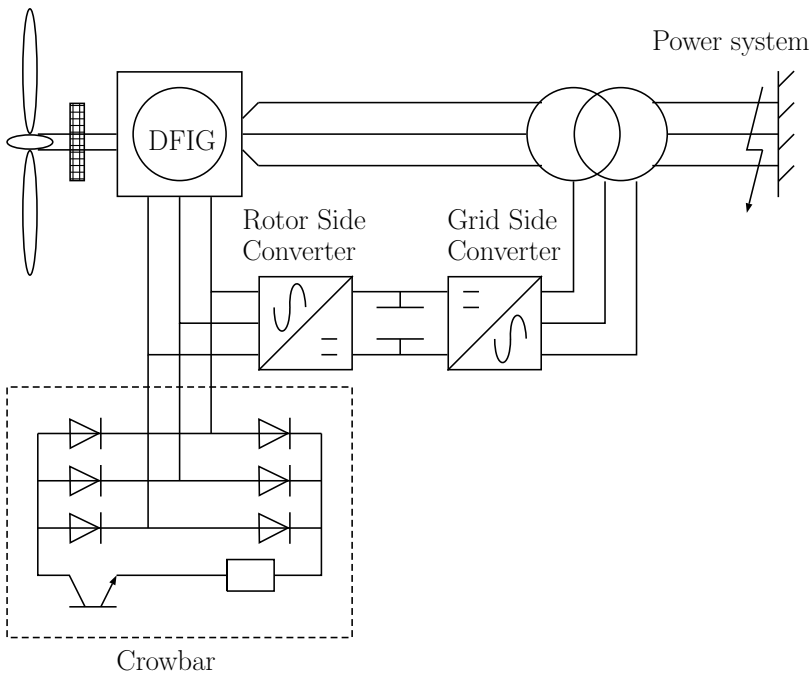

Figure 2.14: LVRT improvement using crowbar.

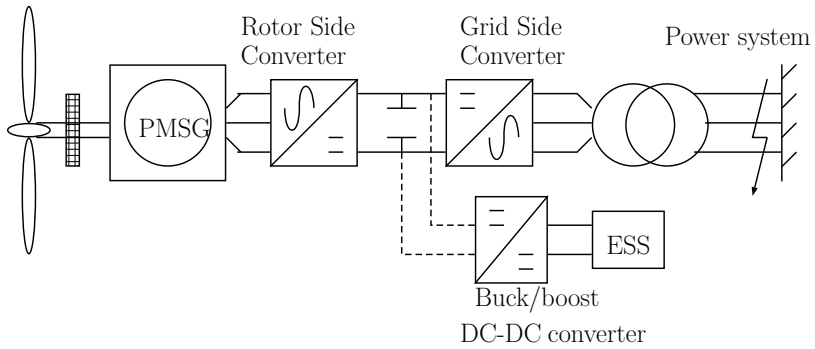

Figure 2.15: LVRT improvement using ESS in PMSG.

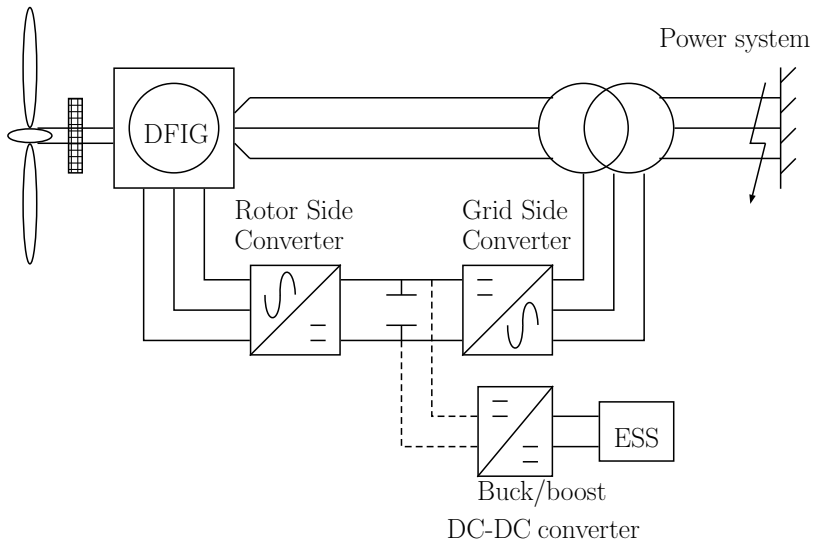

Figure 2.16: LVRT improvement using ESS in DFIG.

However, during the grid fault, the crowbar needs to protect the rotor side power converter from over-current. Since during this time, the controllability of the DFIG is lost, as the DFIG behaves as a conventional squirrel cage induction generator. Further, the installation of a crowbar with each individual wind turbine requires an additional control system and therefore increases the control complexity of the system.

2.5.2 Energy Storage System

ESS is a helpful group of devices to protect the dc-link of the converters from over-voltage during faults with the PCC, which enhances the LVRT capability of wind turbines [86–89]. ESS is usually connected to the dc link side of back-to-back converters. Fig. 2.15 and Fig. 2.16 show the ESS installed with PMSG and DFIG .

The ESS used for improvement of LVRT capability could be classified into several different types: battery energy storage system (BESS) [90, 91], flywheel energy storage system (FESS) [92], superconducting magnetic energy storage system (SMESS) [93], electrical double-layer capacitor (EDLC) [94] and so on.

Battery energy storage system is one of the most popular energy storage devices used in power system to improve the LVRT capability. In [95–97], the BESS is installed in parallel with the dc-link of wind generators which is used to store the energy in the ESS device during the faults. This reduces the power absorbed by the dc-link of the wind generators which otherwise could cause over-voltage. This is helpful to keep the wind generators connected with the grid during the fault without loss of generators, which is essentially LVRT improvement. Similar to the operation of BESS, EDLC also known as super-capacitor, is another group of effective option for LVRT improvement [98, 99]. Besides, there is another electro-mechanical based ESS device called FESS, where the energy is stored in the form of kinetic energy. Its effectiveness has been demonstrated in several applications of LVRT improvement in wind turbines [92]. Different from these devices mentioned above, a SMESS stores the energy in a magnetic field which is created by a DC current through a large super-conducting oil [93, 100, 101]. Moreover, SMESS could be more flexible in the connection with the wind generators except with dc-link. For example, [102] proposes a SMESS devices with a different connection which is in parallel with the rotor side of each DFIG, and its effectiveness has also been studied by different LVRT strategies in the DFIGs based wind farm under several fault conditions.

However, there are some drawbacks of these ESS devices, such as energy loss in the process of conversion, high installation and maintenance costs, requirements of infrastructure and space [103], short operation duration and high self-discharge losses in FESS [104, 105]. Further, the ESS devices also have disadvantages similar to crowbars, which could increase the control complexity of the system.

2.5.3 Series dynamic resistor

Series dynamic resistor (SDR) is usually applied in the rotor or stator of wind turbines to limit the over-current and to reduce the oscillations and settling time of transient response during the voltage dip [106]. Its effectiveness in LVRT enhancement has been widely studied by many researchers [85, 107–116].

Fig. 2.17 shows the connection of SDR installed in series with the stator

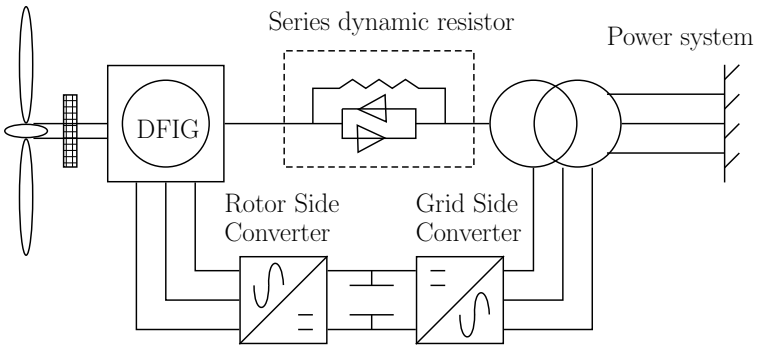

Figure 2.17: LVRT improvement using series dynamic resistor installed in series with stator

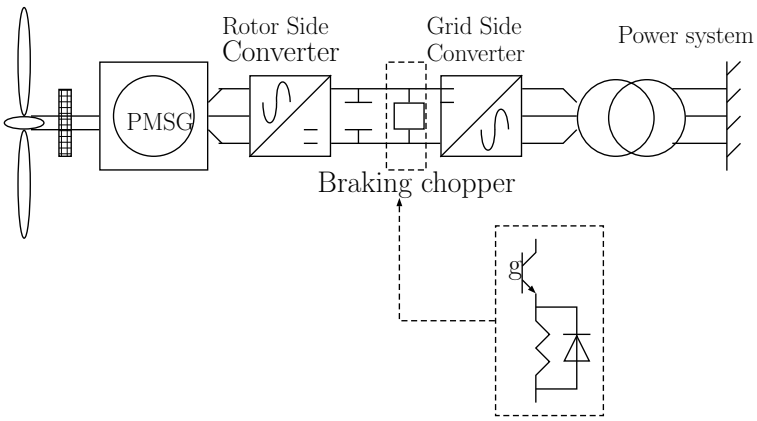

Figure 2.18: LVRT improvement using braking chopper

of DFIG. In the event of system fault, e.g., when the voltage drops, the SDR is switched in series with the stator of DFIG, which increases the equivalent reactance of stator. Otherwise, the SDR is deactivated in normal operation.

2.5.4 Braking chopper

Braking chopper connected in the dc-link to improve the LVRT capability of PMSG based wind turbines is often proposed as another effective option in the literature [108, 117–120]. Fig. 2.18 shows the connection of braking chopper with a PMSG.

A typical braking chopper consists of a high power resistor in series with a switch g [118]. The control signal S_g to activate the switch g is dependent on the difference between the output power of the generator P_{gen} and the grid power P_{grid}, which is expressed as (2.3) [119]:

$$S_g = \frac{R_{BC}}{V_{dc}^2} P_{BC} \tag{2.3}$$

where, R_{BC} is the resistance of the braking chopper; $P_{BC} = P_{gen} - P_{grid}$, is the power dissipated by the braking chopper; V_{dc} is the voltage of dc-link where the braking chopper is connected.

2.5.5 FACTS

An alternate attractive solution to achieve LVRT is through the use of FACTS devices which are usually installed at the PCC and therefore do not increase the overall complexity.

FACTS device group could be classified into three different types: series branch based FACTS, shunt branch based FACTS and combined FACTS. Series FACTS are usually connected in series with transmission lines in the power system, and are usually effective in the transient stability improvement, e.g., dynamic series compensator. Shunt FACTS are connected in parallel with the power grid, such as STATCOM, static VAR compensator (SVC) and so on. The combined FACTS devices consist of both series and shunt compensations, and are considered as the most versatile FACTS devices which could both regulate the series voltage and inject power flow into the grid [121], such as UPFC and CSC.

Many researchers have studied various effects of FACTS on power system, such as improvement of small-signal stability [21, 122, 123], voltage stability [124–129], transient stability [130–142], power oscillation damping [143, 144], optimization of power flow [145], enhancement of security [146] and reliability [147], and attenuation of sub-synchronous resonance in wind farm integration [148].

The effectiveness of some of FACTS devices such as STATCOM, SVC,DVR and TCSC to improve the LVRT capability has been thoroughly investigated by researchers. For example, in [149], a comparative study has been carried out to improve LVRT capability using STATCOM and SVC and it has shown that STATCOM is better than SVC. In [150], a robust controller for STATCOM with the objective of LVRT capability improvement was designed. Besides these shunt devices which are used to provide reactive power to the power system, other researchers have also applied series FACTS devices to improve the LVRT capability by compensating the voltage sags, such as Dynamic Voltage Restorer (DVR) [151–153], thyristor controlled series capacitor (TCSC) [154] and so on.

However, all these FACTS devices in terms of LVRT improvement are either series branch based or shunt branch based FACTS devices. To the best knowl-

edge of the author, the performance of combined FACTS devices such as UPFC and CSC to improve the LVRT capability have not been investigated yet and this will be the focus of the present investigation.

2.5.6 Control Approaches

Besides the devices mentioned above, the control approach also has significant effect on the LVRT capability of wind turbines. During past decades, various controllers have also been designed for various devices to adjust the reactive power injected into the power system in order to improve LVRT capability of wind turbines.

In [155], a decentralized controller using a linear quadratic (LQ) output-feedback control design method is proposed to control a STATCOM, which improves the LVRT capability of fixed-speed wind turbines. In [75], an advanced control strategy is designed for both grid side converter and rotor side converter. With this strategy, the rotor side converter could convert the imbalanced power into kinetic energy of wind turbine by speeding up the rotor. This strategy also enables a reactive compensation in the grid side control scheme to smooth the DC-link fluctuation. [156] presents a fuzzy controller which is tuned by genetic algorithm for grid side converter of DFIG to improve its LVRT capability.

In this study, the major focus is on designing reinforcement learning controllers to achieve LVRT capability by using several FACTS devices and determine the optimum combination of the FACT device and controller.

Chapter 3

Improvement of Transient Stability of a Power System using Reinforcement Learning Controllers

Transient stability analysis and improving its limit in a modern power power system have been recognized as one of the major problems amongst researchers during the past few decades [63, 157, 158]. The transient stability analysis essentially investigates whether a power system has the ability to remain in synchronism following a large disturbance, such as loss of load or generators, faults in the transmission lines and so on.

Considerable research has been dedicated to addressing power system transient stability issues [159]. For example, FACTS devices such as SSSC, STATCOM, UPFC and Inter line Power Flow Controller [160] have been proposed during the last few decades for improving transient stability of power systems. Further, different types of controllers, such as PID control [161], bang-bang control [162], sliding mode control [163], self-tuning control [164] have been proposed to provide additional damping to the power system following a disturbance to damp out the transient oscillations quickly. Each of these methods of transient stability improvement has both merits and demerits.

However, the power system network is nonlinear which operates in a constantly changing environment where loads, generator outputs and key operating parameters change continually. To effectively account for these scenarios, various intelligent control methods, such as fuzzy PID controller [165], and genetic

algorithm based fuzzy control [166], have been proposed. Although the classical fuzzy based controllers are effective to improve the transient stability margin of the power system, they offer a sub-optimal solution to various scenarios in the power system. For example, the initial rule base of fuzzy inference system (FIS), which is only based on the knowledge given by an experts' experience, could not conform to all the situations the power system might be exposed to.

An alternative approach of improving the transient stability is to use DFQL based controllers for the power system. In DFQL scheme, Q-learning is being used to adjust the prior knowledge of fuzzy rule base through the learning process. Thus, the system does not rely on the user-defined fuzzy rule base. Instead, the DFQL controller could self-learn and redefine the fuzzy rules from the environment and lead to optimal performance adaptively. In [27, 167, 168], the DFQL controller is proposed and successfully implemented in robots, boat problems, the cart-pole balancing problem and the mountain-car problem. In these literatures, a DFQL controller showed superiority of other related controllers. In this chapter, both a Q-learning based controller, and a DFQL controller, which can automatically change the fuzzy rules to adapt for various scenarios of the power system, are proposed for transient stability improvement. The effectiveness of these controllers is demonstrated considering both a single machine infinite bus and three-machine system and is compared with a BBC. Note that, sub-synchronous resonance is not considered in this study.

3.1 Modelling of Synchronous Generator

3.1.1 Single machine infinite bus system with series compensator

The dynamics of SMIB, shown in Fig. 3.1, is described as follows [169]:

$$\frac{d\delta}{dt} = \omega \tag{3.1}$$

$$\frac{d\omega}{dt} = \frac{1}{2H}(P_m - P_e) \tag{3.2}$$

where, δ, ω, and E_g represent the rotor angle, rotor speed and output voltage of the synchronous machine respectively. P_m is the mechanical input; P_e is the

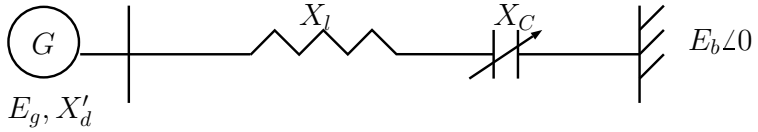

Figure 3.1: A single machine infinite bus system with series compensator

electrical output which is expressed as:

$$P_e = \frac{E_g E_b}{X} \sin\delta \tag{3.3}$$

where, $X{=}X'_d{+}X_l{-}X_c$; X'_d is the transient reactance of synchronous machine; X_l and X_c donate the reactance of the transmission line and the series compensator, respectively.

3.1.2 Modelling of multi-machine power system

Consider a power system consisting of m number of synchronous generators (m-machine system). The dynamics of ith generator in the synchronous rotating frame is described as [169]:

$$\frac{d\delta_i}{dt} = \omega_i \tag{3.4}$$

$$\frac{d\omega_i}{dt} = \frac{1}{M_i}(P_{mi} - P_{ei} - D\omega_i), \qquad (i = 1, \ldots, m) \tag{3.5}$$

The power output of the i_{th} generator, P_{ei} in (3.5) is given as:

$$\begin{aligned} P_{ei} &= \sum_{j=1}^{m} E_i E_j (G_{ij}\cos\delta_{ij} + B_{ij}\sin\delta_{ij}) \\ &= E_i^2 G_{ii} + \sum_{\substack{j=1 \\ \neq i}}^{m} (C_{ij}\sin\delta_{ij} + D_{ij}\cos\delta_{ij}) \end{aligned} \tag{3.6}$$

where

$$\delta_{ij} = \delta_i - \delta_j \tag{3.7}$$

$$C_{ij} = E_i E_j B_{ij} \tag{3.8}$$

$$D_{ij} = E_i E_j G_{ij} \tag{3.9}$$

$$\overline{Y}_{ij} = G_{ij} + jB_{ij} \tag{3.10}$$

$\overline{Y}_{int}$ is the admittance matrix reduced to internal nodes; $\overline{Y}_{ij}$ is the elements of $\overline{Y}_{int}$.

In most of the transient stability studies, researchers have used another frame of reference, called center of inertia (COI) frame, to represent the dynamics of the machines [170]. In this study, we have used the machine models in center of inertia frame. The derivation of the model in this frame proceeds by first computing the mean motion of COI which is defined as:

$$\delta_o = \frac{1}{M_T}\sum_{i=1}^{m} M_i\delta_i \tag{3.11}$$

where, $M_T = \sum_{i=1}^{m} M_i$.

The swing equations (3.4 - 3.5) in synchronous rotating frame when transformed into COI frame give:

$$\frac{d\theta_i}{dt} = \tilde{\omega_i} \tag{3.12}$$

$$M_i\frac{d\tilde{\omega_i}}{dt} = \frac{1}{2H_i}[T_{mi} - T_{ei} - D(\omega_{mi} - \omega_{mi0})] \qquad (i = 1, 2, 3) \tag{3.13}$$

where, $\theta_i = \delta_i - \delta_o$.

3.2 Controller design for series compensator

In this chapter, the performance of both Q-learning based and DFQL based controllers is compared with BBC. It is therefore appropriate to discuss the design procedure of these controllers, which are detailed below.

3.2.1 Q-learning based controller

Q-learning is one of the most popular algorithms in reinforcement learning where the *agent* learns from interactions with the *environment* to achieve a goal. From the control perspective, the *agent* is known as the controller and the system to be controlled is called the *environment*. In the terminology of Q-learning, the output of the system (i.e., the *environment*) is known as the *state* and the output of the controller (i.e., the *agent*) is called the *action*. The basic philosophy of Q-learning is shown in the schematic of Fig. 3.2, and the flowchart of designing

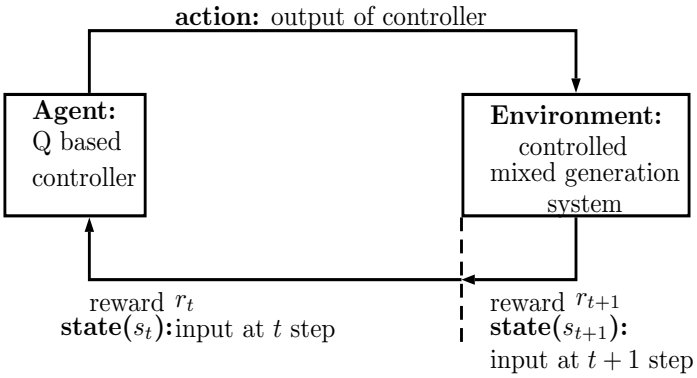

Figure 3.2: Interactions in Q-learning

Q-learning based controller is illustrated in Fig. 3.3.

The Q-learning based controller essentially selects the most suitable action for a given state from an infinite set of possible actions in order to achieve the control goal. The strategy of selecting the action a^t in the state $x(t)$ strongly influences the performance of the controller. In this study, we have used ϵ-greedy policy [171] which can effectively balance the *exploration* and *exploitation* and result in better controller performance. This is achieved as follows:

The algorithm starts with initialization of states x^0, Q-value matrix and probability matrix P of possible actions for all the states. Define the action set $\mathcal{A}$=$[a_1, a_2, \cdots, a_m]$ and state set $\mathcal{X}$=$[x_1, x_2, \cdots, x_n]$, where m and n are the numbers of all possible actions and states respectively. Let $P(x^t, a_i)$ denote the probability of selecting the action a_i for a given state x^t. This is updated by

$$a^t \leftarrow \begin{cases} a_i \in arg\max_a Q(x^t, a), & \text{with probability } (1-\epsilon) \\ random\ action, & \text{with probability } \epsilon \end{cases}$$

where, $\epsilon \in (0, 1)$ is the exploration probability; $a_i \in arg\max_a Q(x^t, a)$ is the action which gives the best Q - value.

After selection of the action a^t, the controller observes the transition state x^{t+1} and receives a reward $r^{t+1} = R(x^{t+1}, a^t)$ which indicates how good the action is. For each transition (x^t, a^t, r^{t+1}, x^{t+1}), it updates the Q - function as [172]:

$$Q(x^t, a^t) \leftarrow Q(x^t, a^t) + \alpha[r^{t+1} + \gamma \max_a Q(x^{t+1}, a) - Q(x^t, a^t)] \tag{3.14}$$

where, $Q(x^t, a^t)$ is the action - value with state x^t and action a^t at t step; $\alpha \in (0, 1)$ is learning rate; γ is the discounted rate; and r^{t+1} is the value of the

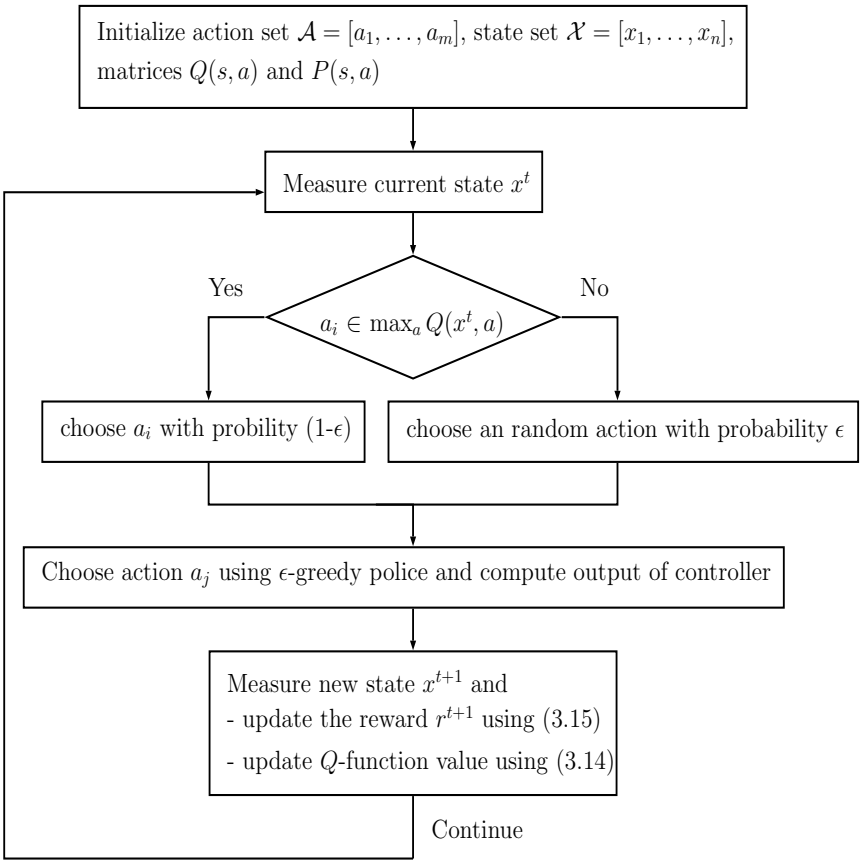

Figure 3.3: Flowchart of designed Q-learning based controller

reward function $R(x^{t+1}, a^t)$.

The reward function is normally decided on the basis of expert's knowledge. In this study, we have used a simple reward function given by

$$R(\hat{x^t}) = \begin{cases} \beta, & \text{if } |\hat{x^t}| \in S_0, \\ -\beta, & \text{else} \end{cases} \tag{3.15}$$

where, $\beta > 0$, and S_0 is the reference of $\hat{x^t}$ with specific error.

This reward function strongly rewards those situations in which the input of controller x^t, which is the error of the reference and actual currents, is approaching towards minimum, i.e., 0. Further, it penalizes those cases when the error tends to be increasing.

3.2.2 Dynamic fuzzy Q-learning based controller

The basic design principle of DFQL is discussed in the following:

The DFQL based controller essentially integrates the concept of Q-learning into the conventional fuzzy controller where the rule base is tuned online using Q-learning algorithm. Note that in conventional FIS, the rule base is developed by *priori* knowledge which makes the conclusion.

The flowchart of DFQL based controller is shown in Fig. 3.4, which proceeds as follows:

Fuzzification of inputs

The design of DFQL controller begins with fuzzification of the input state $\boldsymbol{x^t}$ $=[x_1,x_2,\ldots,x_N]$, where N is the number of the input variables of DFQL. The input x_i is usually divided into j_i number of partitions $X_i=[\chi_{i,1},\chi_{i,2},\ldots,\chi_{i,j_i}]$, where i=1,2,...,n, and j_i is the number of membership functions. X_i is a fuzzy set on the domain of x_i and $\mu_{\chi_{j_i}}$ is the membership degree of x_i.

There are many different types of membership functions. In this study, without loss of generality, we have taken triangular function as the fuzzy membership function.

Fuzzy rules of DFQL

For each fuzzy rule $\mathcal{R}_r$, there are m_r number of possible discrete actions $\mathcal{A}_r=[a_{r,1},a_{r,2},...,a_{r,m_r}]$, and each action is associated with a q-value. The rule base describing DFQL is as follows:

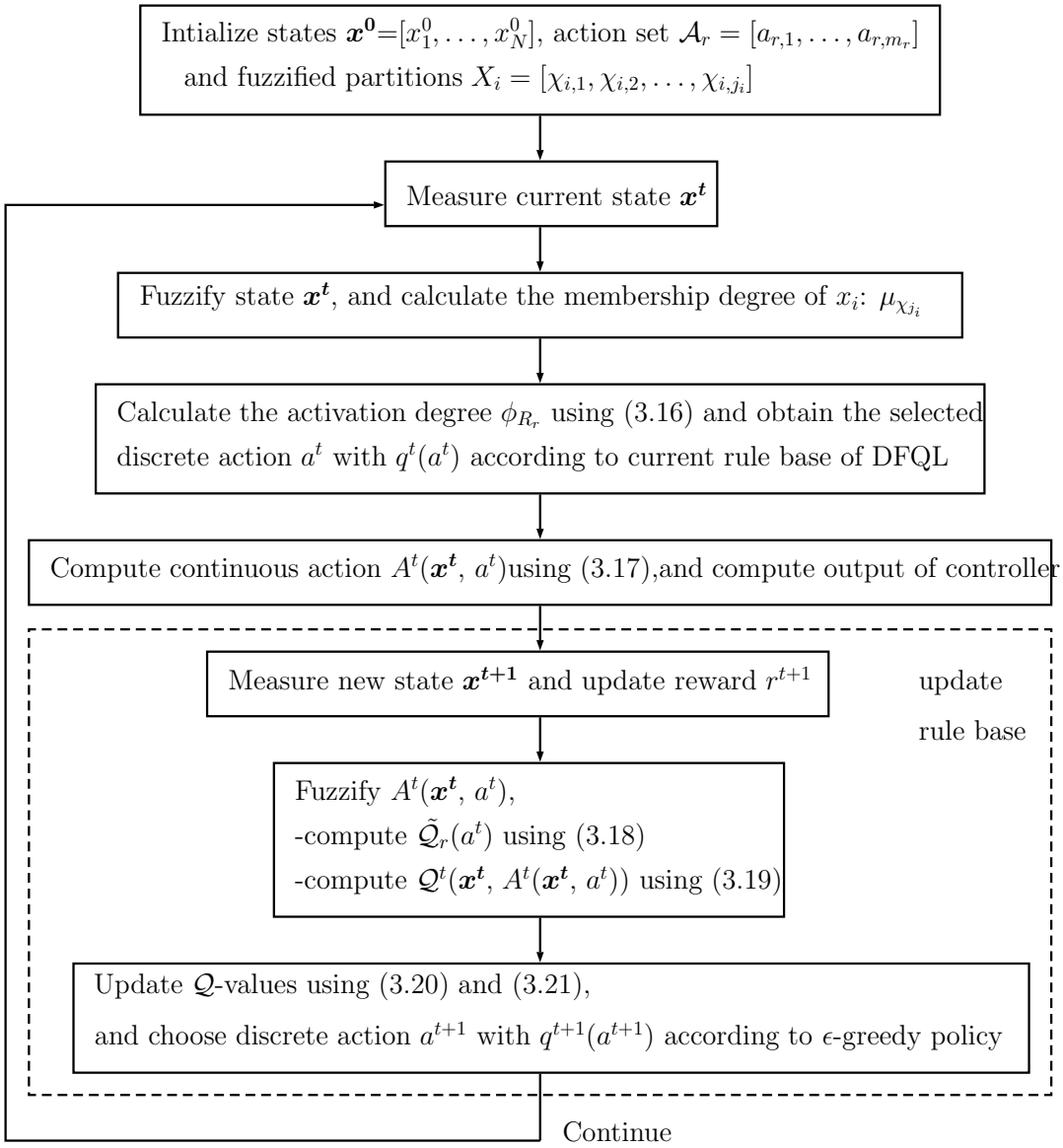

Figure 3.4: Flowchart of designed DFQL based controller

$\mathcal{R}_r$: **IF** x_1 is χ_{1,j_1} **AND** x_2 is χ_{2,j_2} ... **AND** x_N is χ_{N,j_N},
THEN y_r=$a_{r,1}$ with $q_{r,1}$
OR y_r=$a_{r,2}$ with $q_{j,2}$
...
OR y_r=a_{r,m_r} with q_{r,m_r}

At each time step, only one discrete action of each activated rule is selected, which is expressed by $\breve{a}_r(\boldsymbol{x^t})$. For example, if the action $a_{r,5}$ is selected, then $\breve{a}_r = a_{r,5}$.

The conclusion of rule $\mathcal{R}_r$ is a discrete action $a_{r,i}$ along with a corresponding action value $q_{r,i}$. In conventional FIS, the conclusion parts of fuzzy rules are both fixed and determined by the expert's knowledge. However, in the designed DFQL controller, the conclusion of fuzzy rule including the discrete action $a_{r,i}$ and its corresponding action value $q_{r,i}$ is dynamically determined by Q-learning algorithm. This allows the controller to keep learning through the interaction with the controlled system and update the fuzzy rules dynamically. The activation degree of the activated fuzzy rule R_r is defined as:

$$\phi_r = \prod_{j_i \in r} \mu_{\chi_{j_i}}(x_i) \tag{3.16}$$

Calculation of continuous action $A^t(\boldsymbol{x^t},a^t)$

After computation of activated degree of fuzzy rules, the selected discrete action $\breve{a}_r(\boldsymbol{x^t})$ of each activated rule R_r is determined. A continuous action $A^t(\boldsymbol{x^t},a^t)$ needs to be computed on the basis of these selected discrete actions of each activated rules. This continuous action $A_t(\boldsymbol{x^t},a^t)$ is actually performed by the controller at state $\boldsymbol{x^t}$ and is computed by a weighted sum of the selected discrete actions of all activated rules described as

$$A^t = \sum \phi_r \cdot \breve{a}_r(\boldsymbol{x^t}) \tag{3.17}$$

where, $\breve{a}_r(\boldsymbol{x^t})$ is the selected discrete action by rule R_r; ϕ_r is the activation degree of rule R_r.

Update fuzzy rule base of DFQL

To update the fuzzy rule base for time step t+1, a secondary FIS is introduced which associates the continuous action $A^t(\boldsymbol{x^t}, a^t)$ to a $\mathcal{Q}$-value.

For each activated fuzzy rule $\mathcal{R}_r$, the continuous action $A^t(\boldsymbol{x^t}, a^t)$, obtained in last step, is fuzzified by fuzzy set $\mathcal{A}_r$=$[\mathcal{A}_{r,1}, \mathcal{A}_{r,2}, \cdots, \mathcal{A}_{r,m_r}]$, which is centered in each discrete action $a_{r,i}$ of rule $\mathcal{R}_r$. Let $\mu_{\mathcal{A}_{r,i}(\boldsymbol{x^t})}$ stand for the membership degree of $A^t(\boldsymbol{x^t}, a^t)$ in rule $\mathcal{R}_r$. The fuzzy rule base of the secondary FIS is described as follows:

$$\tilde{\mathcal{R}}_{r,1}: \quad \textbf{IF } a \text{ is } \mathcal{A}_{r,1} \textbf{ THEN } \mathcal{Q}=q_{r,1}$$

$$\tilde{\mathcal{R}}_{r,2}: \quad \textbf{IF } a \text{ is } \mathcal{A}_{r,2} \textbf{ THEN } \mathcal{Q}=q_{r,2}$$

$$\cdots$$

$$\tilde{\mathcal{R}}_{r,m_r}: \quad \textbf{IF } a \text{ is } \mathcal{A}_{r,m_r} \textbf{ THEN } \mathcal{Q}=q_{r,m_r}$$

where, m_r is the number of the discrete action set associated to the rule R_r.

The corresponding $\mathcal{Q}$-value of action a^t in activated rule $\mathcal{R}_r$ is $\tilde{\mathcal{Q}}_r(a^t)$ and it is expressed by

$$\tilde{\mathcal{Q}}_r(a^t) = \sum_{i=1}^{m_r} \mu_{\mathcal{A}_{r,i}}(a^t) q_{r,i}^t. \tag{3.18}$$

Thus, the final $\mathcal{Q}$-value of the continuous action $A^t(\boldsymbol{x^t}, a^t)$ is computed as:

$$\begin{aligned} \mathcal{Q}^t(\boldsymbol{x^t}, a^t) &= \sum_{r=1}^{n_R} \phi_r(\boldsymbol{x^t}) \tilde{\mathcal{Q}}_r(a^t) \\ &= \sum_{r=1}^{n_R} \sum_{i=1}^{m_r} \phi_r(\boldsymbol{x^t}) \mu_{\mathcal{A}_{r,i}}(a^t) q_{r,i}^t, \end{aligned} \tag{3.19}$$

where, n_R is the number of activated fuzzy rules of DFQL.

After the computation of the action - value $\mathcal{Q}^t(\boldsymbol{x^t}, a^t)$ of continuous action $A^t(\boldsymbol{x^t}, \boldsymbol{a^t})$, the next step is to update the $\mathcal{Q}$-value function following Q-learning algorithm.

It is demonstrated that in the problems characterized by continuous state and action spaces, the update of $\mathcal{Q}$-value could be maximum effect achievable along the gradient direction [173]. Thus, it is shown as

$$q_{r,i}^t = q_{r,i}^t - \alpha \varepsilon_{\mathfrak{Q}}^t \cdot \bigtriangledown_{q_{r,i}^t} \mathcal{Q}^t(\boldsymbol{x^t}, A^t(\boldsymbol{x^t})), \tag{3.20}$$

$$\varepsilon_{\mathcal{Q}}^t = r_{\boldsymbol{x^t}, A^t(\boldsymbol{x^t})}^t + \gamma \max_a \mathcal{Q}(\boldsymbol{x^{t+1}}, a) - \mathcal{Q}^t(\boldsymbol{x^t}, A^t(\boldsymbol{x^t})), \tag{3.21}$$

where,

$\nabla_{q^t_{r,i}} \mathcal{Q}^t(\boldsymbol{x^t}, a^t)$: the partial derivative of $\mathcal{Q}^t(\boldsymbol{x^t}, a^t)$ with respect to $q^t_{r,i}$;

α : learning rate;

γ : discounted rate;

$r^t(\boldsymbol{x^t}, A^t(\boldsymbol{x^t}))$: the value of reward function which is the same as that of Q-learning in (3.15).

Note that the maximum value of $\mathcal{Q}(\boldsymbol{x^{t+1}}, a^t)$ is the greatest $\mathcal{Q}$-value in the state $\boldsymbol{x^{t+1}}$, and it lies in the correspondence of one of the discrete action sets $\mathcal{A}_r$ of the activated rule $\mathcal{R}_r$:

$$\begin{aligned}\max_a \mathcal{Q}(\boldsymbol{x^{t+1}}, a) &= \max_{a \in \sum_{i=1}^{m_r} A_i} \sum_{r=1}^{n_R} \sum_{i=1}^{m_r} \phi_r(\boldsymbol{x^{t+1}}) \mu_{\mathcal{A}_{r,i}(a)} q^t_{r,i} \\ &= \sum_{r=1}^{n_R} \phi_r(\boldsymbol{x^{t+1}}) \max_i q^t_{r,i}.\end{aligned} \tag{3.22}$$

After updating the $\mathcal{Q}$-value, the discrete action a^{t+1} of each activated rule is selected according to ϵ-greedy policy.

3.2.3 Bang-bang controller

The inputs to the BBC in this study are rotor angle θ and speed ω of generator in COI frame. The discrete control strategies of BBC are shown in Fig. 3.5. The switching policies of BBC are described as:

$$X_c = \begin{cases} X_{cmax}, & \text{when } \omega > 0 \text{ and } \theta > \theta_{ref} \\ X_{cmin}, & \text{when } \omega < 0 \text{ and } \theta < \theta_{ref} \\ X_{c0}, & \text{else} \end{cases} \tag{3.23}$$

where, X_c is the series compensation value; X_{cmax}, X_{cmin} and X_{c0} are the maximum value, minimum value and nominal value of X_c, respectively; and θ_{ref} is the reference angle of generator in post-fault system which is taken as the stable equilibrium point (SEP) θ^s in this study. Note that the performance of BBC is highly dependent on the selected thresholds, *i.e.*, X_{cmin}, X_{cmax}.

Due to non-linear nature of the system, the selection of threshold (X_{cmin}, X_{cmax}) of BBC is approached as an optimization problem based on particle

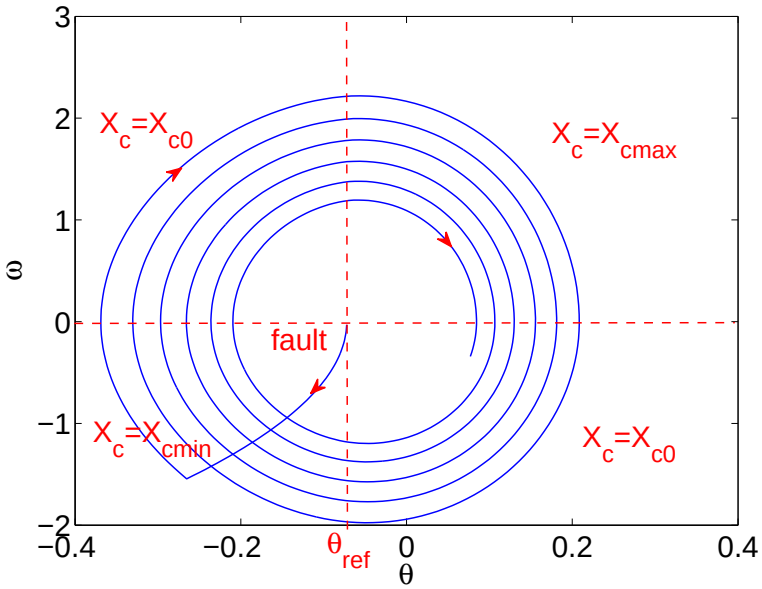

Figure 3.5: Control strategies of BBC

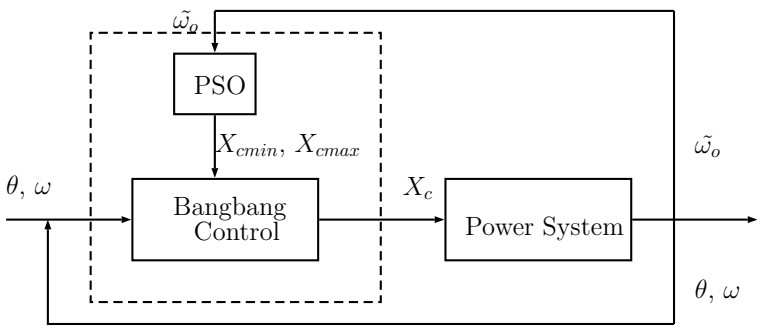

Figure 3.6: PSO Based Bang-Bang Controller

swarms with the objective to minimize the *fitness function*:

$$min\ f = C * \sum_{k=1}^{n} \tilde{\omega_o}(k) \tag{3.24}$$

where, C is a constant; $\tilde{\omega_o}=\frac{d\delta_o}{dt}$; δ_o is expressed in (3.11), and n is the number of generators.

The schematic structure of designed PSO based bang-bang control is shown in Fig. 3.6.

The PSO relies on social co-operation among group of mass-less objects referred to as '*particle*'. Each particle has two memory attributes: *cognitive* and *social*. In each iteration, the movement or '*velocity*' of a particle is determined on the basis of its current position and the memory attributes. Throughout the search process, guided by the velocity, each particle visits several solutions on

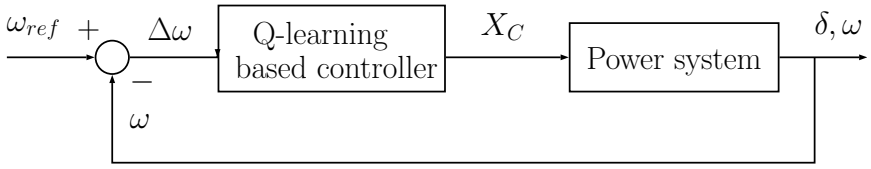

Figure 3.7: Framework of series compensator control using Q-learning based controller

the search landscape. In canonical PSO [174, 175], at any given iteration, d^{th} dimension of the ith particle is updated on the basis of following velocity and position update rule:

$$v_{i,d} = (\varpi \times v_{id}) + \phi_1(\hat{x}_{i,d} - x_{i,d}) + \phi_2(\acute{x}_d - x_{i,d}) \tag{3.25}$$

$$x_{i,d} = x_{i,d} + v_{i,d} \tag{3.26}$$

where, $\hat{x}_i$ is the personal best position of the ith particle, $\acute{x}$ is the best position of the swarm, ϖ is the *inertia weight* and $\phi_1, \phi_2 \in [0, 2]$ are *uniform random numbers*. Following the guidelines of [175], ϖ is set to decrease with iteration form 0.9 to 0.4.

3.3 Simulation Results

The simulation is conducted in MATLAB (R2017b) environment, and the solver used in the program is *ode*45. The Q-learning and DFQL based controllers are designed first for a single machine infinite bus system and later for a multi-machine system consisting of 3-number of synchronous generators.

The schematic of Q-learning and DFQL based controllers are shown in Fig. 3.7 and Fig. 3.8, respectively. Note that the input to the Q-learning based controller is the error in the rotor speed; and that of the DFQL based controller is the error in the rotor angle. Although the inputs to both controllers can either be rotor speed error or rotor angle error, it will be shown later that the performance of Q-learning controller is better with rotor speed input and DFQL based controller performs better with rotor angle input.

3.3.1 Results for SMIB

The SMIB system considered in this chapter is shown in Fig. 3.1. The initial value of the power angle δ_0 is calculated to be 30° for $P_m = 1$, $P_e^{max} = 2$ and

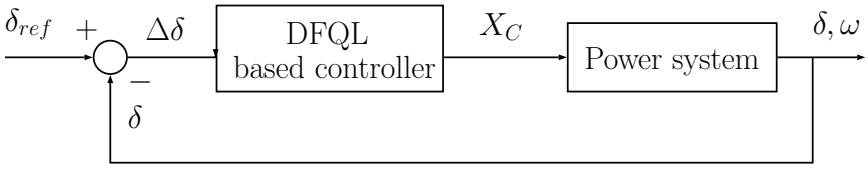

Figure 3.8: Framework of series compensator control using DFQL based controller

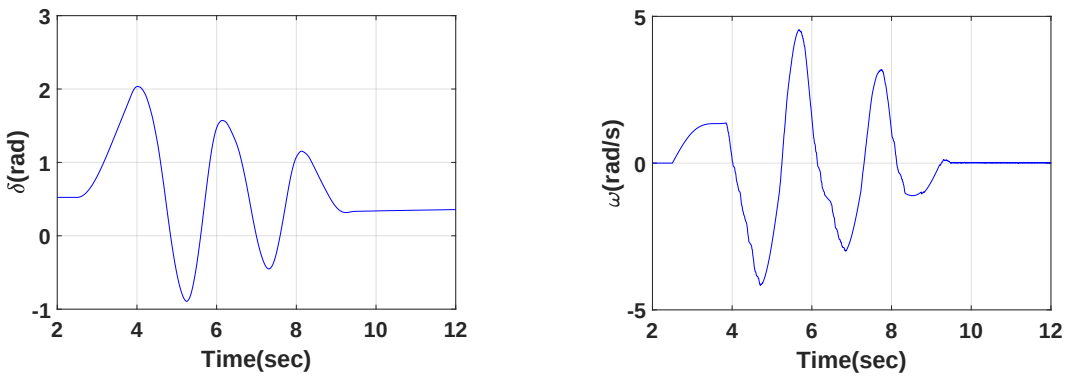

(a) Variations of rotor angle of SMIB system with Q-learning based controller

(b) Variations of rotor speed of SMIB system with Q-learning based controller

Figure 3.9: Responses of Q-learning based controller in SMIB

$M = 0.2$. A fault is simulated in the transmission line by changing the maximum value of the electric output P_e^{max} from 2 to 1. The fault is applied at $t = 2.5$ sec and is assumed to be cleared at $t = 3.85$ sec.

Results of Q-learning based controller

The input of Q-learning controller is $\Delta\omega = \omega_{ref} - \omega$, and the output is the value of series compensator X_c. The variations of rotor angle and rotor speed are shown in Fig. 3.9a and Fig. 3.9b. It can be observed that the Q-learning based controller could damp out the oscillations after 9 sec.

Results of DFQL based controller

The inputs of the DFQL controller are $\Delta\delta = \delta_{ref} - \delta$ and the deviation of $\Delta\delta$, where δ_{ref} is δ_s, the SEP of the synchronous machine in post-fault SMIB. Both of the error and its deviation are divided into 7 partitions, $X_1 = [\chi_{1,1}, \chi_{1,2}, \ldots, \chi_{1,7}]$ and $X_2 = [\chi_{2,1}, \chi_{2,2}, \ldots, \chi_{2,7}]$. The output of DFQL controller is used to modify the value of the series compensator.

The variations of rotor angle and rotor speed are shown in Fig. 3.10a and

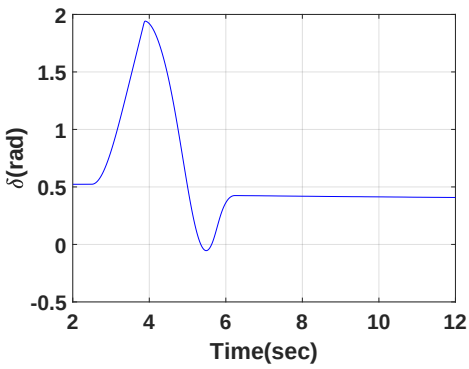

(a) Variation of rotor angle of SMIB system with DFQL based controller

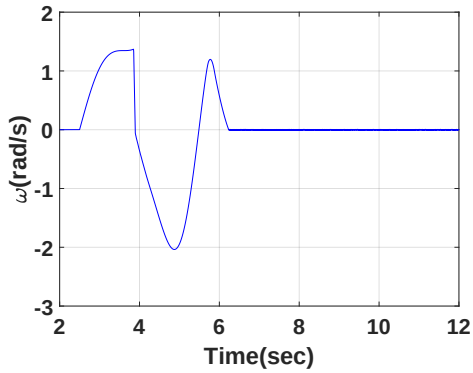

(b) Variation of rotor speed of SMIB system with DFQL based controller

Figure 3.10: Responses of DFQL based controller in SMIB

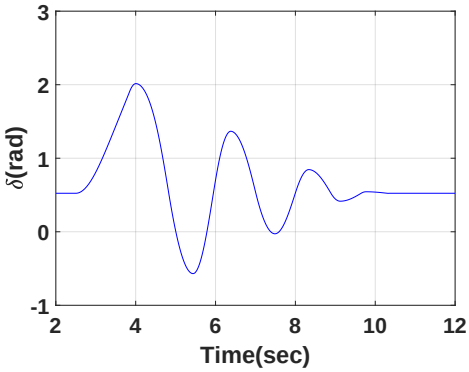

(a) Variations of rotor angle of SMIB system with BBC

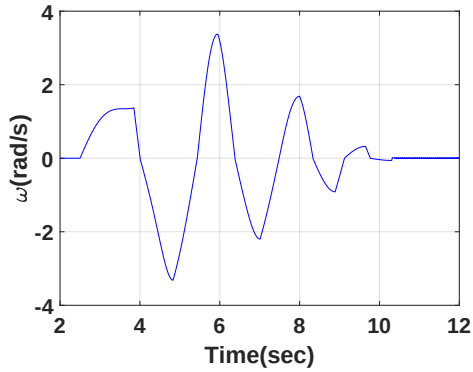

(b) Variations of rotor speed of SMIB system with BBC

Figure 3.11: Responses of BBC in SMIB

Fig. 3.10b. From the figure, it is observed that the DFQL based controller could damp out the transient oscillation around 6 sec, which is much faster than BBC and Q-learning based controller.

Results of bang-bang controller

As mentioned previously, the inputs of BBC is the rotor angle δ and rotor speed ω. The variations of rotor angle and rotor speed of the SMIB system using BBC are shown in Fig. 3.11a and Fig. 3.11b. It can be observed that BBC could make the system stable in 10 sec, which is slower than that of DFQL based controller.

3.3.2 Results for a multi-machine system

After designing the reinforcement controllers for single machine system, their performance in improving transient stability for a 3-machine system are investigated. The 3-machine system, considered in this study, is shown in Fig. 3.12. The initial conditions are taken as: $E = [1.056, 1.1076, 1.042]$, $P = [0.716, 1.63, 0.85]$, $M = [0.125, 0.034, 0.016]$, $D = [0.1 * M(1), 0.2 * M(2), 0.3 * M(3)]$; where $E(i)$, $P(i)$, $M(i)$ and $D(i)$ represent respectively the voltage, electrical power, inertial constant and damping coefficient of i_{th} generator, $i = 1, 2, 3$.

In this chapter, a three-phase short-circuit fault is applied on bus 4, which implies that the voltage at bus 4 is 0. The fault is assumed to be cleared by removing line 4 - 6 after 0.25 sec. Two different locations of series compensator controlled by both 4 different controllers i.e Q-learning based controller, DFQL based controller, BBC and PSO based BBC are considered: . The compensator is installed either in line 4 - 5 or in line 5 - 7.

Results of Q-learning based controller

The input of designed Q-learning with series compensator installed in line 4 - 5 is $\Delta\omega_1$; and for the other case with series compensator installed in line 5 - 7, the input of Q-learning is $\Delta\omega_2$.

The dynamics of rotor angles with series compensation in line 4 - 5 and line 5 - 7 are shown in Fig. 3.13a and Fig. 3.13b, respectively. From the figures, it is observed that the Q-learning based controller could provide correct series compensation and make the system stable irrespective of the lines selected for compensation. However, it takes longer time to stabilise compared to other controller (to be shown below).

Results of DFQL controller

The inputs of the designed DFQL based controller vary with the installation location of the series compensator. When the series compensator is installed in line 4 - 5, the inputs are $\Delta\theta = \theta_{ref1}$ - θ_1 and deviation of this error, where θ_{ref1} is the SEP of machine 1 in post-fault system. While the series compensator is installed in line 5 - 7, the inputs are $\Delta\theta = \theta_{ref2}$ - θ_2 and deviation of this error, where θ_{ref2} is the SEP of machine 2 in post-fault system.

The dynamics of rotor angles with series compensation in line 4 - 5 and line 5 - 7 are shown in Fig. 3.14a and Fig. 3.14b, respectively. It can be seen that the

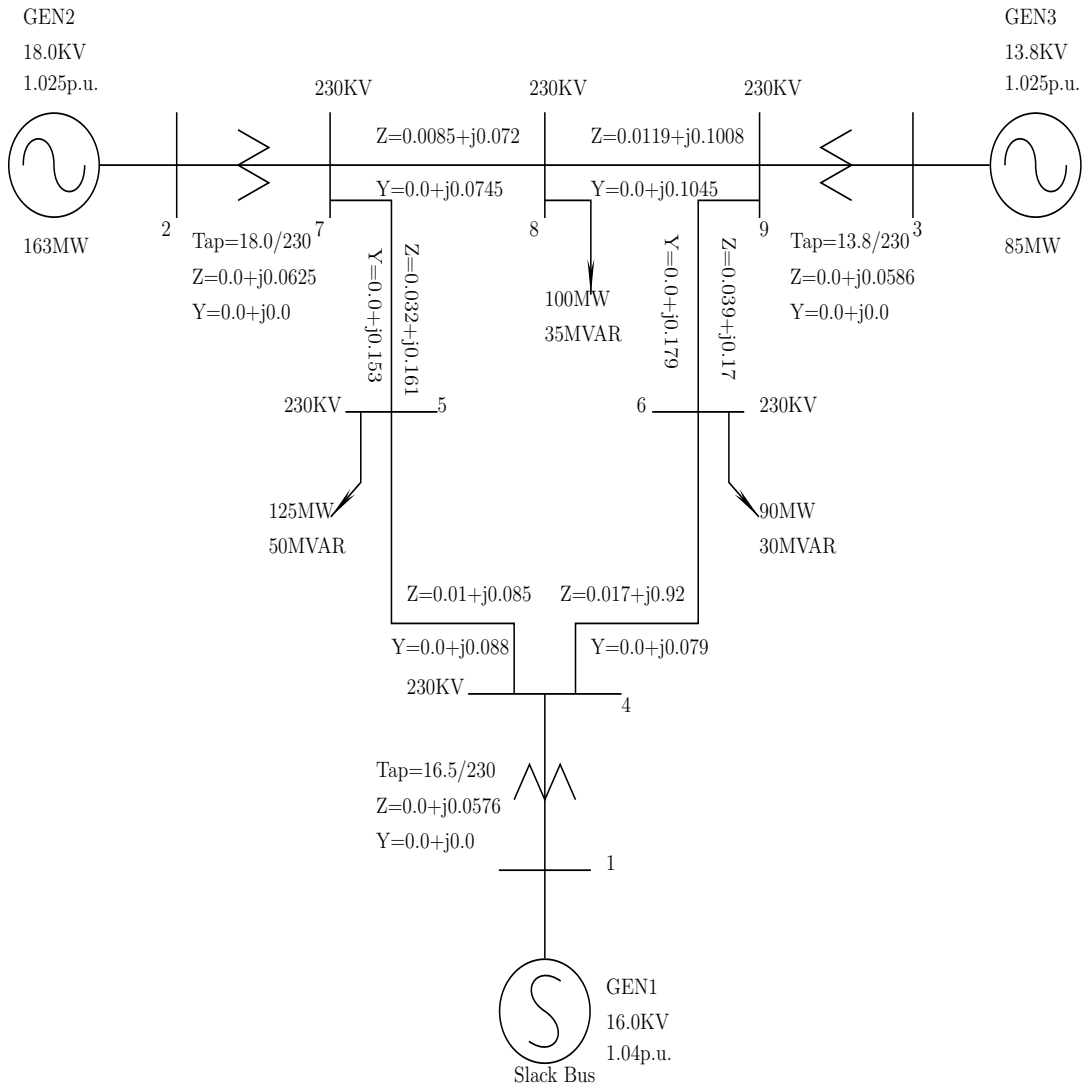

Figure 3.12: A three-machine nine-bus synchronous power system

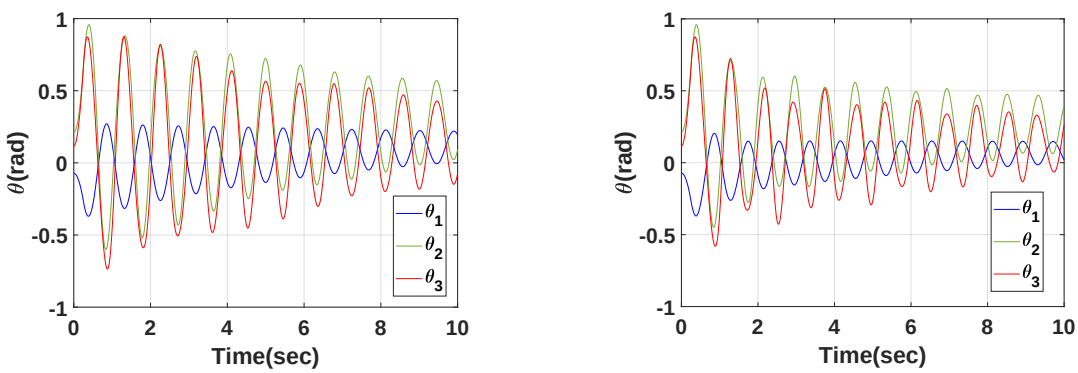

(a) Variations of rotor angles with series compensator installed in line 4 - 5

(b) Variations of rotor angles with series compensator installed in line 5 - 7

Figure 3.13: Responses of Q-learning based controllers in 3-machine power system

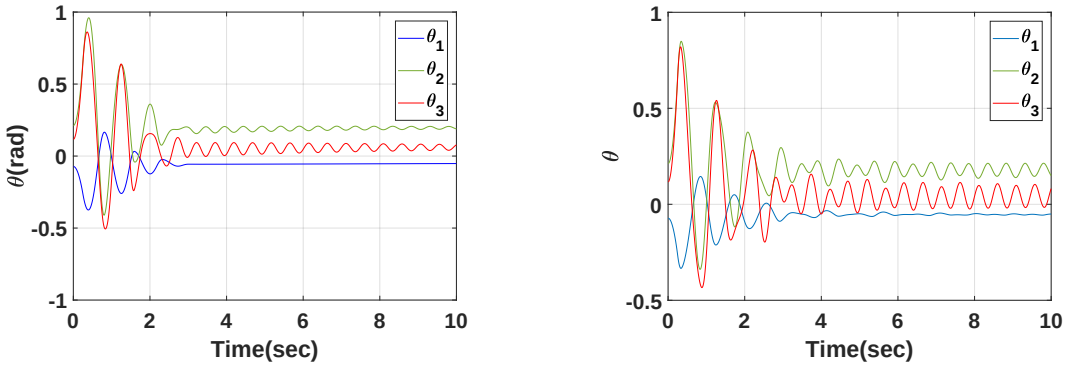

(a) Variations of rotor angles with series compensator installed in line 4 - 5

(b) Variations of rotor angleswith series compensator installed in line 5 - 7

Figure 3.14: Responses of DFQL based controller in 3-machine power system

controller could successfully damp out the oscillations with series compensation installed in both lines.

Results of BBC

The inputs of the designed BBC and PSO based BBC are θ_1 and ω_1 with series compensator in line 4 - 5; and θ_2 and ω_2 with series compensator in line 5 - 7, where θ_1, ω_1, θ_2 and ω_2 represent the rotor angle and speed of machine 1 and 2 respectively. The value of series compensator X_c is discretely changing between $(X_{c_{min}}, X_{c_{max}})$. Therefore, the switching policies of designed controller are:

$$X_c = \begin{cases} X_{cmax}, & \text{when } \omega_1 > 0 \text{ and } \theta_1 > \theta_1^s \\ X_{cmin}, & \text{when } \omega_1 < 0 \text{ and } \theta_1 < \theta_1^s \\ X_{c0}, & \text{else} \end{cases} \tag{3.27}$$

where, X_c is the series compensation value; X_{cmax}, X_{cmin} and X_{c0} are the maximum value, minimum value and nominal value of X_c, respectively; and θ^s is the SEP of generator in post-fault system.

Series compensation in both line 4 - 5 and line 5 - 7 are simulated using both BBC. Fig. 3.15a and Fig. 3.15b show the dynamics of rotor angles with series compensation.

In PSO based BBC, each particle represents the thresholds of the bang-bang controller, *e.g.*, $x_i = \{X^i_{cmin}, X^i_{cmax}\}$. Due to stochastic nature of the PSO, 10 independent optimization runs were performed. Each run was set to terminate after 2000 Function Evaluation (FEs). Fig. 3.16 shows the convergence behavior

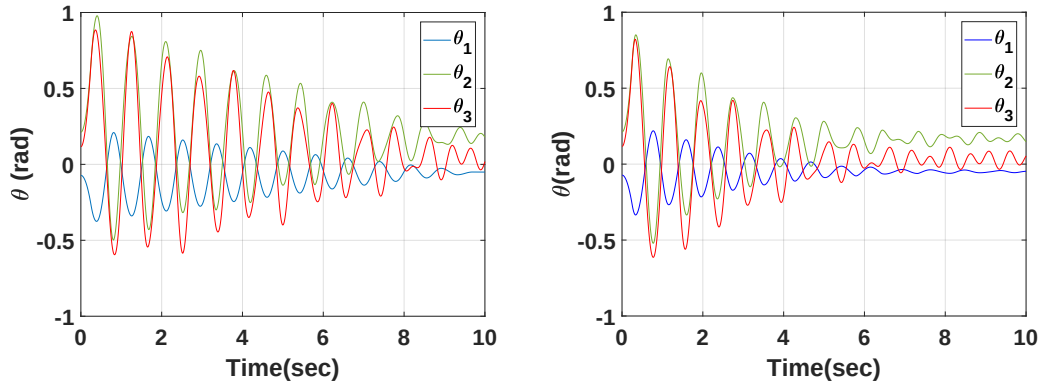

(a) Variations of rotor angles with series compensator installed in line 4 - 5

(b) Variations of rotor angles with series compensator installed in line 5 - 7

Figure 3.15: Responses of BBC in 3-machine power system

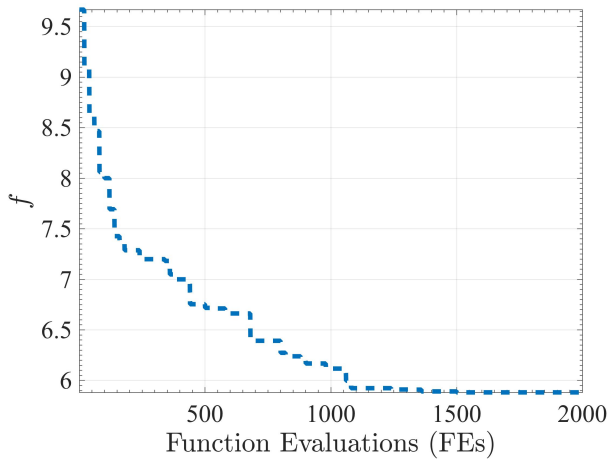

Figure 3.16: Convergence characteristic of PSO

of PSO averaged over 10 runs. The solution with the minimum fitness out of 10 runs is selected for the further analysis. The rotor speed and rotor angles with series compensator controlled by PSO based BBC are shown in Fig. 3.17a and Fig. 3.17b.

From the figures, we can see that the system controlled by BBC and PSO based BBC is transiently stable. Both controllers could damp out the rotor angle oscillations, but slower than that of DFQL based controller.

3.4 Conclusion

Q-learning and DFQL based controllers have been designed and implemented for improving the transient stability of a single machine infinite bus and multi-

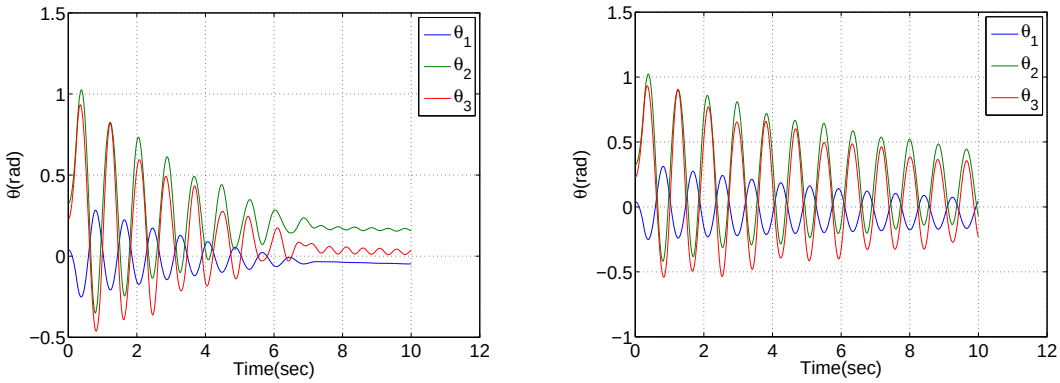

(a) Variations of rotor angles with series compensator installed in line 4 - 5

(b) Variations of rotor angles with series compensator installed in line 5 - 7

Figure 3.17: Response of PSO based BBC in 3-machine power system

machine synchronous generation power system. The proposed Q-learning based controller exploits the learning feature of the Q-learning and DFQL based controller, and even integrates it into the classical fuzzy controller to make the overall controller adaptive. These two designed controllers could both learn the actions by trying to yield the most reward. The difference between them is that the DFQL controllers give continuous control actions, while the normal Q-learning based controllers can only deal with the discrete ones. The performance of the controllers are compared with that of a bang-bang controller and particle swarm optimization based bang-bang controller. It has been shown DFQL based controller is superior to other controllers. The proposed Q-learning and DFQL based controllers will be designed for wind power and hybrid power in the following chapters.

Chapter 4

Q-learning and Dynamic Fuzzy Q-learning Based Controllers for Rotor Side Control of Wind Energy Conversion System

Wind power, which is usually generated by wind turbines coupled with different kinds of generators, has been widely implemented in industry. In modern WECS, the wind generators are often divided into several categories: SCIG, WRIG and DFIG. As DFIGs are usually cheaper with the same capacity and have higher energy transfer efficiency, DFIG based wind turbine has attracted more and more attention in wind energy generation systems [39, 40].

During the past few years, many research results on modelling and control of renewable energy systems including the DFIG have been reported [40, 63–65]. Detailed modelling of both mechanical and electrical dynamics are presented in [62, 66]. In the DFIG control scheme, the controllers could either be applied to RSC or to GSC. In this study, only RSC control, which focuses on the active and reactive power from the rotor side is considered. Many different types of controllers have been designed to improve the performance of the rotor side converter, for example, sliding-mode control [64], and fuzzy logic control [176]. In [177], modelling of DFIG using MATLAB/SIMULINK was introduced first and vector control of the rotor side of DFIG was investigated effectively in a multi-machine power system with penetration of wind energy. Conventional PI controllers and adaptive self-tuning controllers were designed and compared in [178], which were used for the current loop to provide the dq-components

of the rotor voltage through rotor side converter. In [179], PID controller was designed to control the active and reactive power from the rotor side converter and tested on a power system considering wind speed variation, local load change and so on.

Among these existing controllers, there are still several drawbacks. First, the tuning process of PID parameters could be rather tough. Furthermore, in traditional structure of RSC control in DFIG, at least four controllers have to be designed. However, by using the concept of Q-learning, it is possible to effectively control the rotor side converter using only two controllers [179]. Further, Q-learning based controller does not require a precise mathematical model of the system.

However, as Q-learning algorithm can only search within discrete action space, DFQL, method which is an extension of both fuzzy logic control and Q-learning, could deal with continuous action space without the need of an accurate mathematical model. Therefore, DFQL based controllers have also been designed for the active and reactive power in RSC. In this DFQL control scheme, the traditional fuzzy rule base which determines the output of the controller has been changed using Q-learning [180].

This chapter investigates the performance of two reinforcement learning controllers for RSC of DFIG used in WECS. The design of these controllers are based on the concept of Q-learning and DFQL. The Q-learning based controller essentially provides discrete control actions unlike the DFQL based controller which generates continuous control actions. The effectiveness of these controllers is studied considering a test wind energy conversion system consisting of 20 wind turbines which are driven by 20 DFIGs. The results of the simulation illustrate that the DFQL based controller performs better compared to Q-learning controller.

4.1 Aggregated modelling of DFIG based WECS

The modern WECS can use several types of wind generators such as SCIG, DFIG, WSIG. However, among all these different kinds of WECS, DFIG based wind farms are the most popular, as they offer significant advantages over other types of wind generators which include requirement of lower capacity of power converters (25%−30% of the nominated power of the machines); higher efficiency and so on. Therefore this study considers DFIG based WECS.

In this study, the wind farm is represented by an aggregated DFIG driven by an aggregated wind turbine.

4.1.1 Wind Turbine Modelling

The mechanical power extracted from the wind is expressed as [40]:

$$P_{m,agg} = 0.5\rho\pi R^2 C_P(\lambda, \beta)v^3/P_{rated}, \tag{4.1}$$

where,

$$C_p(\lambda, \beta) = c_1(\frac{c_2}{\lambda_i} - c_3\beta - c_4)\exp^{(} - \frac{c_5}{\lambda_i}) + c_6\lambda. \tag{4.2}$$

P_{rated} represents the rated power (= 5 MW in this study) of aggregated wind turbine; v is the wind speed (= 15 m/s in this study). The other parameters considered in simulation are c_1=0.5176; c_2=116; c_3=0.4; c_4=5; c_5=21; c_6=0.0068; R=58.6m; ρ=1.225kg/m^3 [181].

4.1.2 Shaft System Modelling

The lumped-mass model of the shaft system is given by [182] :

$$\frac{d\omega_{m,agg}}{dt} = \frac{1}{2H_{m,agg}} * (T_{m,agg} - T_{e,agg} - D_{m,agg} * \omega_{m,agg}), \tag{4.3}$$

$$H_{m,agg} = (H_t + H_g) * N, \tag{4.4}$$

where N is the total number of DFIGs; H_t and H_g are the inertia constant of each individual wind turbine and DFIG respectively; $H_{m,agg}$ and $D_{m,agg}$ are the lumped inertia constant and damping coefficient of the aggregated model respectively; $\omega_{m,agg}$ is the rotational speed of the system. The aggregated mechanical torque $T_{m,agg}$ is given by

$$T_{m,agg} = P_{m,agg}/\omega_{m,agg}. \tag{4.5}$$

The aggregated electrical torque $T_{e,agg}$ is computed from (4.10). In this study, we have considered N=20; H_t=4; H_g=0.1$*H_t$ and $\omega_{m,agg}$ equals to the generator rotor speed ω_r [181].

4.1.3 Aggregated DFIG Modelling

The dynamics of DFIG in synchronous reference dq-frame [183] is given by

$$\frac{dI_{qs}}{dt} = \frac{\omega_b}{L'_s}(-R_1 I_{qs} + \omega_s L'_s I_{ds} + \frac{\omega_r}{\omega_s} E'_{qs} - \frac{1}{T_r \omega_s} E'_{ds} - v_{qs} + K_{mrr} v_{qr}), \tag{4.6}$$

$$\frac{dI_{ds}}{dt} = \frac{\omega_b}{L'_s}(-\omega_s L'_s I_{qs} - R_1 I_{ds} + \frac{1}{T_r \omega_s} E'_{qs} + \frac{\omega_r}{\omega_s} E'_{ds} - v_{ds} + K_{mrr} v_{dr}), \tag{4.7}$$

$$\frac{dE'_{qs}}{dt} = \omega_b \omega_s [R_2 I_{ds} - \frac{E'_{qs}}{T_r \omega_s} + (1 - \frac{\omega_r}{\omega_s}) E'_{ds} - K_{mrr} v_{dr}], \tag{4.8}$$

$$\frac{dE'_{ds}}{dt} = \omega_b \omega_s [-R_2 I_{qs} - (1 - \frac{\omega_r}{\omega_s}) E'_{qs} - \frac{E'_{ds}}{T_r \omega_s} + +K_{mrr} v_{qr}], \tag{4.9}$$

where, ω_b is the electrical base speed; ω_s is the synchronous speed; ω_r is the rotor speed; I_{qs} and I_{ds} are dq-components of stator currents; E'_{qs} and E'_{ds} are dq-components of internal stator voltage.

The electrical torque and reactive power generated by the aggregated DFIGs are calculated as:

$$T_{e,agg} = [(\frac{E'_{qs}}{\omega_s}) I_{qs} + (\frac{E'_{ds}}{\omega_s}) I_{ds}] * N, \tag{4.10}$$

$$Q_{s,agg} = [V_{qs} I_{ds} - V_{ds} I_{qs}] * N. \tag{4.11}$$

The values of other parameters of this model considered here [181] are L_m=4; L_{ss}= 1.01; L_{rr}=1.005; R_s=0.005; R_r=1.1 $*$ R_s; K_{mrr}=$\frac{L_m}{L_{rr}}$; L'_s=$L_{ss} - L_m K_{mrr}$; R_2=$K^2_{mrr} R_r$; R_1=$R_s + R_2$; T_r=L_{rr}/R_r.

This model assumes that the stator transients are negligible. Further, it is assumed that the reactive power Q_r=0, and the excessive active power P_r of the rotor passes through the grid side converter to the power grid . This implies that $P_{tot} = P_s + P_r$ and $Q_{tot} = Q_s$.

4.2 Control of Rotor Side Converter

In this chapter, we focus on the applications of two RL controllers where the objective is to investigate the effectiveness of these controllers for controlling

the RSC in WECS. The performance of both Q-learning and DFQL based controllers are compared with classical PID controller and $\Delta\Sigma$ based PID controller. The design procedure of Q-learning and DFQL controller has been discussed in Chapter 3. The design principles of a classical PID controller are well established in literature [179]. In this study, a new type of PID controller based on $\Delta\Sigma$ modulation has been designed and it is applied to control the rotor side converter. Since the design of this controller are relatively new, it is appropriate to discuss briefly the concept of $\Delta\Sigma$ modulator and $\Delta\Sigma$ based PID controller. This is discussed in the following.

4.2.1 Technique of $\Delta\Sigma$ Based Control System

Most of the current control systems use micro controllers and digital signal processors for implementing digital controllers. Typically, these micro controllers and digital signal processors are optimized for a fixed width binary words, for example, $8-$bit, $16-$bit or $32-$bit [184]. There are some critical factors that determine the choice of word size namely the hardware cost, the control algorithm that is being used, the signal-to-noise ratio (SNR) and most importantly dynamic range that is required. Although the implementation of controllers using these processors is not difficult for single-input-single-output systems, there are some disadvantages of these micro controllers and digital signal processors. For example, these multi-bit implementations require high information rate between control subsystems despite their success in implementation. Hence, it often becomes computationally extensive and requires large routing area and more valuable silicon area on an Field Programmable Gate Arrays (FPGAs) [185].

Recently, an alternative technique has been proposed based on bit-stream ($\Delta\Sigma$ modulators) for selected control applications, primarily due to many advantages [185, 186]. Amongst the many benefits, this method offers, the key benefit is that each signal is represented by a single bit which eases place and route operations for the FPGA systems reducing input/output use to one pin for a particular signal. It will make isolation of systems using optocouplers easy and is a significant advantage.

Bit-stream based control systems have been investigated in various applications, such as control of induction motor [187], DC motor [188], servo control [189] and so on. The main objective of this study is to design bit-stream-based $\Delta\Sigma$ modulator for RSC in DFIG based WECS, and to compare its performance with Q-learning based and DFQL based controllers.

4.2.2 $\Delta\Sigma$ Based PID Controller

The design principle of $\Delta\Sigma$-based PID controller is briefly described in the following section. $\Delta\Sigma$ modulator is one of the key components of the $\Delta\Sigma$-based control system. It consists of two main components, a $\Delta\Sigma$ encoder ($\mathcal{E}_{\Delta\Sigma}$) and a $\Delta\Sigma$ decoder ($\mathcal{D}_{\Delta\Sigma}$). The schematic of $\mathcal{E}_{\Delta\Sigma}$ and $\mathcal{D}_{\Delta\Sigma}$ is shown in Fig. 4.1. The encoder and the decoder are connected through a communication channel. As represented in Fig. 4.1, the thick solid lines show the weighted signal and the dotted line shows the bit-stream (BS) signal. The input signal $\hat{e}$ is encoded into a BS signal $\hat{\delta}$ by $\mathcal{E}_{\Delta\Sigma}$ which consists of one integrator, one two-level quantizer and a multiplexer. The decoder $\mathcal{D}_{\Delta\Sigma}$, which consists of single multiplexer, reconstructs the estimated input of $\mathcal{E}_{\Delta\Sigma}$. The conversion of the input of $\mathcal{E}_{\Delta\Sigma}$ is done through error feedback.

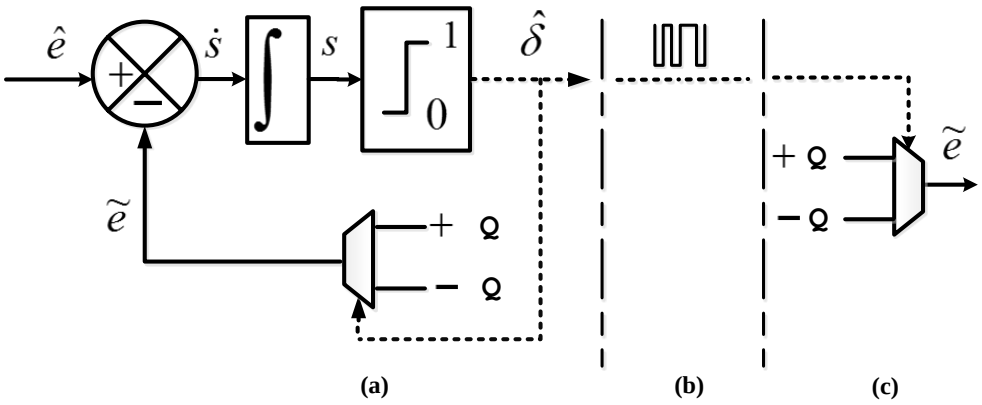

Figure 4.1: $\Delta\Sigma$-based encoder/decoder. (a). Encoder (b). Communication Channel (c). Decoder

Note that, the conventional linear controller design technique is based on an approximate linear model of a system. This linear model can be obtained by perturbing the system dynamics around a desired operating point. Therefore, the linear controller behaves optimally around the linearisation point. In the following, we, therefore, briefly describe the feedback control design of $\Delta\Sigma$ based control design under the assumption that the system is linear.

Consider a linear time-invariant (LTI) plant described by,

$$\begin{aligned} \dot{x} &= Ax + Bu \\ y &= Cx \end{aligned} \tag{4.12}$$

where $x \in \mathbb{R}^n$, $u \in \mathbb{R}^m$ and $y \in \mathbb{R}^p$ denote the states of the linearised plant, the inputs and the output of the linearised plant, respectively. Here, an analogue controller is used to stabilize the system described in (4.12) asymptotically. The dynamics of the analogue controller is described as:

$$\begin{aligned} \dot{x}_c &= A_c x_c + B_c e \\ u &= C_c x_c + D_c e \end{aligned} \tag{4.13}$$

where $x_c \in \mathbb{R}^v$ and e denote respectively the states of the controller and the error signals. Without loss of generality,it is assumed that the reference signal to be zero ($r = 0$); hence $e = -y$. By combining (4.13) with (4.12) gives the dynamics of the closed loop system as:

$$\dot{x}_{cl} = A_{cl} x_{cl} \tag{4.14}$$

where

$$x_{\text{cl}} = \begin{bmatrix} x \\ x_c \end{bmatrix}, \; A_{cl} = \begin{bmatrix} A - BD_cC & BC_c \\ -B_cC & A_c \end{bmatrix} \tag{4.15}$$

Assume that the controller (4.13) has been designed such that, A_{cl} is strictly stable. Note that by inserting the $\Delta\Sigma$ based encoder and decoder in the control system gives the $\Delta\Sigma$ based control system which is shown in Fig. 4.2. Here, $\mathcal{E}_{\triangle\Sigma}$ encodes feedback signals to BS signals at the transmitter. Then those BS signals go through $\mathcal{D}_{\triangle\Sigma}$ to produce $\tilde{e}$. Ideally $\hat{e} = \tilde{e}$.

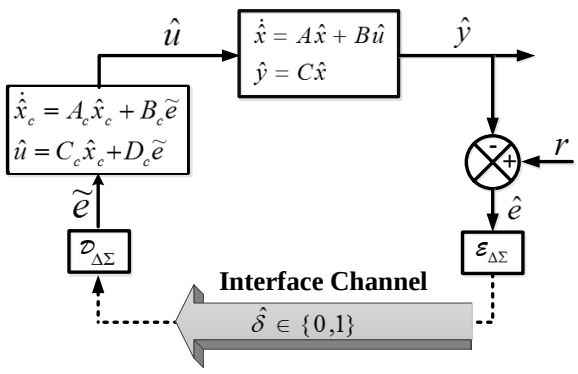

Figure 4.2: Configuration of $\Delta\Sigma$ based control system.

It is important to consider the problem of incorporating $\mathcal{E}_{\triangle\Sigma}$ and $\mathcal{D}_{\triangle\Sigma}$ with the system described in (4.14). Note that $\boldsymbol{Q}$ matrix is of dimension $p \times p$ and is

positive definite. Here, p is the number of $\triangle\Sigma$-Modulators that is being used. The estimated signals which is also the output of $\mathcal{D}_{\triangle\Sigma}$, are defined by,

$$\begin{aligned} \tilde{e} &= \operatorname{diag}\left\{\mathcal{E}_{\triangle\Sigma_j} \circ \mathcal{D}_{\triangle\Sigma_j}\right\} * \hat{e} \\ &= \boldsymbol{Q}\,\operatorname{sgn}(s) \end{aligned} \tag{4.16}$$

where $\dot{s} = \hat{e} - \tilde{e}$. The states of the feedback system can be defined as,

$$\begin{bmatrix} \dot{\hat{x}}_{cl} \\ \dot{s} \end{bmatrix} = \begin{bmatrix} A_1 & \mathbf{0} \\ A_2 & \mathbf{0} \end{bmatrix} \begin{bmatrix} \hat{x}_{cl} \\ s \end{bmatrix} + \begin{bmatrix} B_1 \\ B_2 \end{bmatrix} \tilde{e} \tag{4.17}$$

where $\hat{x}_{cl} = [\hat{x} \quad \hat{x}_c]^T$ and

$$\begin{aligned} A_1 := \begin{bmatrix} A & BC_c \\ \mathbf{0} & A_c \end{bmatrix}, \quad B_1 := \begin{bmatrix} BD_c \\ B_c \end{bmatrix} \\ A_2 := [-C \quad 0], \quad B_2 := -I_p \end{aligned} \tag{4.18}$$

with $A_1 \in \mathbb{R}^{(n+v)\times(n+v)}$, $A_2 \in \mathbb{R}^{p\times(n+v)}$ $B_1 \in \mathbb{R}^{(n+v)\times p}$ and $B_2 \in \mathbb{R}^{p\times p}$.

From (4.16) we can see that the feedback signals are switched signals. However, the system described in (4.17) becomes a differential equation with a discontinuous right hand side. According to [190,191], (4.17) can be analyzed using equivalent control method. Detailed analysis of the stability conditions and convergence analysis of $\Delta\Sigma$ (BS) based controllers shown in Fig.4.3 can be found in [184] and in [192–200].

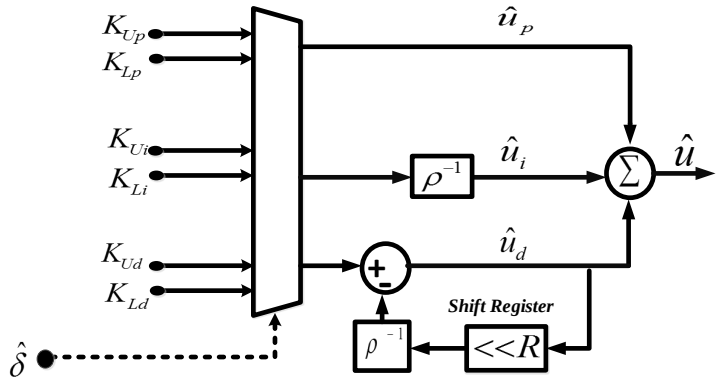

Figure 4.3: $\Delta\Sigma$-based PID controller.

Fig.4.3 shows the schematic diagram of $\Delta\Sigma$-based PID controller. Here, $[K_{Lp}, K_{Up}]$,$[K_{Li}, K_{Ui}]$,$[K_{Ud}, K_{Ud}]$, and N_d denote respectively the lower and upper bounds of the proportional gains, the integral gains, the differentiator gains, and the filter coefficient of the differentiator. Following measures are

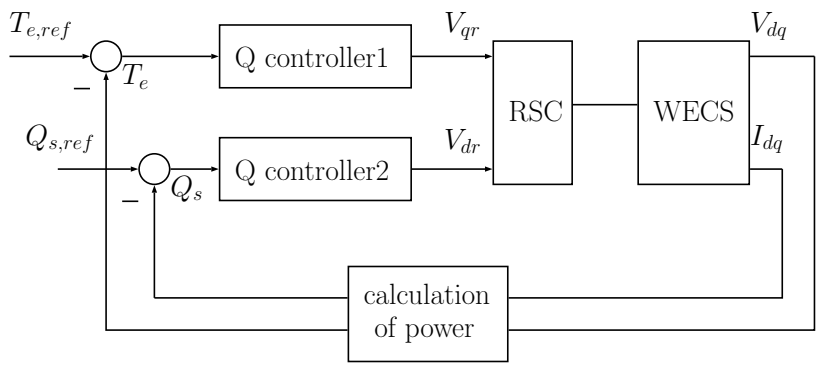

Figure 4.4: Control of RSC using Q-learning based controllers

taken to lower hardware consumption. To replace the multiplier with a *shift register* N_d can be selected such that $N_d h = 2^{-R}$, where $R \in \mathbb{N}_0$. The output of the $\Delta\Sigma$-based PID controller is given by [190]:

$$\hat{u}(t) = K_p + \frac{K_i h}{\rho} + \frac{K_d N_{d\rho}}{\rho + N_d h} \tag{4.19}$$

4.2.3 Q-learning based controller

Q-learning based controller used in RSC has some advantages. First, it is possible to effectively control the rotor side converter using only two controllers. Further, Q-learning based controller does not require precise mathematical model of the system. The structure of a classical Q-learning based controller for rotor side converter is shown in Fig. 4.4. The design procedures of Q-learning based controller is the same as that in Section 3.2.1.

4.2.4 DFQL based controller

As Q-learning algorithm can only search within discrete action space, DFQL, a method which is an extension of both fuzzy logic control and Q-learning, could deal with continuous action space without accurate mathematical model as well. Therefore, DFQL based controllers have also been designed for the RSC. In this DFQL control scheme [180], the traditional fuzzy rule base which determines the output of the controller has been changed using Q-learning. The control structure of DFQL based controller is shown in Fig. 4.5. The design procedures of DFQL based controllers is the same as that in Section 3.2.2.

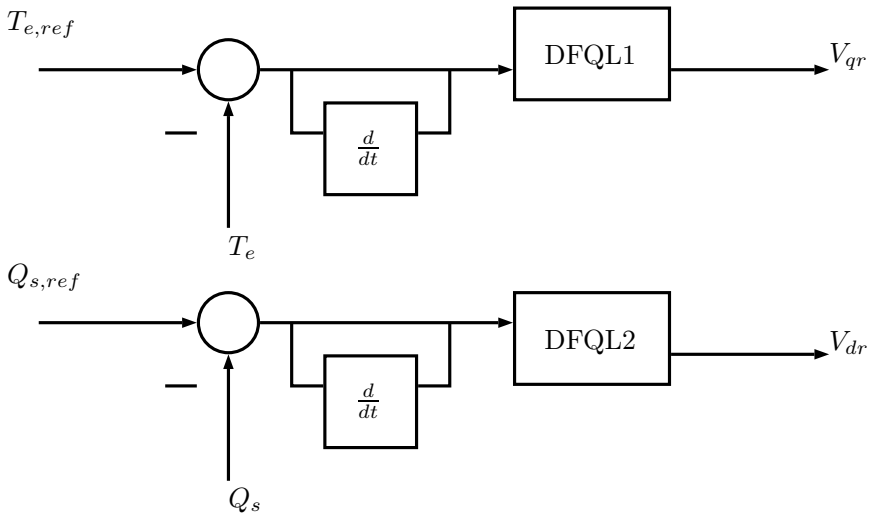

Figure 4.5: Control for RSC using DFQL based controllers

4.2.5 Classical PID controller

Classical PID controller was a popular controller that was usually designed to control the active and reactive power from the rotor side converter and its effectiveness has been demonstrated in simulated system. The control structure of classical PID controller in RSC is shown in Fig. 4.6.

4.3 Simulation results

The wind energy conversion system considered in this study is shown in Fig. 4.7. The fault is simulated by changing the reactance of the transmission line X_e from 5 to 0.5 at $t = 5\,sec$. This is equivalent to the occurrence of some kind of fault; as the fault causes the change of reactance of transmission line.

The inputs of classical PID, $\Delta\Sigma$ PID and Q-learning controller are $\Delta T_e = T_{e,ref} - T_{e,agg}$ and $\Delta Q_s = Q_{s,ref} - Q_{s,agg}$. The reference values of electrical torque ($T_{e,ref}$) and reactive power ($Q_{s,ref}$) are given by

$$T_{e,ref} = K_{opt}\omega_r^2 \tag{4.20}$$

$$Q_{s,ref} = 0 \tag{4.21}$$

where, $K_{opt} = 0.5787$, is a constant. The outputs of controllers are the dq-components of rotor voltage V_{qr} and V_{dr}.

However, the inputs of the designed DFQL controllers are different from that of other three controllers. DFQL controllers use two inputs (unlike other three

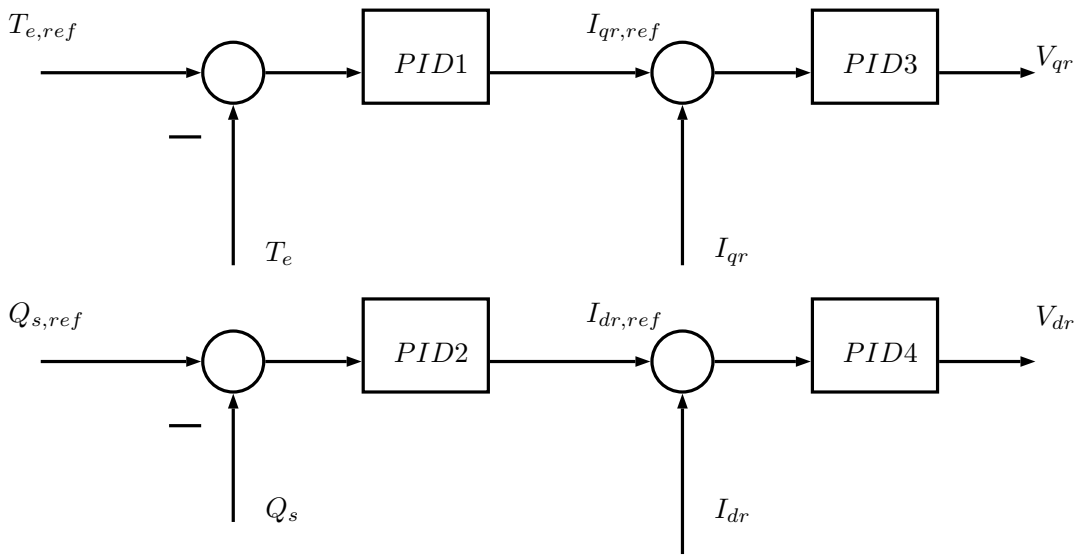

Figure 4.6: Control for RSC using conventional PID controllers

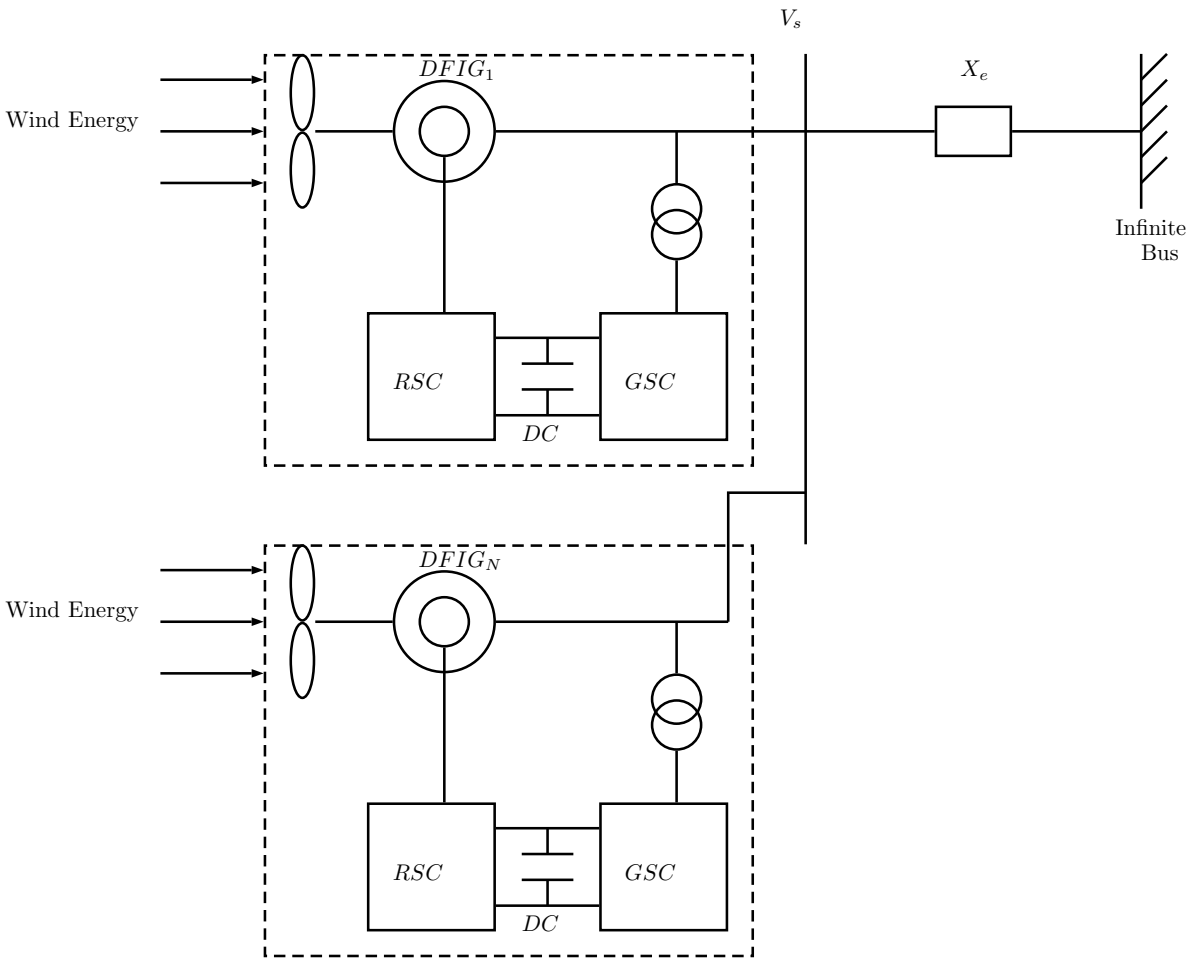

Figure 4.7: DFIGs based WECS

controllers which use one input). The inputs of DFQL controller1 are $T_{e,err} = T_{e,ref} - T_e$ and the deviation of $T_{e,err}$; and the output of this controller is the q-axis component of rotor voltage V_{qr}. Similarly, the inputs of DFQL controller2 are $Q_{s,err} = Q_{s,ref} - Q_s$ and its deviation; and the output is corresponding d-axis voltage V_{dr}. Note that the outputs of DFQL controllers are continuous unlike the outputs of Q-learning controllers which are discrete.

The variations in rotor speed ω_r, electrical and mechanical torques T_e, T_m and reactive power Q_s of the faulted system with various controllers are shown in Fig. 4.8 - Fig. 4.19. Note that variations are shown in p.u.

It is evident from the rotor speed responses in Fig. 4.8 - Fig. 4.11 that the $\Delta\Sigma$ based PID, Q-learning based controller and DFQL based controller stabilize the rotor speed of DFIG after a few seconds, whereas the classical PID controller takes a longer time.

The variations in the electrical torque T_e and mechanical torque T_m of the WECS using 4 controllers are shown in Fig. 4.12 - Fig. 4.15. From these figures, it can be observed that it takes a few seconds for the Q-learning based and DFQL based controllers to stabilize the torques, which are longer than that of other two controllers. The reason is that the RL controllers take some time to learn and react with the system to obtain the optimal actions.

Finally, the variations in reactive power Q_s are also plotted in Fig.4.16 - Fig.4.19. We can see from these figures that the DFQL based controller could stabilize the reactive power in a fastest time with some practically acceptable error . Further, in terms of overshoot, DFQL based controller also performs best among these controllers.

4.4 Conclusion

The performance of both Q-learning and DFQL controllers are compared with a classical PID controller and $\Delta\Sigma$ based PID controller in controlling the rotor side converter of a wind energy conversion system . The $\Delta\Sigma$ based PID controller is essentially a 1-bit controller and needs less hardware resources compared to other traditional controllers which are implemented in multi-bit. The results of the comparative investigation show that both DFQL controller and $\Delta\Sigma$ based PID controller perform better than other two controllers. However, Q-learning and DFQL controller have a longer learning process than the $\Delta\Sigma$ based PID controller.

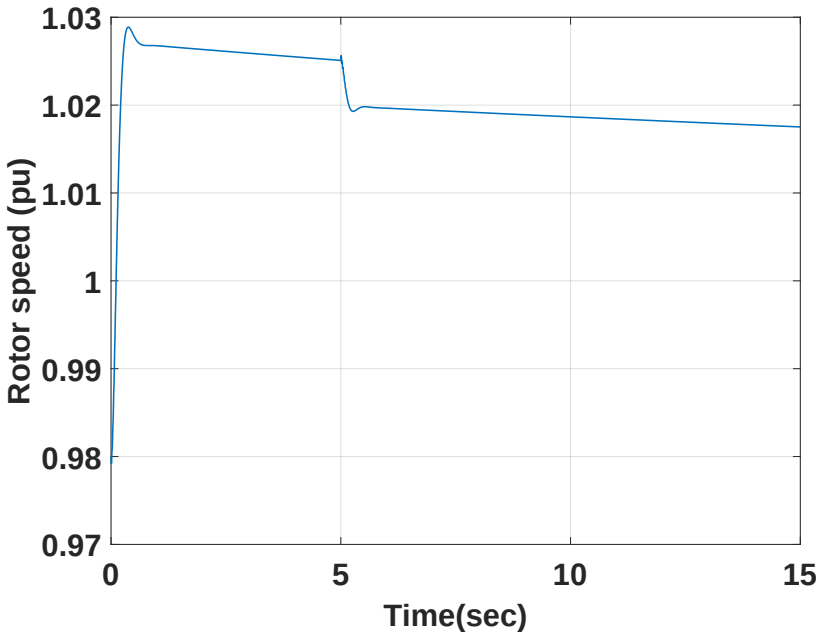

Figure 4.8: Variations in rotor speed of DFIG with classical PID controllers

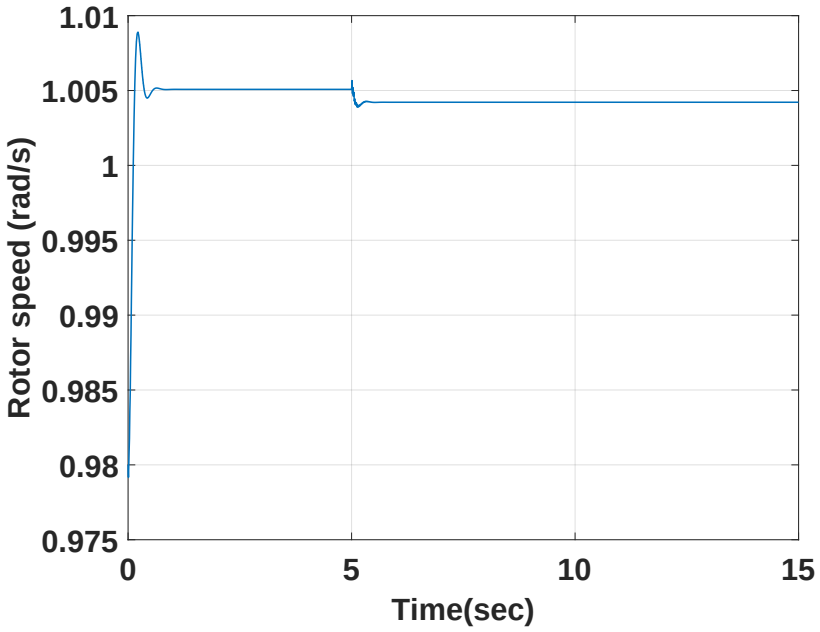

Figure 4.9: Variations in rotor speed of DFIG with $\Delta\Sigma$ based PID controllers

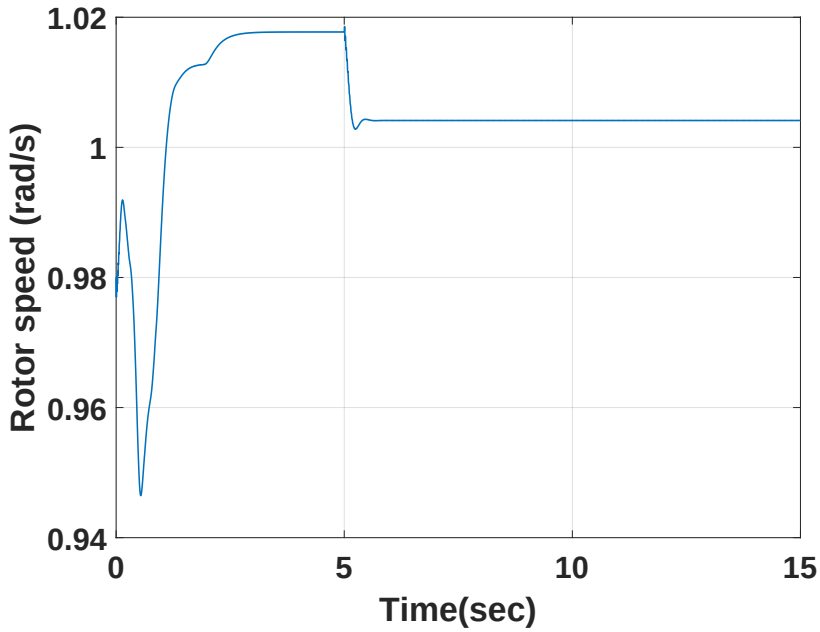

Figure 4.10: Variations in rotor speed of DFIG with Q-learning based controllers

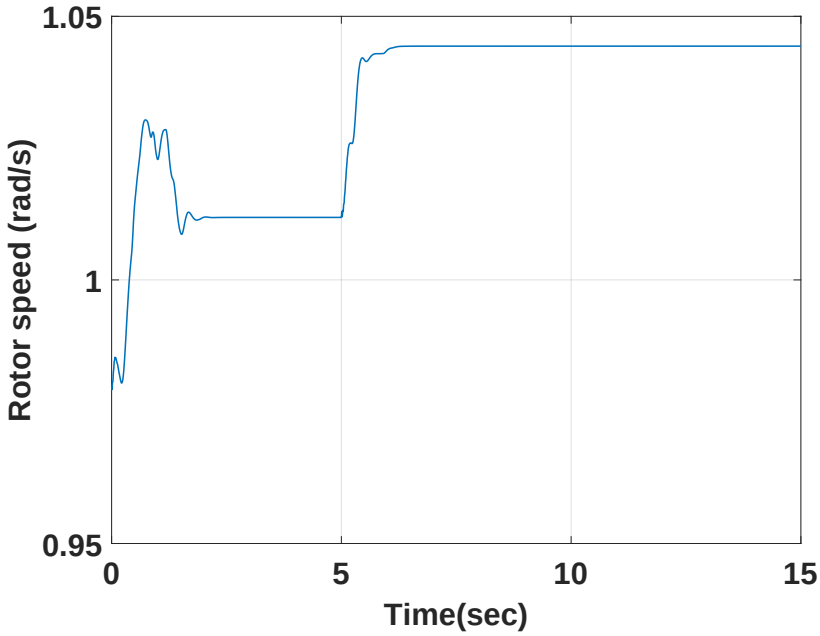

Figure 4.11: Variations in rotor speed of DFIG with DFQL based controllers

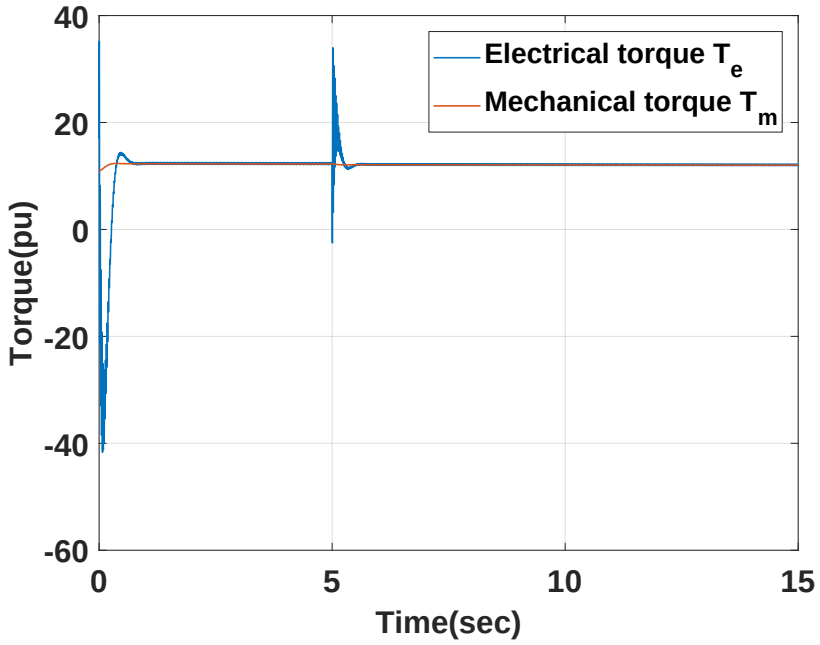

Figure 4.12: Variations in torque of DFIG with classical PID controllers

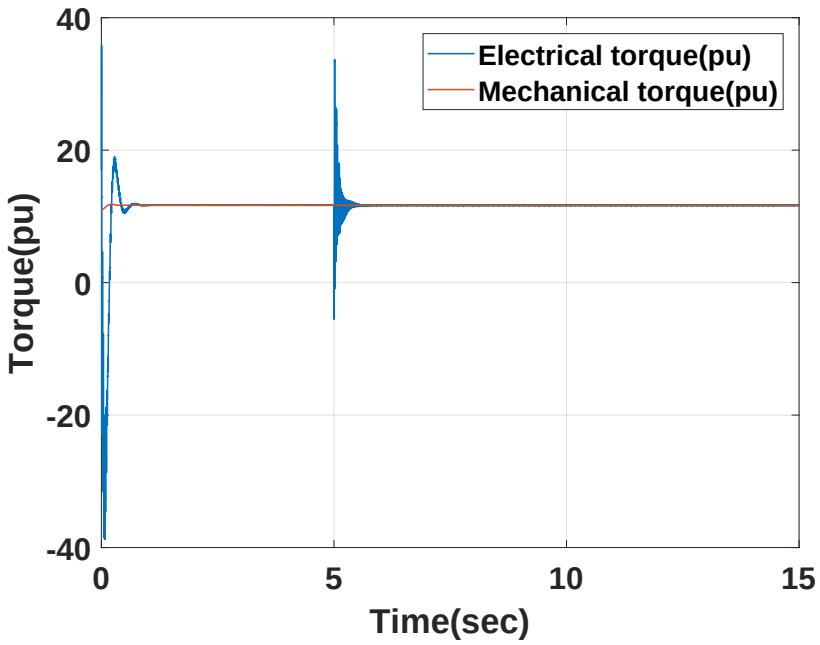

Figure 4.13: Variations in torque of DFIG with $\Delta\Sigma$ based PID controllers

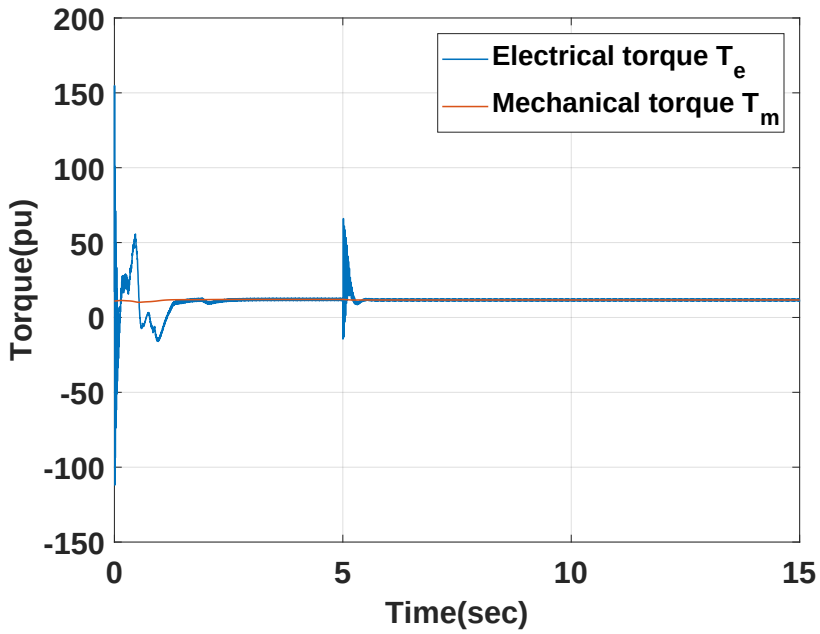

Figure 4.14: Variations in torque of DFIG with Q-learning based controllers

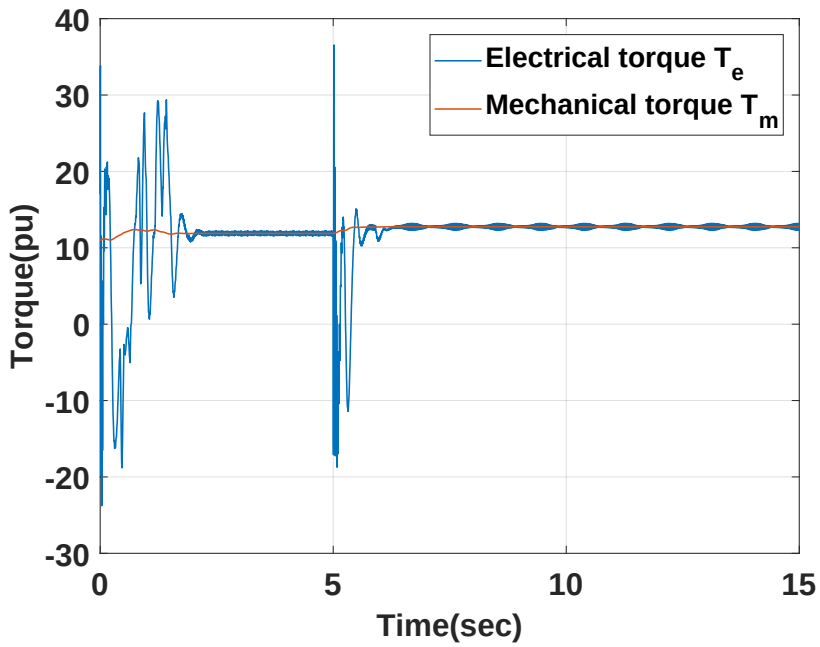

Figure 4.15: Variations in torque of DFIG with DFQL based controllers

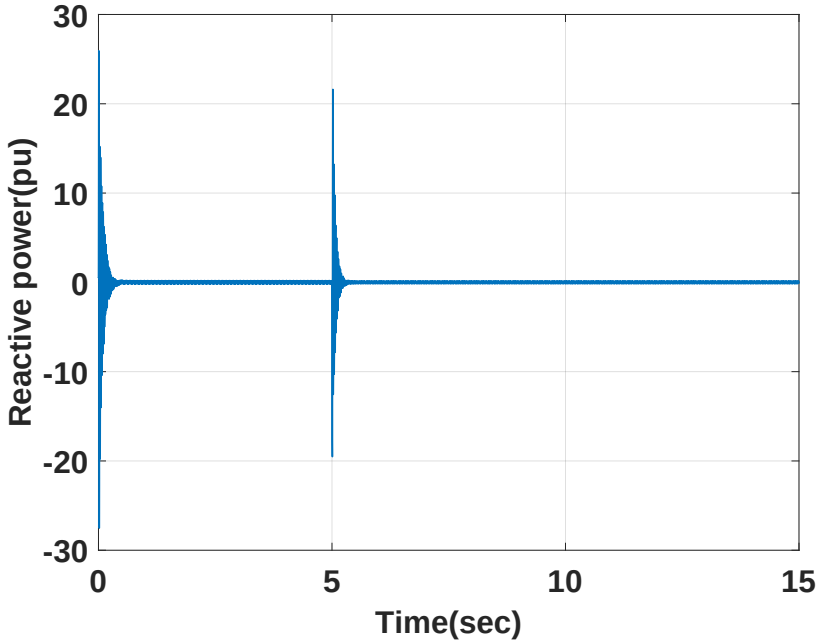

Figure 4.16: Variations in reactive power of DFIG with classical PID controllers

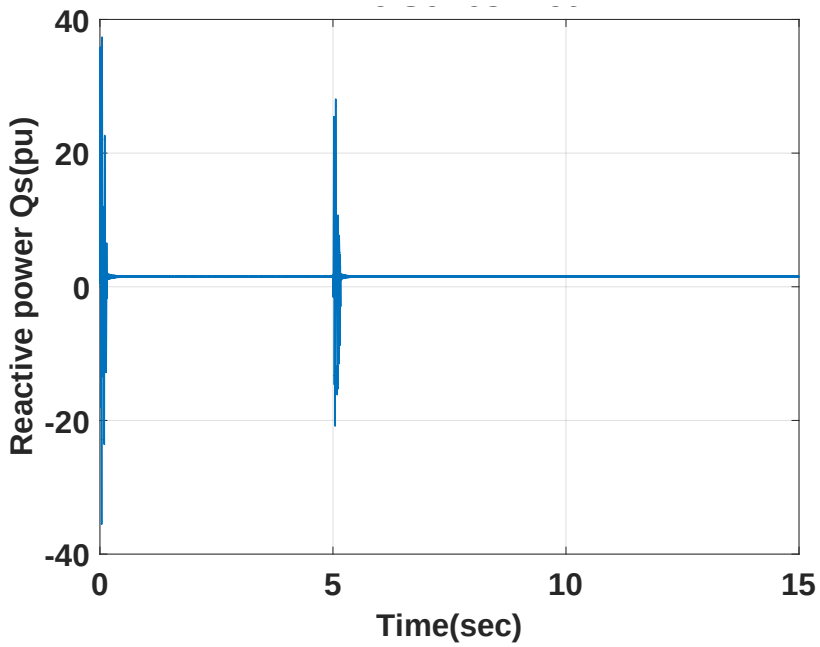

Figure 4.17: Variations in reactive power of DFIG with $\Delta\Sigma$ based PID controllers

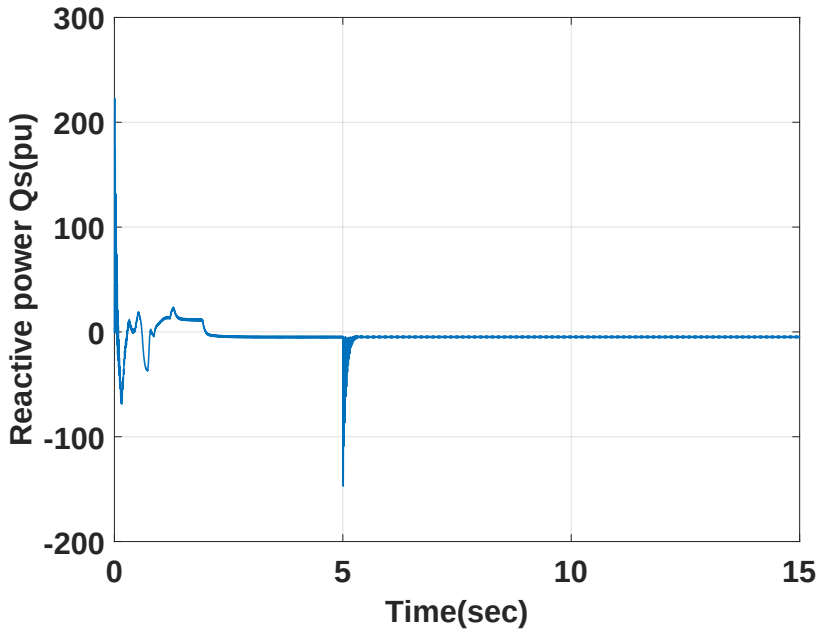

Figure 4.18: Variations in reactive power of DFIG with Q-learning based controllers

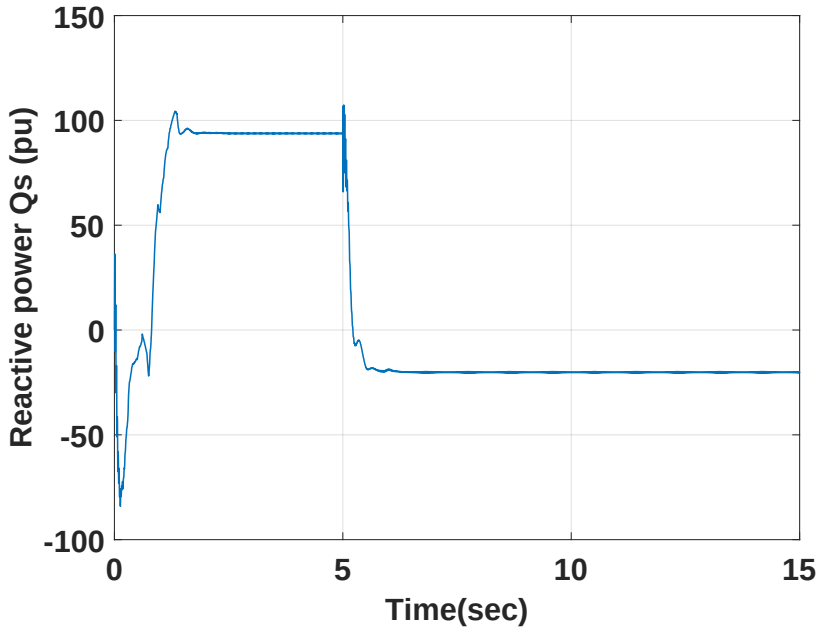

Figure 4.19: Variations in reactive power of DFIG with DFQL based controllers

Chapter 5

Design of UPFC for LVRT Improvement in Hybrid Power System

In recent years, several researchers have developed various methods and suggested both hardware and software solutions (e.g., crowbar, series dynamic resistors, DC link chopper, flexible AC transmission system) to enhance the LVRT capability of WECS [72, 73]. Some of these include crowbar protection using external crowbar resistors to short circuit the rotor side converter of the DFIG [201], installation of stator damping resistor in series with the stator or rotor of DFIG [202], DC link chopper in parallel with the DC link capacitor [119], insertion of flexible AC transmission system (FACTS) [203] and so on. Further, many control algorithms, such as fuzzy controller tuned by genetic algorithm [156], type-2 fuzzy logic control [204] etc. have been proposed for LVRT solutions.

One of the most popular approaches to improve the LVRT capability is through installation of FACTS devices. For example, STATCOM [205] and SVC [206] have been investigated for the enhancement of both LVRT capability and transient stability of the power system. In these shunt connected FACTS devices, different controllers have been designed to adjust the reactive power injected into the power system. In [155], a decentralized controller using a LQ output-feedback control design method is proposed to control a STATCOM, which improves the LVRT capability of fixed-speed wind turbines. Besides these shunt devices which are used to provide reactive power to the power system, other researchers have also applied series FACTS devices to improve the LVRT

capability by compensating the voltage sags, such as DVR [151–153], TCSC and SBR [116] and so on.

UPFC is one of the most versatile FACTS device which could both regulate the series voltage and inject power flow into the grid [121]. Various applications of the UPFC include improvement of power oscillation damping [143, 144], optimization of power flow [145], enhancement of power system transient stability [141, 142], security [146] and reliability [147], attenuation of sub-synchronous resonance in wind farm integration [148], coordination with power system stabilizer to eliminate small-signal oscillations [123] etc.

However, the effectiveness of UPFC to enhance the LVRT capability in WECS has not received enough attention from researchers except in [207], where a hysteresis current controller and PI controllers are designed for UPFC to improve the LVRT of wind turbines, and [208] where the performance of UPFC in fault ride-through has been shown better than STATCOM. This device could improve the LVRT capability by injecting reactive current through its shunt branch and compensating the voltage sag by its series branch. The success of UPFC in satisfying the LVRT requirements of various grid codes requires injection of the correct amount of reactive current and determining the degree of compensation for voltage sags. One of the approaches to achieve this is through the use of various types of controllers. In the past few decades, Q-learning based controller has been very successful in several applications [209, 210], as these controllers do not require the model of the systems (model-free controllers) and they are based on the principle of reinforcement learning (unsupervised learning) which is usually a good choice to successfully obtain optimal controls [23]. This property of Q-learning has been exploited in this study to determine the correct value of reactive power injection and accurate level of voltage compensation, so that the Q-learning based controllers can make the UPFC device compatible with the power system.

However, there is still a challenge existing in Q-learning as it essentially operates in discrete space where the input variables are first discretised and then used to generate discrete control actions. The controller may not give accurate outputs due to the fixed discrete control actions. Therefore, another control method needs to be addressed to handle continuous inputs and produce continuous control actions. In this study, we have therefore used DFQL to generate continuous control actions. The DFQL based controller essentially combines the principle of Q-learning with fuzzy controller where Q-learning is effectively used to update the initial fuzzy rule base and make it self-adaptive

[26,27]. Further, from the perspective of Q-learning, fuzzy control could provide the agent with continuous actions, and overcome the disadvantages of 'curse of dimension' associated with Q-learning.

This chapter investigates the application and performance of a UPFC device based on two different reinforcement learning based controllers to improve the LVRT capability of a three-machine hybrid power system consisting of two synchronous generators and one DFIG based wind farm. The UPFC essentially provides control of the power flow of transmission line. It consists of both a series and a parallel branch where each branch is represented by a controllable voltage source with a series impedance. The proposed controllers enable the UPFC to control the series and shunt compensation of the system.

5.1 Modelling of hybrid power system

5.1.1 Modelling of synchronous generators

In this chapter, the two-axis model of the synchronous generators, which does not account for sub-transient reactances and saturation have been considered. Further, the dynamics of turbine governor is also ignored, which implies that the mechanical torque $T_{M_i}, i = 1, 2$ is kept constant. The dynamics of i_{th} synchronous generator with IEEE type-I excitation system, which is employed here, is described as [170]:

$$\frac{d\delta_i}{dt} = \omega_i - \omega_0 \tag{5.1}$$

$$\frac{d\omega_{mi}}{dt} = \frac{1}{2H_i}[P_{mi} - P_{ei} - D(\omega_{mi} - \omega_{mi0})] \tag{5.2}$$

$$\frac{dE'_{qi}}{dt} = \frac{1}{T'_{d0i}}[-E'_{qi} + (X_{di} - X'_{di})I_{di} + E_{fdi}] \tag{5.3}$$

$$\frac{dE'_{di}}{dt} = \frac{1}{T'_{q0i}}[-E'_{di} - (X_{qi} - X'_{qi})I_{qi}] \tag{5.4}$$

$$T_{Ei}\frac{dE_{fdi}}{dt} = -(K_{Ei} + S_{Ei}(E_{fdi}))E_{fdi} + V_{Ri} \tag{5.5}$$

$$T_{Fi}\frac{dR_{fi}}{dt} = -R_{fi} + \frac{K_{Fi}}{T_{Fi}}E_{fdi} \tag{5.6}$$

$$T_{Ai}\frac{dV_{Ri}}{dt} = -V_{Ri} + K_{Ai}R_{fi} - \frac{K_{Ai}K_{Fi}}{T_{Fi}}E_{fdi} + K_{Ai}(V_{refi} - V_{ti}) \tag{5.7}$$

where, i=1, 2; ω_0 is the synchronous rotating speed.

The expression for electrical power of i_{th} machine P_{ei} is expressed by

$$P_{ei} = E'_{di}I_{di} + E'_{qi}I_{qi} + (X'_{di} - X'_{qi})I_{di}I_{qi}. \tag{5.8}$$

The stator equations of i_{th} synchronous machine are given by

$$E'_{qi} + X'_{di}I_{di} = V_{qi}, \tag{5.9}$$

$$E'_{di} - X'_{qi}I_{qi} = V_{di}. \tag{5.10}$$

The network equations are described as:

$$I_i = \sum_{k=1}^{m} Y_{int}(i,k)\dot{E}'_k e^{j\delta_k} \tag{5.11}$$

where, Y_{int} is the admittance matrix of the transmission network reduced to internal nodes [170]. The process of obtaining Y_{int} is shown in [170]. E'_k is the voltage at internal node $k, (k = 1, 2)$ and expressed as:

$$\dot{E}'_k = E'_{qk} + j[E'_{dk} + (X'_{dk} - X'_{qk})I_{qk}] \tag{5.12}$$

5.1.2 Modelling of DFIG based wind farm

The model of a DFIG-based wind-farm used in this chapter is the same as that which was established in Chapter 4 except the bus node with voltage V_s, shown in Fig. 4.7, is replaced by a bus node of hybrid power system. This is also considered as the PCC.

5.2 Modelling of UPFC

A typical UPFC consists of a series unit, a shunt unit and a control unit [211]. The equivalent circuit of UPFC is shown in Fig. 5.1 where the voltage sources in both the branches are controllable voltage sources.

The dynamics of the series and shunt branches are given by

$$\frac{d}{dt}\begin{bmatrix} I_{q,se} \\ I_{d,se} \end{bmatrix} = \begin{bmatrix} \frac{-R_{se}\omega}{L_{se}} & \omega \\ -\omega & \frac{-R_{se}\omega}{L_{se}} \end{bmatrix}\begin{bmatrix} I_{q,se} \\ I_{d,se} \end{bmatrix} + \frac{\omega}{L_{se}}\begin{bmatrix} V_{qi} - V_{qj} + V_{q,se} \\ V_{di} - V_{dj} + V_{d,se} \end{bmatrix} \tag{5.13}$$

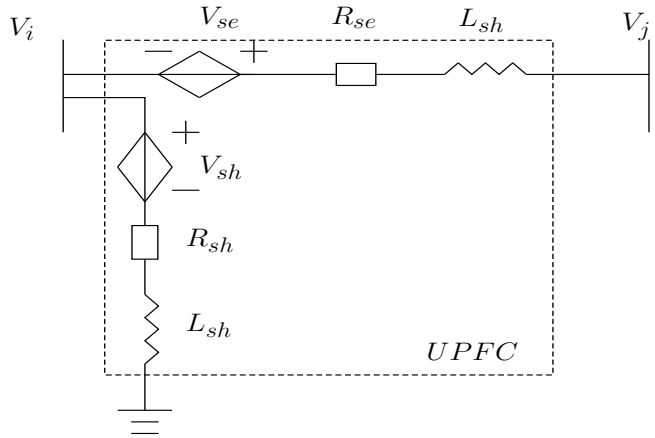

Figure 5.1: Equivalent circuit of an UPFC

$$\frac{d}{dt}\begin{bmatrix} I_{q,sh} \\ I_{d,sh} \end{bmatrix} = \begin{bmatrix} \frac{-R_{sh}\omega}{L_{sh}} & \omega \\ -\omega & \frac{-R_{sh}\omega}{L_{sh}} \end{bmatrix} \begin{bmatrix} I_{q,sh} \\ I_{d,sh} \end{bmatrix} + \frac{\omega}{L_{sh}} \begin{bmatrix} V_{qi} - V_{q,sh} \\ V_{di} - V_{d,sh} \end{bmatrix} \tag{5.14}$$

where, $I_{q,se}$, $I_{d,se}$ and $I_{q,sh}$, $I_{d,sh}$ are the dq - components of series current and shunt current, respectively.

The configuration of feedback control system of the series and shunt branch of UPFC is shown in Fig. 5.2. The series current I_{se} and shunt current I_{sh} are determined by a vector control system shown in Fig. 5.3. Let $x_{1,se}$, $x_{2,se}$, $x_{1,sh}$ and $x_{2,sh}$ be the outputs of the individual controllers in current control subsystem of series and shunt branch respectively. These are expressed as:

$$x_{1,se} = \frac{\omega}{L_{se}}(V_{qi} - V_{qj} + V_{q,se}) \tag{5.15}$$

$$x_{2,se} = \frac{\omega}{L_{se}}(V_{di} - V_{dj} + V_{d,se}) \tag{5.16}$$

$$x_{1,sh} = \frac{\omega}{L_{sh}}(V_{qi} - V_{q,sh}) \tag{5.17}$$

$$x_{2,sh} = \frac{\omega}{L_{sh}}(V_{di} - V_{d,sh}) \tag{5.18}$$

In the series branch, the reference current $I_{se,ref}$ is calculated by the reference power flow and voltage. A controlled injected voltage of series branch V_{se} is then generated using (5.15 - 5.16).

In the shunt branch, the dq - components of reference shunt current $I_{q,sh,ref}$ and $I_{d,sh,ref}$ are obtained by the outputs of the reference current controllers. The active reference current $I_{q,sh}$ is determined by regulating the DC capacitor voltage by a feedback controller. The reactive current $I_{d,sh}$ is controlled to support the voltage.

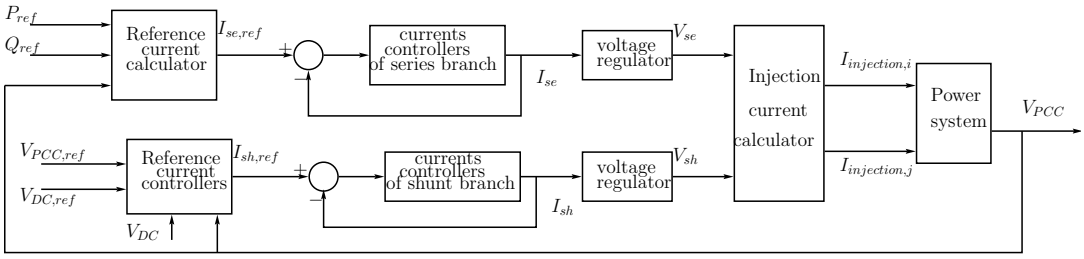

Figure 5.2: Diagram of Controlling Shunt and Series Branch of UPFC.

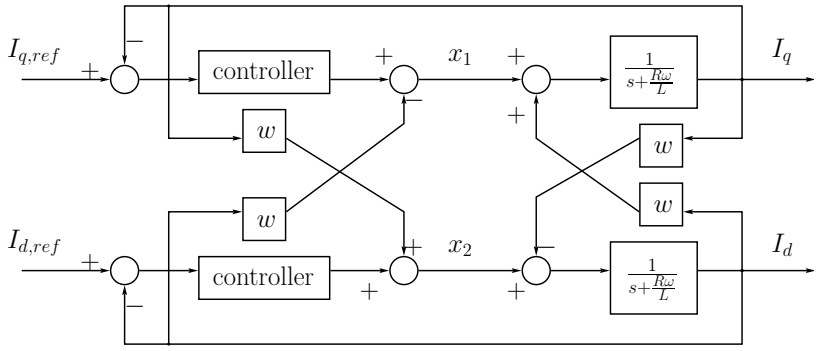

Figure 5.3: Diagram of current controllers in UPFC.

5.3 Low-voltage ride-through requirements

Due to increasing penetration of wind farms into the existing transmission system, there is a need for specific grid codes which allows the wind farms to be connected to the grid in the event of network faults and disturbances. The grid codes of various countries, stipulate that the wind farms connected to high voltage grids must withstand voltage dips to a certain percentage of nominal voltage for a specified duration. These requirements are popularly known as fault ride-through (FRT) or LVRT and these vary from one country to another.

In this study, we have designed various controllers to meet the LVRT requirements of Gemany (E.ON) [212], Canada (Hydro Quebec) [213] and New Zealand (North Island) [214]. Fig. 5.4 shows the LVRT requirements of these countries and Table 5.1 summarizes the main characteristics of these limit curves [215,216].

According to the grid code requirement of wind farms in Germany (E.ON), these farms must withstand voltage drops down to 0% of the nominal voltage at PCC for up to 9 cycles (150 ms), taking the frequency $f = 1/60$ Hz. According to the LVRT requirements for Canada (Hydro Quebec), the wind farms should remain connected in the grid with voltage dips down to 0% of the nominal voltage for maximum duration of 10.8 cycles (0.18 sec), and the voltage at PCC should be recovered to 0.75 p.u. in 1s. In New Zealand, the wind power should

Table 5.1: Characteristics of LVRT requirements in international grid codes

Indexes		Germany (E.ON)	Canada (Hydro Quebec)	New Zealand (North Island)
On-fault	$V_{min}(p.u.)$	0	0	0
	$T_{max}(cycles)$	9	10.8	8.4
post-fault	$V_{min}(p.u.)$	0.9	0.75	0.76
	$T_{max}(s)$	1.5	1	1.3

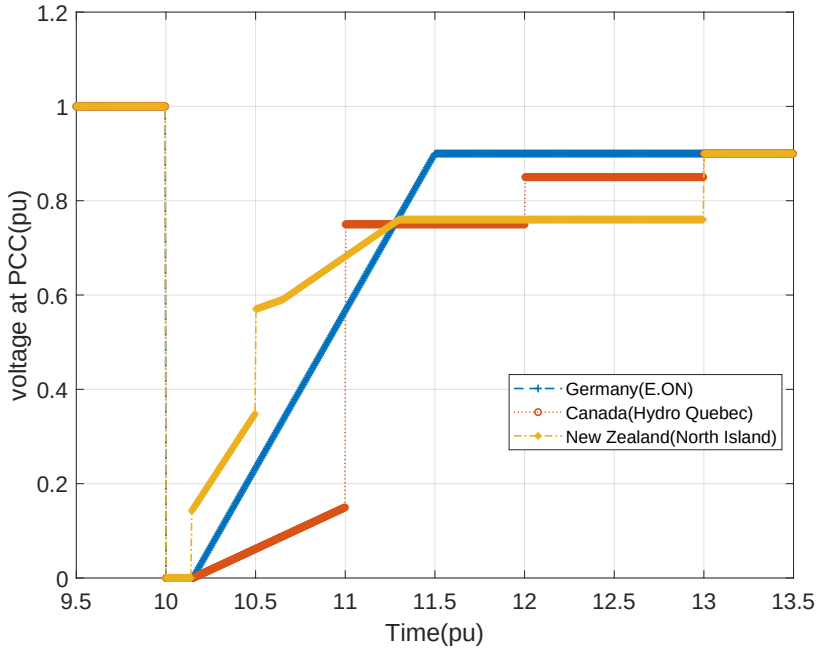

Figure 5.4: Limit curves for LVRT requirements in international grid codes.

be capable of remaining electrically connected in the transmission system for up to 8.4 cycles (0.14 sec) and recovering to 0.76 p.u. in 1.3 sec.

5.4 Controller design for UPFC

In this study, both Q-learning and dynamic fuzzy Q-learning controllers are designed for UPFC to improve the LVRT capability of a three-machine hybrid system consisting of two synchronous machines and a wind farm. The design procedures of Q-learning and DFQL based controllers are the same as that of Chapter 3. Their performances are further compared with classical PID controller.

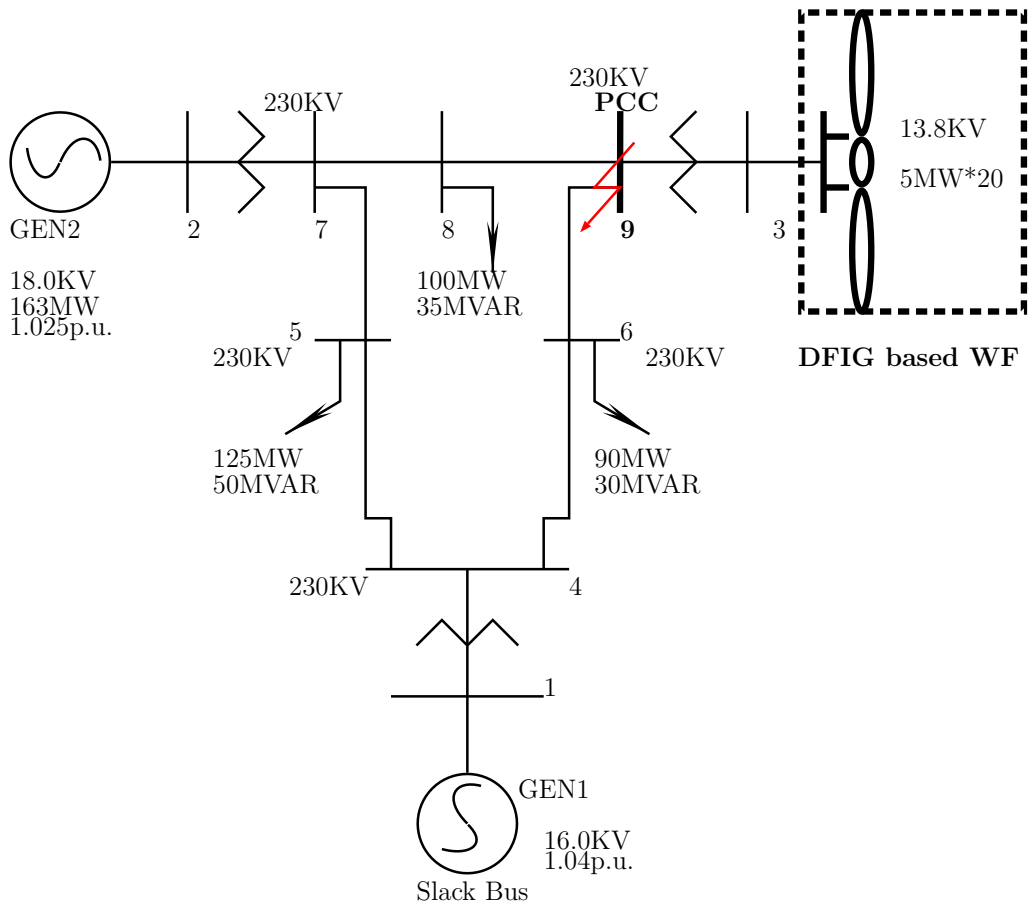

Figure 5.5: A three machine hybrid power system.

5.5 Simulation results

5.5.1 Simulated Hybrid Power System

The effectiveness of Q-learning based and DFQL based controllers are demonstrated considering a hybrid power system consisting of an aggregated DFIGs based wind farm and two synchronous generators. This is shown in Fig. 5.5.

Note that the wind farm, considered here, is an aggregated wind farm consisting of 20 DFIGs based wind turbines; each with a capacity of 5 MW. The simulated system is a modified version of the three-machine system of Western System Coordinating Council (WSCC) where one of the synchronous generator is replaced with the aggregated wind-farm. The initial conditions of this system is the same as the powerflow results of the WSCC system. All the parameters and powerflow results of the three-machine system of WSCC are given in

Apprendice A.1.

5.5.2 Simulation Framework

Throughout the simulation, the bus 9 in Fig.5.5 is regarded as PCC. A three-phase fault occurs at PCC at $t = 10$ sec and is cleared after some cycles by removing different lines. The performance of the controllers are studied considering the LVRT requirements of Germany (E.ON), Canada (Hydro Quebec) and New Zealand (North Island).

5.5.3 Results

The objective of this study is to investigate whether the system could satisfy the LVRT requirements of various international grid codes following a fault of varying duration both with and without the use of UPFC. The UPFC, in this study, is controlled either by Q-learning or DFQL based controller. The following two cases are taken up for study.

Case 1: A three-phase fault occurred at $t = 10$ sec and it is cleared after 9.9 cycles by removing the line 6 - 9. The UPFC is switched into the line 6 - 9 at the moment of fault clearance. It is worth mentioning that the critical clearing time for this system, where the fault is cleared by removing line 6 - 9, is 9.9 cycles. Therefore, for this case the fault duration is set at 9.9 cycles.

The LVRT capability of the system, both with and without UPFC, (controlled by Q- and DFQL controllers), are shown in Fig. 5.6.

From Fig. 5.6, it is observed that, without UPFC, the voltage at the PCC failed to meet the LVRT requirement of any of Germany (E.ON), Canada (Hydro Quebec) or New Zealand (North Island). Although both Q-learning based and DFQL based UPFC satisfied the LVRT grid codes of all the countries under investigation, the DFQL based UPFC provided best performance in improving LVRT capability.

Case 2:

In this case, the duration of the fault is increased from 9.9 cycles to 15.1 cycles. In contrast to Case 1, where the fault is cleared by removing the line 6 - 9, this is cleared by removing the line 8 - 9. Note that this simulation condition is the worst scenario for this system.

The LVRT capability of the system are studied using the three cases i.e without UPFC and with UPFC (which is controlled either by Q- or DFQL-)

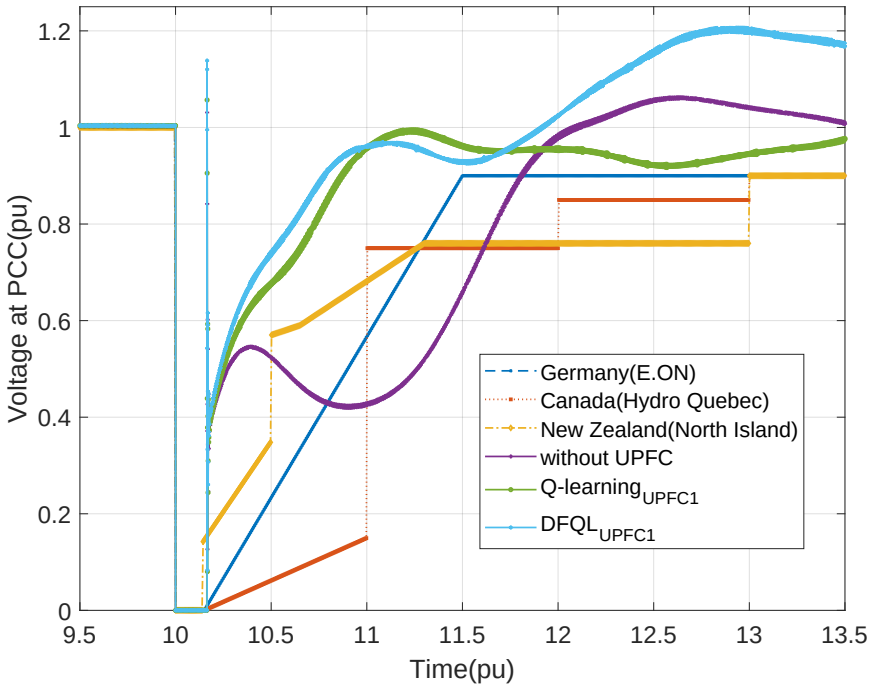

Figure 5.6: LVRT capability of UPFC1 in Case 1 (Fault duration is 9.9 cycles, and the fault is cleared by removing line 6 - 9).

controllers are shown in Fig. 5.7. From Fig. 5.7, it is observed that, without UPFC, the voltage at the PCC could only meet the LVRT requirement of Germany (E.ON) but could not satisfy the LVRT grid code of Canada (Hydro Quebec) and New Zealand (North Island). However, both Q-learning and DFQL based UPFC satisfied the LVRT requirements of all the 3 countries under investigation.

5.6 Conclusion

Both Q-learning and DFQL based controllers are designed to achieve and improve the low-voltage ride through capability of a hybrid power system through UPFC. The main difference between Q-learning and DFQL based controller is that Q-learning deals with discrete states and actions while DFQL could solve continuous action problem. The outputs of these controllers essentially decide the amount of series and shunt compensation to be provided by the UPFC. The performance of these controllers have been studied by considering the possible worst case scenario (i.e. three-phase fault of 9.9 - and 15.1 - cycle duration). The results of comparative study show that the performance of DFQL based UPFC is better and it could achieve and satisfy the LVRT grid codes of differ-

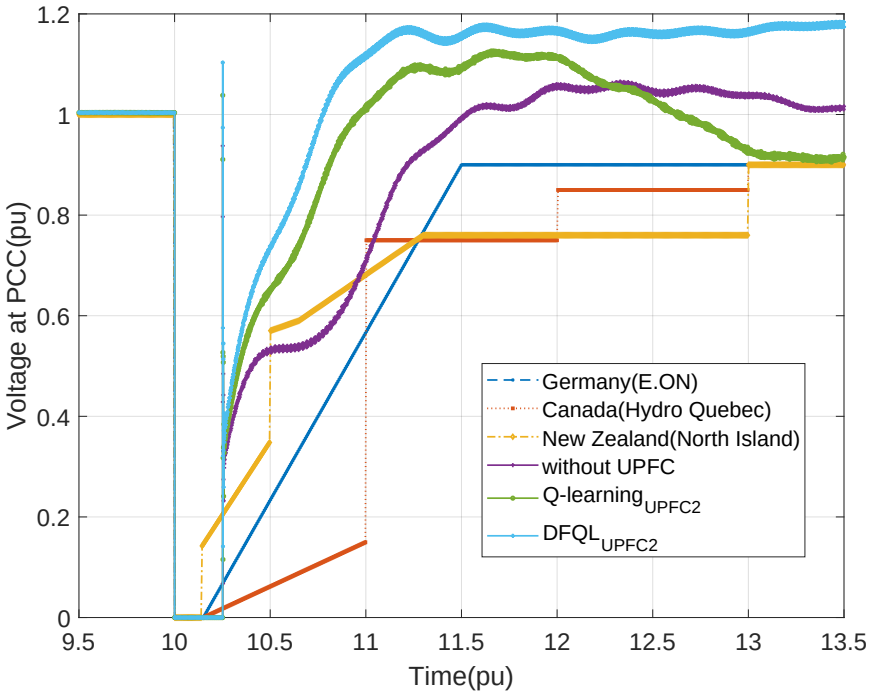

Figure 5.7: LVRT capability using UPFC2 in Case 2 (Fault duration is 15.1 cycles and cleared by removing line 8 - 9).

ent countries.

Chapter 6

Design of CSC for LVRT Improvement in Hybrid Power System

The focus of this research is to investigate if CSC can be used to achieve the LVRT capability of a hybrid power system.

The advantages of CSC is well established which include its versatility, flexibility and multi-functionality provided by more than one degrees of freedom [211]. It can be configured into various FACTS devices such as SSSC, one STATCOM, two STATCOMs, UPFC, IPFC etc., and has been shown to provide voltage support and power flow control both efficiently and effectively. Although the performance of combined FACTS have been investigated in improving the voltage stability [217], small-signal stability and transient stability [218], transfer path stability [219] of power systems, their effectiveness to achieve LVRT has not been received much attention from researchers and not been thoroughly investigated yet.

The goal of this study is to investigate if reinforcement learning controllers, in conjunction with CSC, could be used to achieve LVRT capability in a hybrid power system consisting of both synchronous and asynchronous generators such as wind generator. In particular the following questions will be answered:

i. *For a given controller, which configuration of CSC, such as STATCOM, UPFC etc., is best for achieving LVRT capability?*

ii. *For a given configuration of CSC, which controller would give better performance?*

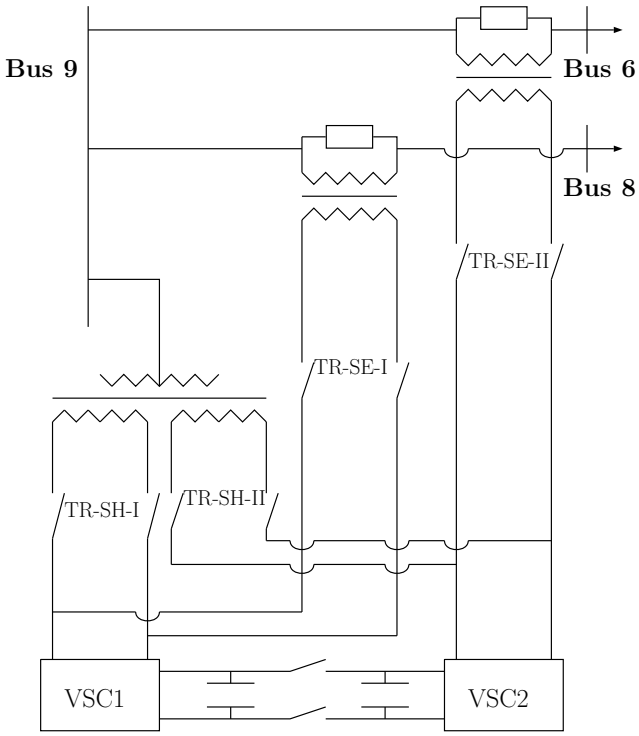

Figure 6.1: Schematic of CSC

iii. *Which combination of CSC configuration and controller could perform best in LVRT capability?*

Therefore, this chapter applies CSC controlled by reinforcement learning controllers to improve the LVRT capability and focuses on the effect of various configurations of CSC on LVRT improvement in a hybrid power system.

6.1 Convertible static compensator

The schematic of CSC is shown in Fig. 6.1 which consists of two voltage-sourced converters and one shunt step-down transformer with two secondary windings [217]. Note that, functionally, either of the converters connected with the system could lead to ten different configurations as shown in Table 6.1. Note that STATCOM-I and STATCOM-II are the same configuration.

Among all these configurations, it is known that SSSC is usually used to support active power and STATCOM is set to provide voltage support to the grid. Further, the benefit provided by UPFC is more than SSSC and STATCOM operated separately, and IPFC is considered not to be more positively supportable than two individual SSSCs. This could be helpful in decreasing the

Table 6.1: Possible configurations of CSC

	TR-SH-I	TR-SH-II	TR-SE-I	TR-SE-II
SSSC-I	-	-	✓	-
SSSC-II	-	-	-	✓
two SSSCs	-	-	✓	✓
IPFC	✓	✓	-	-
one STATCOM (STATCOM-I)	✓	-	-	-
one STATCOM (STATCOM-II)	-	✓	-	-
UPFC-I	✓	-	✓	-
UPFC-II	-	✓	-	✓
SSSC-I+ STATCOM-II	-	✓	✓	-
SSSC-II+ STATCOM-I	✓	-	-	✓
two STATCOMs	✓	✓	-	-

configuration numbers of CSC considered in this study. In order to carry out this simulation efficiently, the configurations considered in this study are as follows: *SSSC-I, SSSC-II, one STATCOM (STATCOM-I, or STATCOM-II), two STATCOMs, UPFC-I* and *UPFC-II*.

6.2 Controller design for CSC

It is worth mentioning that in this study two reinforcement learning controllers based on Q-learning and DFQL have been used for various advantages they offer in non-linear dynamic systems. The Q-learning controller is a self-adaptive and self-learning controller [220], which provides optimal control actions (discrete in nature) by interacting with the system. On the contrary, the DFQL based controller which is essentially a combination of both fuzzy control and Q-learning based controller, provides continuous control actions and has been shown to be more accurate and robust [27, 180, 221].

The inputs of designed controllers $\hat{x}^t$ are the voltages at those nodes where CSC is installed; and outputs of controllers are the currents injected from CSC into the power system. However, it is worth mentioning that the success of the reinforcement learning controllers is often critically dependent on the choice of the reward function which is often selected based on the knowledge of the experts. In this study, the reward function of both Q-learning and DFQL based

Table 6.2: Configurations of CSC considered in different scenarios

Configuration	Scenario	
	Case-I	Case-II
SSSC-I	✓	-
SSSC-II	-	✓
STATCOM-I	✓	-
STATCOM-II	-	✓
UPFC-I	✓	-
UPFC-II	-	✓
two STATCOMs	✓	✓

controllers are chosen as the same as that used in previous chapters:

$$R(\hat{x^t}) = \begin{cases} \beta, & \text{if } |\hat{x^t}| \in S_0, \\ -\beta, & \text{else} \end{cases} \tag{6.1}$$

where, $\beta > 0$, and S_0 is the reference of $\hat{x^t}$ with specific error.

6.3 Simulation results

6.3.1 Simulation

The effectiveness of the proposed reinforcement learning controllers are demonstrated considering a hybrid power system consisting of two synchronous generators and one DFIG based wind-farm shown in Fig. 5.5. Note that the 100 MW wind-farm consists of 20 wind turbines, of which the capacity is 5 MW.

To investigate the LVRT capability of different configurations of CSC, the system shown in Fig. 5.5 in two scenarios are considered in this study. The behaviour of voltage at PCC in two different scenarios is analyzed to evaluate the influence of each configuration and controller on LVRT capability. The considered cases are as follows:

Case-I

A three-phase fault is assumed to occur at PCC (bus 9) at time = 10 sec, and it was cleared by removing the transmission line 6 - 9 after 0.165 sec, i.e. at 10.165 sec. Note that the critical clearing time for this post-fault configuration has been found to be 0.165 sec.

Case-II

In this scenario, similar to Case-I a three phase fault was introduced at PCC (bus 9) at time = 10 sec. However, instead of clearing fault by removing line 6 - 9, it is cleared by removing the transmission line 8 - 9 at time = 10.251 sec; because the critical clearing time for this post-fault configuration is found to be 0.251 sec.

The simulations were carried out by configuring the CSC shown in Table 6.2. In Case-I, the CSC is configured to operate as *SSSC-I, STATCOM-I, two STATCOMs* and *UPFC-I*. In Case-II, different transmission line has been removed to clear the fault, series compensation was installed in line 8 - 9. Thus, the CSC is configured as *SSSC-II, STATCOM-II, two STATCOMs* and *UPFC-II*. In both scenarios, three controllers such as PID controllers, Q-learning and DFQL based controllers are designed to control various configurations of CSC which alternately achieve LVRT capability.

6.3.2 Results

The investigation in this study is carried out progressively in three stages.
Stage 1: For a given controller such as PID, Q-learning and DFQL based controller, the performance of four different configurations of CSC are studied.
Stage 2: For a given configuration of the CSC, the performance of all the three controllers are investigated.
Stage 3: For a given LVRT grid code of a specific country, the performance of different combinations of CSC configurations and controllers are studied.

Results of Case-I

Stage 1: The voltage at the PCC for Case-I with 4 configurations of CSC are computed. These responses for PID, Q-learning and DFQL based controllers are shown respectively in Fig. 6.2 - Fig. 6.4. From the figures, it is observed that PID controller could achieve the LVRT grid codes only when the CSC is configured as UPFC-I. In contrast, both Q-learning and DFQL could satisfy the LVRT grid codes for three configurations of CSC. The performance of all these controllers with SSSC-I is poor except for the DFQL controller which satisfies the grid code of one of the countries - that is Germany (E.ON).

Stage-2: In this stage,the performance of three configurations of CSC with all the three controllers are investigated. Since the performance of SSSC-I is poor

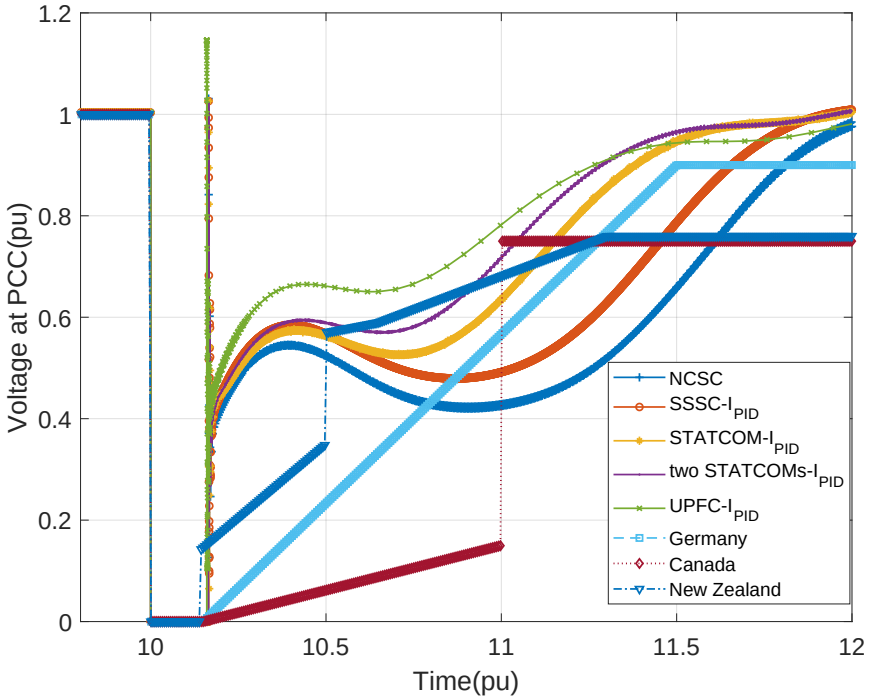

Figure 6.2: Performance of PID controller in Case-I

compared to other configurations, it is therefore not studied further. The results for STATCOM-I, two STATCOMs, UPFC-I are shown respectively in Fig. 6.5 - Fig. 6.7. From Fig. 6.5, it is observed that Q-learning and DFQL based controllers could achieve LVRT requirements while the PID controller failed to satisfy LVRT codes. The results in Fig. 6.6 for two STATCOMs gives similar results as with STATCOM-I which is shown in Fig. 6.5. The results in Fig. 6.7 show that when the CSC is configured as UPFC-I, all the 3 controllers could achieve LVRT grid codes for all the three countries and is therefore recommended for use.

Stage-3: The last stage studied which combination of CSC configuration and controller would provide better performance in the LVRT compliance of Germany (E.ON), Canada (Hydro Quebec) and New Zealand (North Island). The results of this investigation are summarized in Table 6.3 - Table 6.5. The recovering time for all combinations of CSC configurations and controllers are summarized in Table 6.6. From the tables, it is observed that DFQL based controller is the best among-st these three controllers in various configurations of CSC.

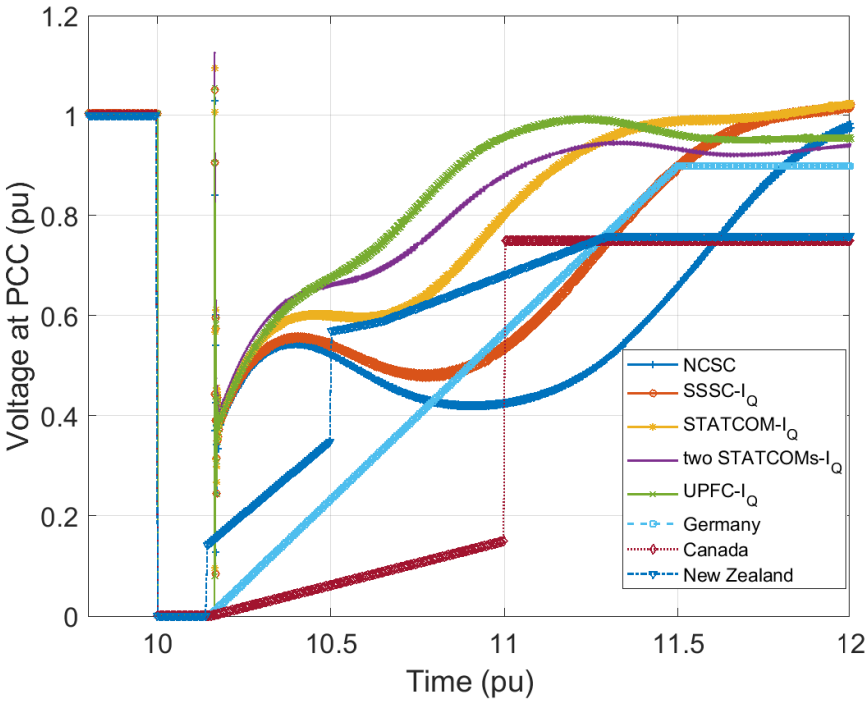

Figure 6.3: Performance of Q-learning based controller in Case-I

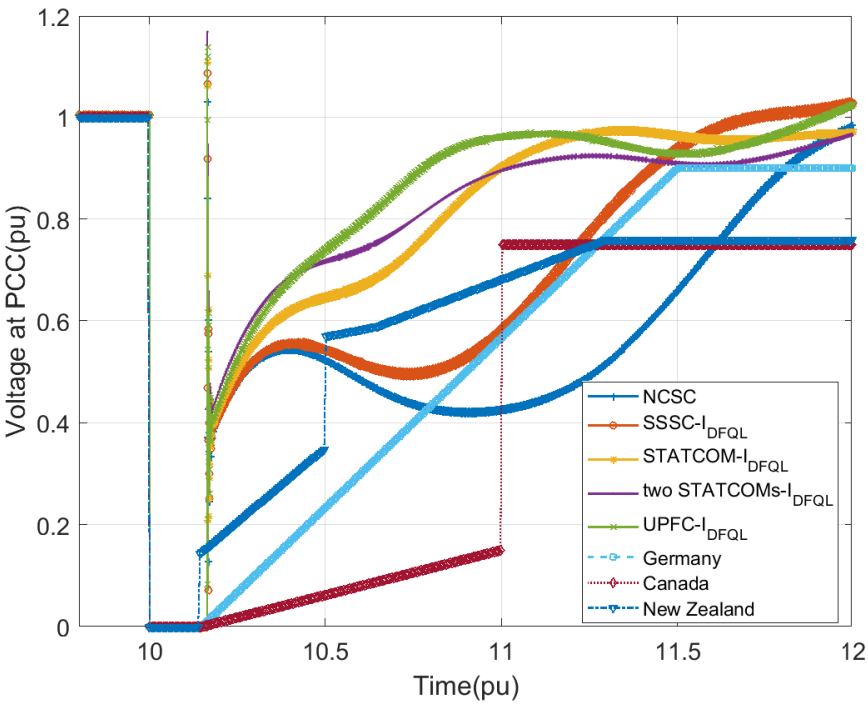

Figure 6.4: Performance of DFQL based controller in Case-I

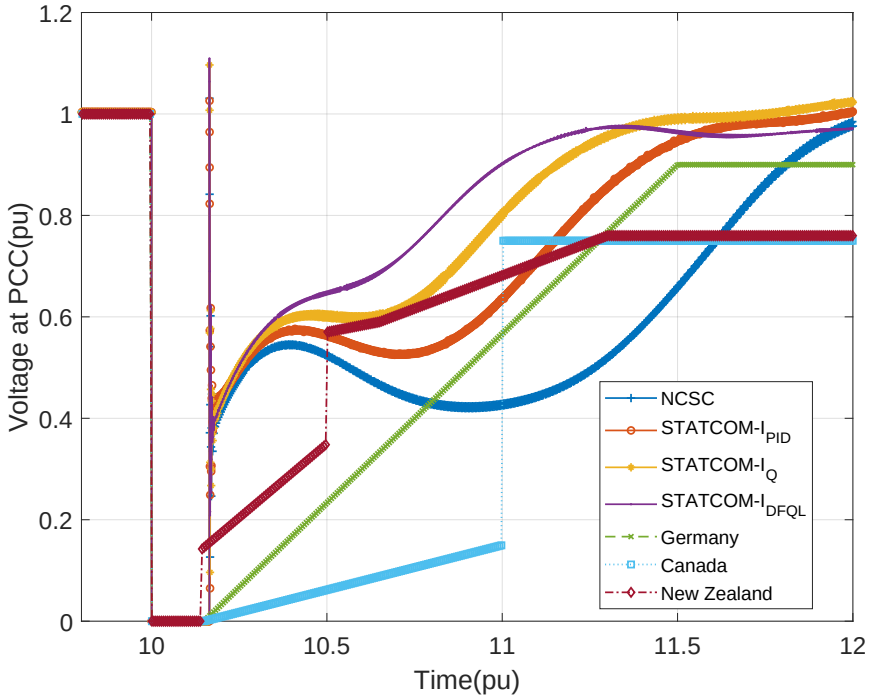

Figure 6.5: Performance of CSC configured as STATCOM-I in Case-I

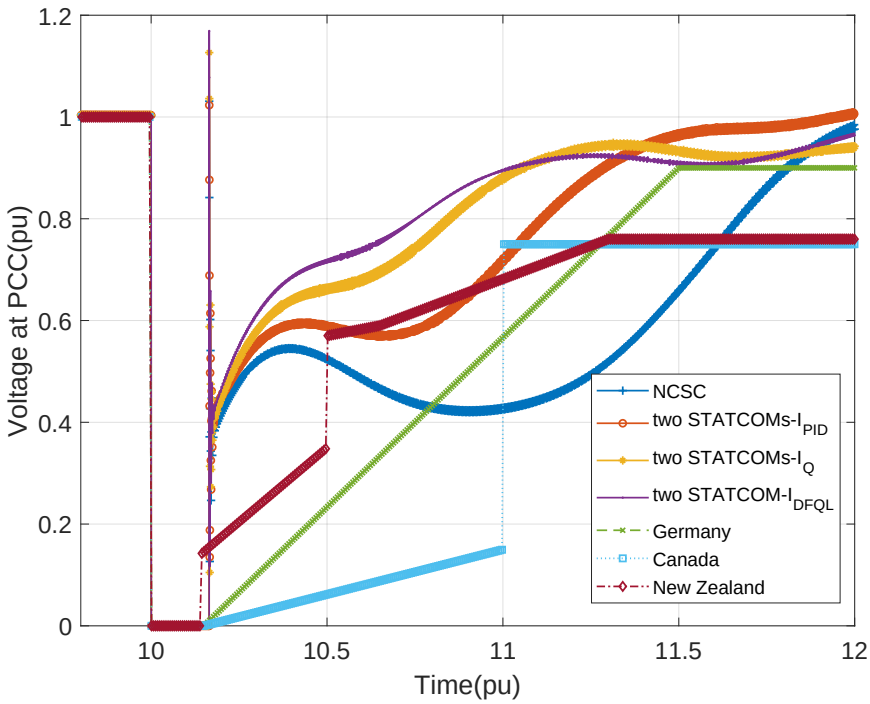

Figure 6.6: Performance of CSC configured of two STATCOMs in Case-I

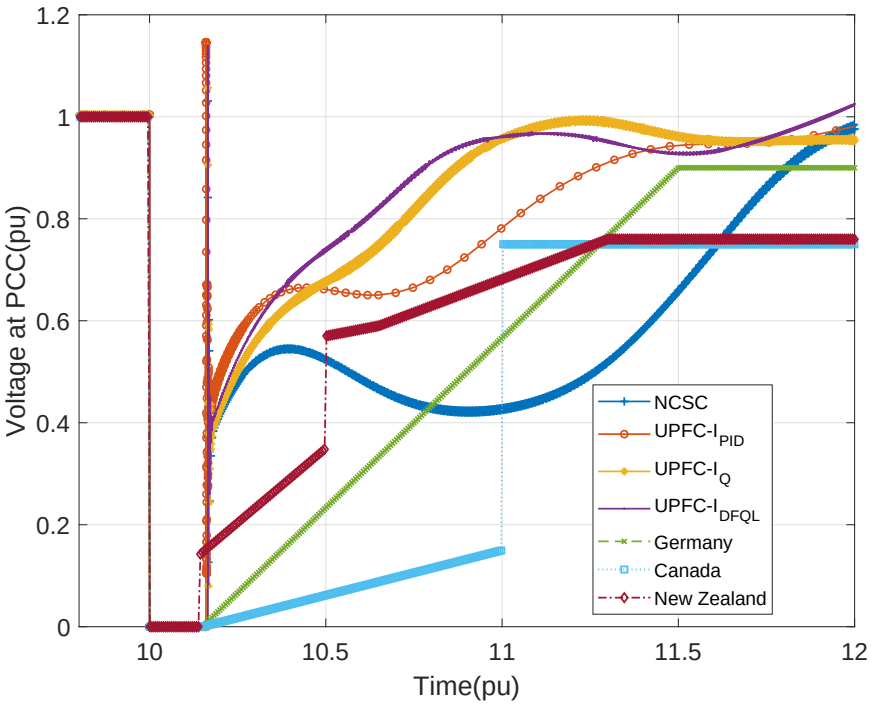

Figure 6.7: Performance of CSC configured of UPFC-I in Case-I

Table 6.3: Performance of different combinations in Case-I in regard to LVRT requirement of Germany (E.ON)

	PID	Q-learning	DFQL
SSSC-I	✗	✗	✓
STATCOM-I	✗	✓	✓
two STATCOMs	✗	✓	✓
UPFC-I	✓	✓	✓

Table 6.4: Performance of different combinations in Case-I in regard to LVRT requirement of Canada(Hydro Quebec)

	PID	Q-learning	DFQL
SSSC-I	✗	✗	✗
STATCOM-I	✗	✓	✓
two STATCOMs	✗	✓	✓
UPFC-I	✓	✓	✓

Table 6.5: Performance of different combinations in Case-I in regard to LVRT requirement of New Zealand (North Island)

	PID	Q-learning	DFQL
SSSC-I	✗	✗	✗
STATCOM-I	✗	✓	✓
two STATCOMs	✗	✓	✓
UPFC-I	✓	✓	✓

Table 6.6: Critical recovering time in Case-I

	PID		Q-learning		DFQL	
	$T_{(V=0.75)}$ (sec)	$T_{(V=0.9)}$ (sec)	$T_{(V=0.75)}$ (sec)	$T_{(V=0.9)}$ (sec)	$T_{(V=0.75)}$ (sec)	$T_{(V=0.9)}$ (sec)
SSSC-I	11.45	11.66	11.29	11.50	11.22	11.42
STATCOM-I	11.15	11.38	10.93	11.16	10.76	11.00
two STATCOMs	11.04	11.28	10.76	11.05	10.63	11.01
UPFC-I	10.94	11.26	10.65	10.87	10.51	10.78

Results of Case-II

In this part of the study, we are interested to know whether the choice of various CSC configurations and the controllers depend on the post fault system configuration. Therefore, in this case, the fault was cleared by removing line 8 - 9 instead of line 6 - 9.

First, the voltage at PCC for Case-II with 4 CSC configurations are computed in Stage 1. The performances of three controllers are shown respectively in Fig. 6.8, Fig. 6.9 and Fig. 6.10. It is observed that configurations of STATCOM-II, two STATCOMs and UPFC-II could satisfy all the LVRT grid codes of three countries while SSSC-II could not. Further, the performances of these three effective CSC configurations are illustrated respectively in Fig. 6.11, Fig. 6.12 and Fig. 6.13. It is shown that all the three controllers meet all the LVRT requirements. Finally, the performances of different combinations of CSC configurations and controllers are studied in Stage 3. The results are summarized in Table 6.7, Table 6.8 and Table 6.9. The recovering time for all combinations of CSC configurations and controllers are summarized in Table 6.10. From the table, it is clear that although all the three controllers for CSC configurations could satisfy the LVRT grid code, the combination of two STATCOMs and DFQL controller help the voltage at PCC recover fastest among all

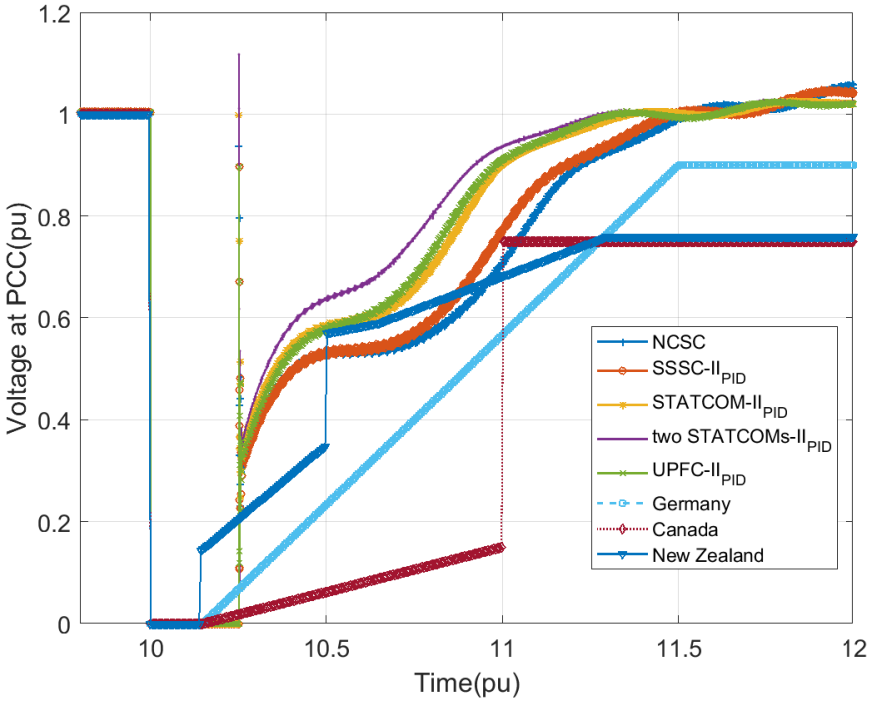

Figure 6.8: Performance of PID controller in Case-II

Table 6.7: Performance of different combinations in Case-II in regard to LVRT requirement of Germany (E.ON)

	PID	Q-learning	DFQL
SSSC-II	✓	✓	✓
STATCOM-II	✓	✓	✓
two STATCOMs	✓	✓	✓
UPFC-II	✓	✓	✓

the combinations.

6.4 Conclusion

In this study, CSC operating in different configurations and controlled by different reinforcement learning based controllers has been investigated to improve the LVRT capability in a hybrid power system consisting of two synchronous generators and one DFIG-based wind-farm.

The simulations have been conducted considering two scenarios, which cleared the fault by removing different transmission lines. The results have demonstrated the effectiveness of CSC in improving the LVRT capability. In Case-I,

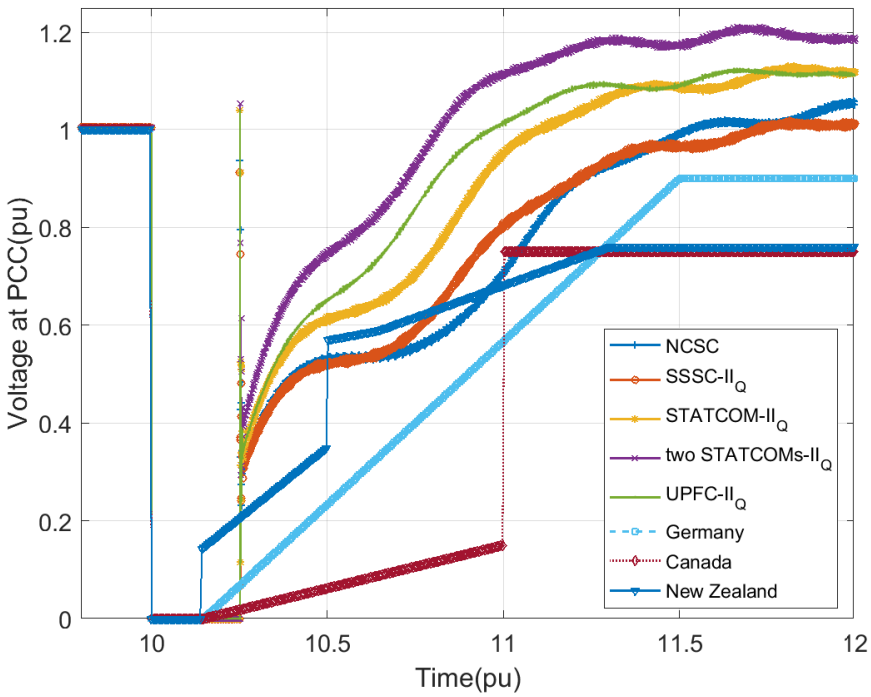

Figure 6.9: Performance of Q-learning based controller in Case-II

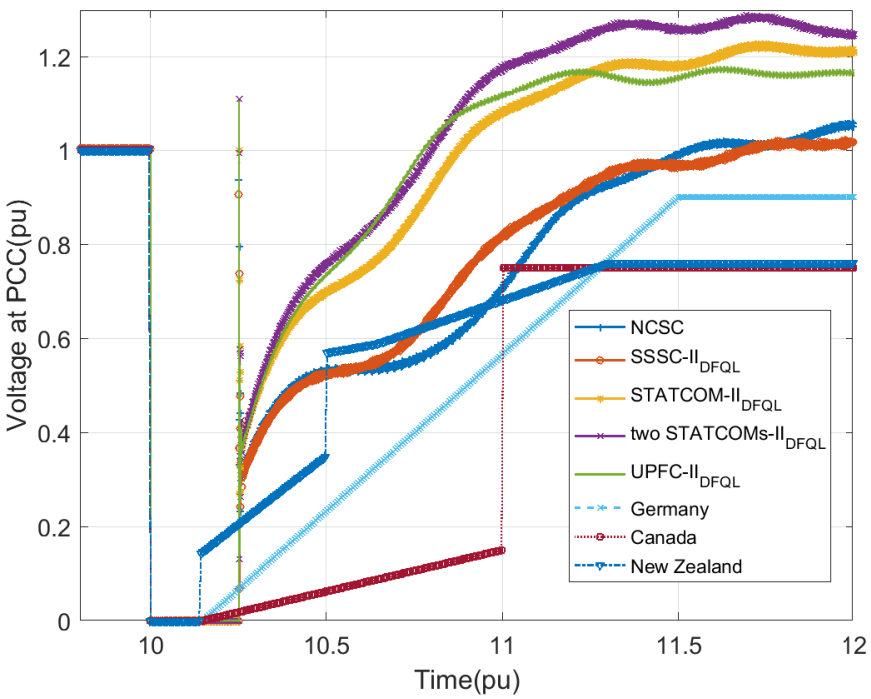

Figure 6.10: Performance of DFQL based controller in Case-II

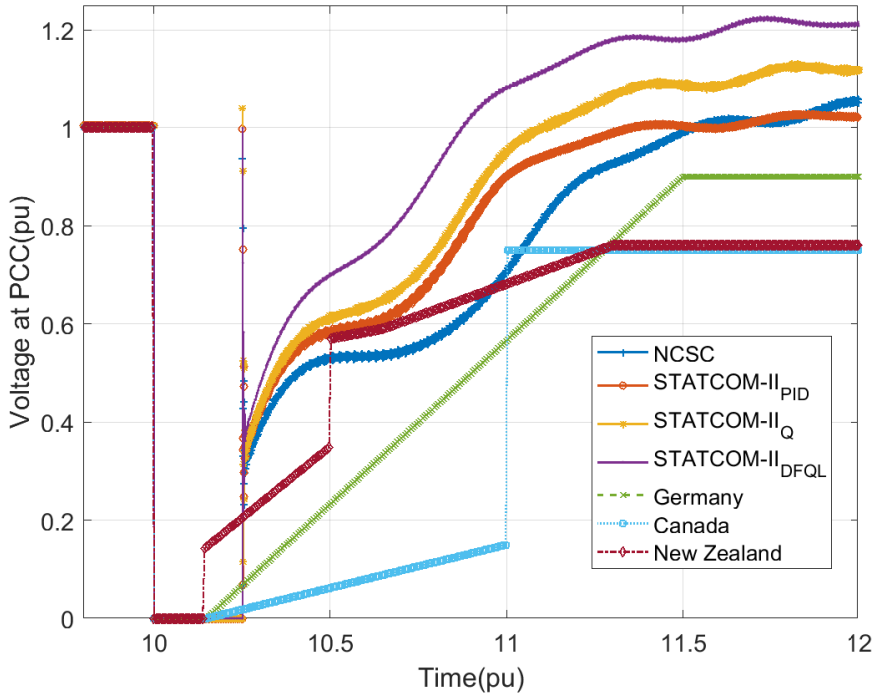

Figure 6.11: Performance of CSC configured as STATCOM-II in Case-II

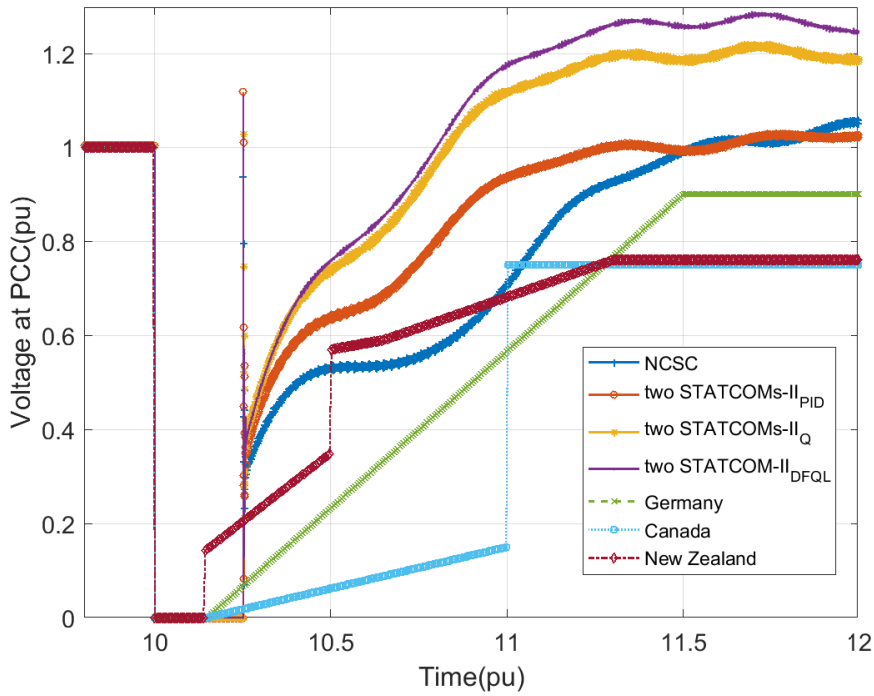

Figure 6.12: Performance of CSC configured as two STATCOMs in Case-II

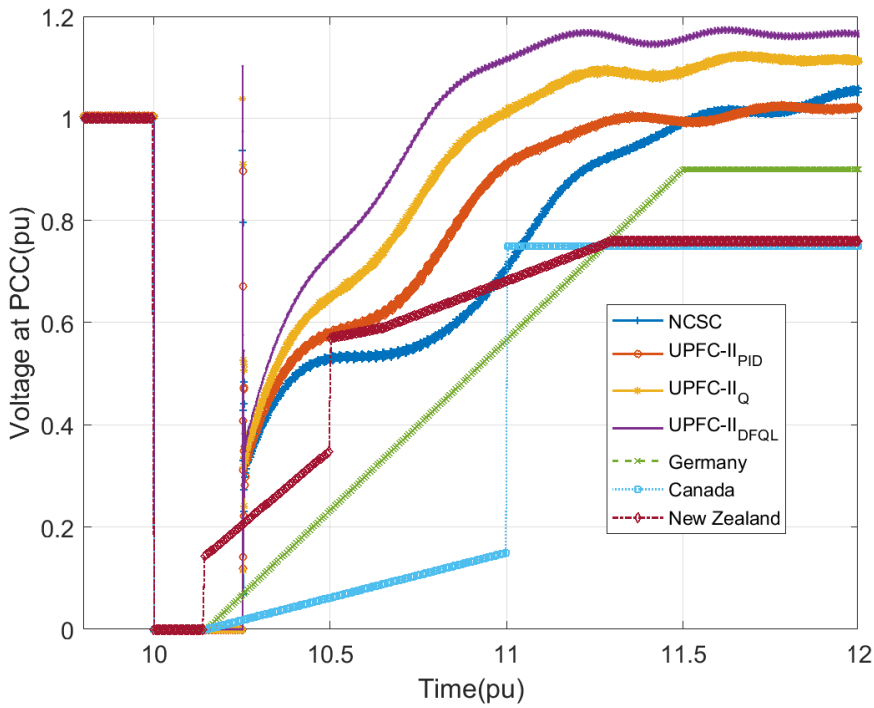

Figure 6.13: Performance of CSC configured as UPFC-II in Case-II

Table 6.8: Performance of different combinations in Case-II in regard to LVRT requirement of Canada (Hydro Quebec)

	PID	Q-learning	DFQL
SSSC-II	✗	✓	✓
STATCOM-II	✓	✓	✓
two STATCOMs	✓	✓	✓
UPFC-II	✓	✓	✓

Table 6.9: Performance of different combinations in Case-II in regard to LVRT requirement of New Zealand (North Island)

	PID	Q-learning	DFQL
SSSC-II	✗	✗	✗
STATCOM-II	✓	✓	✓
two STATCOMs	✓	✓	✓
UPFC-II	✓	✓	✓

Table 6.10: Critical recovering time in Case-II

	PID		Q-learning		DFQL	
	$T_{(V=0.75)}$ (sec)	$T_{(V=0.9)}$ (sec)	$T_{(V=0.75)}$ (sec)	$T_{(V=0.9)}$ (sec)	$T_{(V=0.75)}$ (sec)	$T_{(V=0.9)}$ (sec)
SSSC-II	10.98	11.81	10.92	11.22	10.90	11.17
STATCOM-II	10.85	11.00	10.80	10.94	10.61	10.78
two STATCOMs	10.74	10.92	10.51	10.74	10.48	10.70
UPFC-II	10.82	10.97	10.66	10.81	10.52	10.70

the configuration of UPFC-I could provide best LVRT performance. In Case-II, the CSC performs better when configured as two STATCOMs than other configurations. Among all the three controllers, DFQL controller provides highest benefit in LVRT capability enhancement for CSC configurations in both scenarios. Finally, the most effective combinations are recommended: configuration of UPFC-I and DFQL based controller for Case-I; and configuration of two STATCOMs and DFQL based controller for Case-II.

Chapter 7

Conclusions and Future Work

7.1 Conclusions

The results presented in this study explore the effective application of reinforcement learning (RL) controllers based on the principle of Q-learning and dynamic fuzzy Q-learning to improve the low-voltage ride-through (LVRT) of a hybrid power system consisting of both synchronous generators and wind energy systems.The present research has been carried out progressively towards achieving this goal.

The research begins with the application of RL controllers to improve the transient stability of both single machine and multi-machine power system consisting of synchronous generators alone. Both Q-learning and DFQL based controllers are designed by proper selection of the input ranges and the reward functions. The output of these controllers are used to determine the degree of series compensation of specific transmission lines. Their performances are compared with bang-bang control (BBC). The parameters of the BBC are optimized using particle swarm optimization (PSO). The simulation results have shown that the DFQL based controller, which offers continuous control outputs, is the fastest in stabilizing both the single and multi-machine power system compared to Q-learning controller which gives discrete control outputs. The PSO based bang-bang controller performs better than the Q-learning controller. However, its performance is poor compared to DFQL controller. It has been shown that the effectiveness of these controllers is not critically dependent on the choice of the compensated line provided these lines are close to the fault location.

After designing RL controllers for single and multi-machine power system with synchronous generators, the research progresses to design these controllers

for wind energy conversion system (WECS). The WECS investigated in this study consists of 20 DFIGs, each with a capacity of 5 MW. The dynamics of WECS is established by an aggregated wind turbine equipped with DFIG. Although WECS can be controlled either by controlling the grid side converter or the rotor side converter, we focus on controlling the system by rotor side converter. In this section, the inputs of RL based controllers are the difference of reference values of torque and reactive power and the actual values from the system; and the output of RL controllers give the rotor side voltage. The performances of designed Q-learning based and DFQL based controllers have been compared with classical PID controller and $\Delta\Sigma$ based PID controller. The controller design based on $\Delta\Sigma$ modulator offers several advantages compared to traditional controllers which are implemented in multi-bit. The simulation results have demonstrated that the DFQL based controller and the $\Delta\Sigma$ based PID controller performed better than other controllers. However, DFQL has a longer learning process.

Unlike the investigation in Chapter 3 and Chapter 4, the next phase of the research focuses on enhancing the low voltage ride through (LVRT) capability of hybrid power system by using unified power flow controller (UPFC). For this purpose, a hybrid three-machine power system consisting of two-synchronous generators and one wind farm are considered. This system is essentially the three-machine system studied in Chapter 3, where one of the synchronous machine is replaced by a wind-farm of the same capacity. The wind farm consists of 20 number of DFIGs, each with a capacity of 5MW. Following similar procedure as in Chapter 3 and Chapter 4, both Q-learning and DFQL based controllers are designed for UPFC. The outputs of RL controllers determine the required voltages and currents in the series and shunt branches of UPFC. Their performances were compared with classical PID controller, and the results show that DFQL based controller performed best among all these three controllers in terms of LVRT compliance of different grid codes.

After successfully achieving the LVRT capability using UPFC through different controllers, the last phase of the study investigated if this can be achieved by different configurations of convertible static compensator (CSC) in the hybrid power system. The CSC is considered as the most versatile flexible alternating current transmission system (FACTS) device which could be operated in 11 different configurations, such as series compensation, one STATCOM, two STATCOMs, UPFC and so on. This study compared the performance of Q-learning and DFQL based controllers with classical PID controller considering

several different configurations of CSC in two different scenarios where the fault is cleared by removing different transmission lines. The results show that all the configurations of CSC when controlled by DFQL based controller give the best performance from the perspective of LVRT enhancement. This is true irrespective of the fault scenarios. However, the configuration of UPFC-I is the best in Case-I where the fault is cleared by removing line 6 - 9; and the performance of CSC when configured as two STATCOMs in Case-II is best provided that the fault is cleared by removing line 8 - 9.

7.2 Future work

The following work is recommended for immediate future research.

- Apply the RL based controllers for FACTS devices in large-scale hybrid power system with varying degree of renewable energy penetration.
- Establish which configurations of CSC is optimum for various fault scenarios in large scale hybrid power system using different controllers.
- Study the feasibility of implementing $\Delta\Sigma$ based controllers (which are single-bit) for LVRT applications and develop better methods of tuning these controllers.

Appendix A

Synchronous Generation Power System

A.1 Three-machine synchronous power system

The parameters of the synchronous machines are listed in Table A.1. The power flow results of the three-machine synchronous power system are shown in Table A.2.

A.2 Excitation system

The excitation system in this study is IEEE-Type I excitation system shown in Fig. A.1, and the parameters are given in Table A.3 [169].

where, $S_{E_i} = 0.0039 * e^{1.555 E_{fd_i}}$, $i = 1, 2, 3$; and other parameter are lised in Table. A.3.

Table A.1: Synchronous machine data

Parameters	M/C1	M/C2	M/C3
$H(sec)$	23.64	6.4	3.01
$X_d(pu)$	0.146	0.8958	1.3125
$X'_d(pu)$	0.0608	0.1198	0.1813
$X_q(pu)$	0.0969	0.8645	1.2578
$X'_q(pu)$	0.0969	0.1969	0.25
$T'_{d0}(sec)$	8.96	6.0	5.89
$T'_{q0}(sec)$	0.31	0.535	0.6

Table A.2: Power flow results of 3-machine synchronous power system

	Node	Voltage magnitude (pu)	Voltage phase (rad)	P_G (pu)	Q_G (pu)	-P_L (pu)	-Q_L (pu)
1	slack bus	1.04	0	0.716	0.27	-	-
2	P-V	1.025	0.162	1.63	0.067	-	-
3	P-V	1.025	0.082	0.85	- 0.109	-	-
4	P-Q	1.026	0.038	-	-	-	-
5	P-Q	0.996	0.070	-	-	1.25	0.5
6	P-Q	1.013	-0.065	-	-	0.9	0.3
7	P-Q	1.026	0.065	-	-	-	-
8	P-Q	1.016	0.012	-	-	1.00	0.3
9	P-Q	1.032	0.035	-	-	-	-

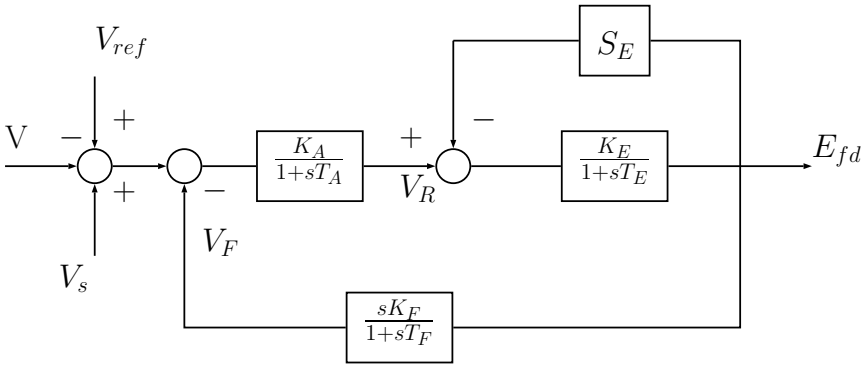

Figure A.1: IEEE-Type I excitation system

Table A.3: Exciter data

Parameters	Exciter 1	Exciter 2	Exciter 3
K_A	20	20	20
$T_A(sec)$	0.2	0.2	0.2
K_E	1.0	1.0	1.0
$T_E(sec)$	0.314	0.314	0.314
K_F	0.063	0.063	0.063
$T_F(sec)$	0.35	0.35	0.35

Bibliography

[1] V. Yaramasu, B. Wu, P. C. Sen, S. Kouro, and M. Narimani, "High-power Wind Energy Conversion Systems: State-of-the-art and Emerging Technologies," *Proceedings of the IEEE*, vol. 103, no. 5, pp. 740–788, 2015.

[2] R. Patnaik and P. Dash, "Impact of wind farms on disturbance detection and classification in distributed generation using modified adaline network and an adaptive neuro-fuzzy information system," *Applied Soft Computing*, vol. 30, pp. 549 – 566, 2015. [Online]. Available: http://www.sciencedirect.com/science/article/pii/S156849461500099X

[3] Y. Hashemi, H. Shayeghi, and M. Moradzadeh, "Design of dual-dimensional controller based on multi-objective gravitational search optimization algorithm for amelioration of impact of oscillation in power generated by large-scale wind farms," *Applied Soft Computing*, vol. 53, pp. 236 – 261, 2017. [Online]. Available: http://www.sciencedirect.com/science/article/pii/S1568494616306615

[4] World Wind Energy Association. WIND POWER CAPACITY WORLDWIDE REACHES 600 GW, 53.9 GW ADDED IN 2018. [Online]. Available: https://wwindea.org/blog/2019/02/25/wind-power-capacity-worldwide-reaches-600-gw-539-gw-added-in-2018/

[5] ——. WIND POWER CAPACITY REACHES 539 GW, 52.6 GW ADDED IN 2017. [Online]. Available: https://wwindea.org/blog/2018/02/12/2017-statistics/

[6] ——. Wwea half-year report: Worldwind wind capacity reached 456 gw. [Online]. Available: https://wwindea.org/blog/2016/10/10/wwea-half-year-report-worldwind-wind-capacity-reached-456-gw/

[7] ——. THE WORLD SETS NEW WIND INSTALLATIONS RECORD: 63,7 GW NEW CAPACITY IN 2015.

[Online]. Available: https://wwindea.org/blog/2016/02/10/the-world-sets-new-wind-installations-record-637-gw-new-capacity-in-2015/

[8] ——. WWEA PUBLISHES HALF-YEAR REPORT 2014. [Online]. Available: https://wwindea.org/blog/2014/09/17/wwea-publishes-half-year-report-2014/

[9] ——. WWEA PUBLISHES HALF-YEAR REPORT 2013. [Online]. Available: https://wwindea.org/blog/2013/10/17/wwea-publishes-half-year-report-2013-2/

[10] ——. WORLD WIND WORLD REPORT 2012 LAUNCHED. [Online]. Available: https://wwindea.org/blog/2013/05/17/world-wind-world-report-2012-launched/

[11] ——. WORLD WIND ENERGY REPORT 2011 LAUNCHED. [Online]. Available: https://wwindea.org/blog/2012/07/01/world-wind-energy-report-2011-launched/

[12] M. Edrah, K. Lo, and O. Anaya-Lara, "Impacts of high penetration of DFIG wind turbines on rotor angle stability of power systems," *Sustainable Energy, IEEE Transactions on*, vol. 6, no. 3, pp. 759–766, 07 2015.

[13] T. Ackermann, *Wind power in power systems.* John Wiley & Sons, Ltd., 2012.

[14] B. Mahdad, "Contribution to the improvement of power quality using multi hybrid model based wind-shunt facts," in *2011 10th International Conference on Environment and Electrical Engineering*, 05 2011, pp. 1–5.

[15] A. Beekmann, J. Marques, E. Quitmann, and S. Wachtel, "Wind energy converters with facts capabilities for optimized integration of wind power into transmission and distribution systems," in *2009 CIGRE/IEEE PES Joint Symposium Integration of Wide-Scale Renewable Resources Into the Power Delivery System*, 07 2009, pp. 1–1.

[16] M. S. Li, T. Y. Ji, Y. Z. Li, and Q. H. Wu, "Optimal voltage control with uncertain wind power using facts devices," in *2013 IEEE Power Energy Society General Meeting*, 07 2013, pp. 1–5.

[17] V. K. Polisetty, S. R. Jetti, G. K. Venayagamoorthy, and R. G. Harley, "Intelligent integration of a wind farm to an utility power network with improved voltage stability," in *Conference Record of the 2006 IEEE Industry Applications Conference Forty-First IAS Annual Meeting*, vol. 3, 10 2006, pp. 1128–1133.

[18] J. R. Williams, D. G. Wilson, and R. D. Robinett, "Transient stability and performance based on nonlinear power flow control design of wind turbines," in *International Symposium on Power Electronics Power Electronics, Electrical Drives, Automation and Motion*, 06 2012, pp. 559–564.

[19] M. Lekshmi and J. Vishnu, "Improvement of transient stability in PMSG based wind integrated system using fod controlled FACTS device," in *2017 International Conference on Circuit ,Power and Computing Technologies (ICCPCT)*, April 2017, pp. 1–8.

[20] H. Nguyen-Duc, L. Dessaint, A. F. Okou, and I. Kamwa, "A power oscillation damping control scheme based on bang-bang modulation of FACTS signals," *IEEE Transactions on Power Systems*, vol. 25, no. 4, pp. 1918–1927, 11 2010.

[21] Y. Li, C. Rehtanz, S. Ruberg, L. Luo, and Y. Cao, "Wide-area robust coordination approach of HVDC and FACTS controllers for damping multiple interarea oscillations," *IEEE Transactions on Power Delivery*, vol. 27, no. 3, pp. 1096–1105, 07 2012.

[22] L. Wang and D. Truong, "Stability enhancement of DFIG-based offshore wind farm fed to a multi-machine system using a STATCOM," *IEEE Transactions on Power Systems*, vol. 28, no. 3, pp. 2882–2889, 08 2013.

[23] "Optimal resource allocation using reinforcement learning for IoT content-centric services," *Applied Soft Computing*, vol. 70, pp. 12 – 21, 2018.

[24] D. Ye, M. Zhang, and D. Sutanto, "A hybrid multiagent framework with Q-learning for power grid systems restoration," *IEEE Transactions on Power Systems*, vol. 26, no. 4, pp. 2434–2441, 11 2011.

[25] J. Duan, H. Xu, and W. Liu, "Q-learning-based damping control of wide-area power systems under cyber uncertainties," *IEEE Transactions on Smart Grid*, vol. 9, no. 6, pp. 6408–6418, 11 2018.

[26] M. J. Er and C. Deng, "Online tuning of fuzzy inference systems using dynamic fuzzy Q-learning," *IEEE Transactions on Systems, Man, and Cybernetics, Part B (Cybernetics)*, vol. 34, no. 3, pp. 1478–1489, 06 2004.

[27] L. Jouffe, "Fuzzy inference system learning by reinforcement methods," *IEEE Transactions on Systems, Man, and Cybernetics, Part C (Applications and Reviews)*, vol. 28, no. 3, pp. 338–355, 08 1998.

[28] R. E. P. N. for the 21st Century (REN21), "Renewables global status report," 2018. [Online]. Available: http://www.ren21.net/status-of-renewables/global-status-report/

[29] M. J. Morshed and A. Fekih, "A probabilistic robust coordinated approach to stabilize power oscillations in DFIG-based power systems," *IEEE Transactions on Industrial Informatics*, pp. 1–1, 2019.

[30] S. Yu, T. Fernando, H. H. Iu, and K. Emami, "Realization of state-estimation-based DFIG wind turbine control design in hybrid power systems using stochastic filtering approaches," *IEEE Transactions on Industrial Informatics*, vol. 12, no. 3, pp. 1084–1092, 06 2016.

[31] S. M. Muyeen, R. Takahashi, T. Murata, and J. Tamura, "A variable speed wind turbine control strategy to meet wind farm grid code requirements," *IEEE Transactions on Power Systems*, vol. 25, no. 1, pp. 331–340, Feb 2010.

[32] A. Das, K. B. Chimonyo, T. R. Kumar, S. Gourishankar, and C. Rani, "Vertical axis and horizontal axis wind turbine- a comprehensive review," in *2017 International Conference on Energy, Communication, Data Analytics and Soft Computing (ICECDS)*, 08 2017, pp. 2660–2669.

[33] M. Tata, F. Massouh, I. Dobrev, and A. Smaili, "Experimental and numerical analysis of a scaled wind turbine near wake," in *2018 International Conference on Wind Energy and Applications in Algeria (ICWEAA)*, 11 2018, pp. 1–6.

[34] M. E. Harrison, W. M. J. Batten, and A. S. Bahaj, "A blade element actuator disc approach applied to tidal stream turbines," in *OCEANS 2010 MTS/IEEE SEATTLE*, 09. 2010, pp. 1–8.

[35] I. Erlich, J. Kretschmann, J. Fortmann, S. Mueller-Engelhardt, and H. Wrede, "Modeling of wind turbines based on doubly-fed induction generators for power system stability studies," *IEEE Transactions on Power Systems*, vol. 22, no. 3, pp. 909–919, 08 2007.

[36] E. J. Bueno, S. Cobreces, F. J. RodrÍguez, A. Hernandez, and F. Espinosa, "Design of a back-to-back NPC converter interface for wind turbines with squirrel-cage induction generator," *IEEE Transactions on Energy Conversion*, vol. 23, no. 3, pp. 932–945, 09 2008.

[37] H. Chen and D. C. Aliprantis, "Analysis of squirrel-cage induction generator with vienna rectifier for wind energy conversion system," *IEEE Transactions on Energy Conversion*, vol. 26, no. 3, pp. 967–975, 09 2011.

[38] R. Pena, J. C. Clare, and G. M. Asher, "Doubly fed induction generator using back-to-back PWM converters and its application to variable-speed wind-energy generation," *IEE Proceedings - Electric Power Applications*, vol. 143, no. 3, pp. 231–241, 05 1996.

[39] S. Muller, M. Deicke, and R. W. De Doncker, "Doubly fed induction generator systems for wind turbines," *IEEE Industry Applications Magazine*, vol. 8, no. 3, pp. 26–33, 05 2002.

[40] A. Tapia, G. Tapia, J. X. Ostolaza, and J. R. Saenz, "Modeling and control of a wind turbine driven doubly fed induction generator," *IEEE Transactions on Energy Conversion*, vol. 18, no. 2, pp. 194–204, 06 2003.

[41] S. Mourad and R. Habib, "Stand alone synchronous operation of wound rotor induction generator," in *2016 7th International Renewable Energy Congress (IREC)*, 03 2016, pp. 1–4.

[42] H. Ashfaq, S. A. Nahvi, and M. S. J. Asghar, "A personal-computer based controller for performance improvement of grid-connected wound-rotor induction generators," in *2006 IEEE International Power and Energy Conference*, 11 2006, pp. 432–436.

[43] S. Bayhan, H. Fidanboy, and S. Demirbas, "Active and reactive power control of grid connected permanent magnet synchronous generator in wind power conversion system," in *2013 International Conference on Renewable Energy Research and Applications (ICRERA)*, 10 2013, pp. 1048–1052.

[44] L. Dong, S. Gao, M. Liu, and X. Liao, "Non-grid-connected wind power generating system with permanent magnet synchronous generator and buck/boost converter," in *2009 World Non-Grid-Connected Wind Power and Energy Conference*, 09 2009, pp. 1–5.

[45] M. S. Ullah Khan, A. I. Maswood, K. Satpathi, M. T. Iqbal, and A. Tripathi, "Analysis of brushless wound rotor synchronous generator with unity power factor rectifier for series offshore dc wind power collection," in *IECON 2018 - 44th Annual Conference of the IEEE Industrial Electronics Society*, 10 2018, pp. 1693–1698.

[46] E. Muljadi and C. P. Butterfield, "Pitch-controlled variable-speed wind turbine generation," *IEEE Transactions on Industry Applications*, vol. 37, no. 1, pp. 240–246, 2001.

[47] A. Abir, D. Mehdi, and S. Lassaad, "Pitch angle control of the variable speed wind turbine," in *2016 17th International Conference on Sciences and Techniques of Automatic Control and Computer Engineering (STA)*, 2016, pp. 582–587.

[48] T. Ackermann, *Wind power in power systems.* A John Wiley & Sons, Ltd., 2012.

[49] L. Holdsworth, X. G. Wu, J. B. Ekanayake, and N. Jenkins, "Comparison of fixed speed and doubly-fed induction wind turbines during power system disturbances," *IEE Proceedings - Generation, Transmission and Distribution*, vol. 150, no. 3, pp. 343–352, 05 2003.

[50] Q. Wang and L. Chang, "An intelligent maximum power extraction algorithm for inverter-based variable speed wind turbine systems," *IEEE Transactions on Power Electronics*, vol. 19, no. 5, pp. 1242–1249, 09 2004.

[51] K. Tan, "Squirrel-cage induction generator system using wavelet petri fuzzy neural network control for wind power applications," *IEEE Transactions on Power Electronics*, vol. 31, no. 7, pp. 5242–5254, 07 2016.

[52] M. Hassan Zamani, G. Hossein Riahy, and M. Abedi, "Rotor-speed stability improvement of dual stator-winding induction generator-based wind farms by control-windings voltage oriented control," *IEEE Transactions on Power Electronics*, vol. 31, no. 8, pp. 5538–5546, 08 2016.

[53] A. M. Howlader, N. Urasaki, T. Senjyu, A. Yona, T. Funabashi, and A. Y. Saber, "Output power leveling of wind generation system using inertia for pm synchronous generator," in *2009 International Conference on Power Electronics and Drive Systems (PEDS)*, 11 2009, pp. 1289–1294.

[54] O. A. Morfin, R. Ruiz-Cruz, F. Ornelas-Tellez, A. Campos-Valdillez, R. Ramírez-Betancour, N. Padilla, and J. A. Gándara, "Maximum wind energy capture in a wind system using a doubly-fed induction generator," in *2018 IEEE International Autumn Meeting on Power, Electronics and Computing (ROPEC)*, 11 2018, pp. 1–6.

[55] M. Chinchilla, S. Arnaltes, and J. C. Burgos, "Control of permanent-magnet generators applied to variable-speed wind-energy systems connected to the grid," *IEEE Transactions on Energy Conversion*, vol. 21, no. 1, pp. 130–135, 03 2006.

[56] Z. Chen, J. M. Guerrero, and F. Blaabjerg, "A review of the state of the art of power electronics for wind turbines," *IEEE Transactions on Power Electronics*, vol. 24, no. 8, pp. 1859–1875, 08 2009.

[57] J. Morren and S. W. H. de Haan, "Ride through of wind turbines with doubly-fed induction generator during a voltage dip," *IEEE Transactions on Energy Conversion*, vol. 20, no. 2, pp. 435–441, 06 2005.

[58] H. Polinder, F. F. A. van der Pijl, G. . de Vilder, and P. J. Tavner, "Comparison of direct-drive and geared generator concepts for wind turbines," *IEEE Transactions on Energy Conversion*, vol. 21, no. 3, pp. 725–733, 09 2006.

[59] A. E. Leon, M. F. Farias, P. E. Battaiotto, J. A. Solsona, and M. I. Valla, "Control strategy of a DVR to improve stability in wind farms using squirrel-cage induction generators," *IEEE Transactions on Power Systems*, vol. 26, no. 3, pp. 1609–1617, 08 2011.

[60] Y. Lin, "Comparison of speed and voltage based critical clearing time of squirrel cage induction generator," in *2010 IEEE 11th International Conference on Probabilistic Methods Applied to Power Systems*, 06 2010, pp. 283–286.

[61] H. Li and Z. Chen, "Overview of different wind generator systems and their comparisons," *IET Renewable Power Generation*, vol. 2, no. 2, pp. 123–138, 06 2008.

[62] J. B. Ekanayake, L. Holdsworth, X. Wu, and N. Jenkins, "Dynamic modeling of doubly fed induction generator wind turbines," *IEEE Transactions on Power Systems*, vol. 18, no. 2, pp. 803–809, 05 2003.

[63] P. K. Naik, N. C. Nair, and A. K. Swain, "Impact of reduced inertia on transient stability of networks with asynchronous generation," *International Transactions on Electrical Energy Systems*, vol. 26, no. 1, pp. 175–191, 2016.

[64] R. K. Patnaik and P. K. Dash, "Fast adaptive back-stepping terminal sliding mode power control for both the rotor-side as well as grid-side converter of the doubly fed induction generator-based wind farms," *IET Renewable Power Generation*, vol. 10, no. 5, pp. 598–610, 2016.

[65] L. Zhou, A. Swain, P. K. Naik, F. Hafiz, and N. K. C. Nair, "Optimum design of series compensation to improve power system transient stability using DFQL and PSO based controllers," in *2017 13th IEEE International Conference on Control Automation (ICCA)*, 07 2017, pp. 1125–1130.

[66] A. Junyent-Ferré, O. Gomis-Bellmunt, A. Sumper, M. Sala, and M. Mata, "Modeling and control of the doubly fed induction generator wind turbine," *Simulation Modelling Practice and Theory*, vol. 18, no. 9, pp. 1365 – 1381, 2010.

[67] E. H. Camm, M. R. Behnke, O. Bolado, M. Bollen, M. Bradt, C. Brooks, W. Dilling, M. Edds, W. J. Hejdak, D. Houseman, S. Klein, F. Li, J. Li, P. Maibach, T. Nicolai, J. Patino, S. V. Pasupulati, N. Samaan, S. Saylors, T. Siebert, T. Smith, M. Starke, and R. Walling, "Characteristics of wind turbine generators for wind power plants," in *2009 IEEE Power Energy Society General Meeting*, 07 2009, pp. 1–5.

[68] M. Tsili and S. Papathanassiou, "A review of grid code technical requirements for wind farms," *IET Renewable Power Generation*, vol. 3, no. 3, pp. 308–332, 09 2009.

[69] "Dynamic characteristic analysis of doubly-fed induction generator low voltage ride-through," *Energy Procedia*, vol. 16, pp. 1526 – 1534, 2012,

2012 International Conference on Future Energy, Environment, and Materials.

[70] K. A. Saleh, M. S. E. Moursi, and H. H. Zeineldin, "A New Protection Scheme Considering Fault Ride Through Requirements for Transmission Level Interconnected Wind Parks," *IEEE Transactions on Industrial Informatics*, vol. 11, no. 6, pp. 1324–1333, 12 2015.

[71] T. H. Nguyen, K. Hassan Al Hosani, and M. El Moursi, "Alternating submodule configuration based MMCs with carrier-phase-shift modulation in HVDC systems for DC-fault ride-through capability," *IEEE Transactions on Industrial Informatics*, pp. 1–1, 2019.

[72] S. Tohidi and M.-I. Behnam, "A comprehensive review of low voltage ride through of doubly fed induction wind generators," *Renewable and Sustainable Energy Reviews*, vol. 57, pp. 412–419, 2016.

[73] A. Howlader and T. Senjyu, "A comprehensive review of low voltage ride through capability strategies for the wind energy conversion systems," *Renewable and Sustainable Energy Reviews*, vol. 56, pp. 643–658, 2016.

[74] S. M. Muyeen, R. Takahashi, T. Murata, and J. Tamura, "A variable speed wind turbine control strategy to meet wind farm grid code requirements," *IEEE Transactions on Power Systems*, vol. 25, no. 1, pp. 331–340, 2 2010.

[75] L. Yang, Z. Xu, J. Ostergaard, Z. Y. Dong, and K. P. Wong, "Advanced control strategy of DFIG wind turbines for power system fault ride through," *IEEE Transactions on Power Systems*, vol. 27, no. 2, pp. 713–722, 05 2012.

[76] J. Lopez, P. Sanchis, E. Gubia, A. Ursua, L. Marroyo, and X. Roboam, "Control of doubly fed induction generator under symmetrical voltage dips," in *2008 IEEE International Symposium on Industrial Electronics*, 06 2008, pp. 2456–2462.

[77] S. Hu, X. Zou, and Y. Kang, "A novel optimal design of DFIG crowbar resistor during grid faults," in *2014 International Power Electronics Conference (IPEC-Hiroshima 2014 - ECCE ASIA)*, 05 2014, pp. 555–559.

[78] X. Yang, L. Li, and F. Jiang, "A control strategy combining sliding mode controller with crowbar circuit for low voltage ride through of direct-drive

wind power system," in *2nd IET Renewable Power Generation Conference (RPG 2013)*, 09 2013, pp. 1–4.

[79] L. Peng, B. Francois, and Y. Li, "Improved crowbar control strategy of DFIG based wind turbines for grid fault ride-through," in *2009 Twenty-Fourth Annual IEEE Applied Power Electronics Conference and Exposition*, 02 2009, pp. 1932–1938.

[80] C. Wessels and F. W. Fuchs, "Fault ride through of DFIG wind turbines during symmetrical voltage dip with crowbar or stator current feedback solution," in *2010 IEEE Energy Conversion Congress and Exposition*, 09 2010, pp. 2771–2777.

[81] and and, "Short circuit current analysis of DFIG-type wg with crowbar protection under grid faults," in *2012 IEEE International Symposium on Industrial Electronics*, 05 2012, pp. 1072–1079.

[82] L. Zhang, X. Jin, and L. Zhan, "A novel LVRT control strategy of DFIG based rotor active crowbar," in *2011 Asia-Pacific Power and Energy Engineering Conference*, 03 2011, pp. 1–6.

[83] S. Hu, X. Lin, Y. Kang, and X. Zou, "An improved low-voltage ride-through control strategy of doubly fed induction generator during grid faults," *IEEE Transactions on Power Electronics*, vol. 26, no. 12, pp. 3653–3665, 12 2011.

[84] J. Vidal, G. Abad, J. Arza, and S. Aurtenechea, "Single-phase dc crowbar topologies for low voltage ride through fulfillment of high-power doubly fed induction generator-based wind turbines," *IEEE Transactions on Energy Conversion*, vol. 28, no. 3, pp. 768–781, 09 2013.

[85] S. Tohidi, H. Oraee, M. R. Zolghadri, S. Shao, and P. Tavner, "Analysis and enhancement of low-voltage ride-through capability of brushless doubly fed induction generator," *IEEE Transactions on Industrial Electronics*, vol. 60, no. 3, pp. 1146–1155, 03 2013.

[86] M. Y. Suberu, M. W. Mustafa, and N. Bashir, "Energy storage systems for renewable energy power sector integration and mitigation of intermittency," *Renewable and Sustainable Energy Reviews*, vol. 35, pp. 499 – 514, 2014.

[87] Y. Shen, D. Ke, Y. Sun, D. S. Kirschen, W. Qiao, and X. Deng, "Advanced auxiliary control of an energy storage device for transient voltage support of a doubly fed induction generator," *IEEE Transactions on Sustainable Energy*, vol. 7, no. 1, pp. 63–76, 01 2016.

[88] N. Saadat, S. S. Choi, and D. M. Vilathgamuwa, "A statistical evaluation of the capability of distributed renewable generator-energy-storage system in providing load low-voltage ride-through," *IEEE Transactions on Power Delivery*, vol. 30, no. 3, pp. 1128–1136, 06 2015.

[89] C. Abbey and G. Joos, "Short-term energy storage for wind energy applications," in *Fourtieth IAS Annual Meeting. Conference Record of the 2005 Industry Applications Conference, 2005.*, vol. 3, 10 2005, pp. 2035–2042 Vol. 3.

[90] M. Kabir, Y. Mishra, G. Ledwich, Z. Dong, and K. Wong, "Coordinated control of grid-connected photovoltaic reactive power and battery energy storage systems to improve the voltage profile of a residential distribution feeder," *IEEE Transactions on Industrial Informatics*, vol. 10, no. 2, pp. 967–977, 2014.

[91] J. I. Y. Ota, T. Sato, and H. Akagi, "Enhancement of performance, availability, and flexibility of a battery energy storage system based on a modular multilevel cascaded converter (MMCC-SSBC)," *IEEE Transactions on Power Electronics*, vol. 31, no. 4, pp. 2791–2799, 04 2016.

[92] M. I. Daoud, A. M. Massoud, A. S. Abdel-Khalik, A. Elserougi, and S. Ahmed, "A flywheel energy storage system for fault ride through support of grid-connected VSC HVDC-based offshore wind farms," *IEEE Transactions on Power Systems*, vol. 31, no. 3, pp. 1671–1680, 05 2016.

[93] W. Guo, L. Xiao, and S. Dai, "Enhancing low-voltage ride-through capability and smoothing output power of DFIG with a superconducting fault-current limiter–magnetic energy storage system," *IEEE Transactions on Energy Conversion*, vol. 27, no. 2, pp. 277–295, 06 2012.

[94] Y. Shen, D. Ke, W. Qiao, Y. Sun, D. S. Kirschen, and C. Wei, "Transient reconfiguration and coordinated control for power converters to enhance the LVRT of a DFIG wind turbine with an energy storage device," *IEEE Transactions on Energy Conversion*, vol. 30, no. 4, pp. 1679–1690, 12 2015.

[95] C. Jin and P. Wang, "Enhancement of low voltage ride-through capability for wind turbine driven DFIG with active crowbar and battery energy storage system," in *IEEE PES General Meeting*, 07 2010, pp. 1–8.

[96] K. Ibrahima and C. Zhao, "Modeling of wind energy conversion system using doubly fed induction generator equipped batteries energy storage system," in *2011 4th International Conference on Electric Utility Deregulation and Restructuring and Power Technologies (DRPT)*, 07 2011, pp. 1780–1787.

[97] T. Gayathri, D. V. N. Ananth, G. V. N. Kumar, and G. Sivanagaraju, "Enhancement in dynamic and LVRT behaviour of an efoc controlled dfig with integrated battery energy storage system," in *2013 Annual IEEE India Conference (INDICON)*, 12 2013, pp. 1–6.

[98] M. Worku and M. Abido, "Fault ride-through and power smoothing control of PMSG-based wind generation using super-capacitor energy storage system," *Arabian Journal for Science and Engineering*, vol. 44, no. 3, pp. 2067–2078, 2019.

[99] A. Rahim and E. Nowicki, "Supercapacitor energy storage system for fault ride-through of a DFIG wind generation system," *Energy Conversion and Management*, vol. 59, pp. 96–102, 2012.

[100] W. Guo, J. Zhang, N. Song, Z. Gao, T. Ma, Z. Zhu, X. Xu, L. Li, Y. Wang, S. Dai, and L. Xiao, "Overview and development progress of a 1-mva/1-mj superconducting fault current limiter-magnetic energy storage system," *IEEE Transactions on Applied Superconductivity*, vol. 26, no. 3, pp. 1–5, 04 2016.

[101] L. Chen, G. Li, H. Chen, Y. Xu, L. Ren, and Y. Tang, "Low-voltage ride-through improvement in a DFIG based wind turbine by integrated use of a sfcl and dc-link regulation of a smes system," in *2018 IEEE International Conference on Applied Superconductivity and Electromagnetic Devices (ASEMD)*, 04 2018, pp. 1–2.

[102] X.-Y. Xiao, R.-H. Yang, Z.-X. Zheng, and Y. Wang, "Cooperative rotor-side smes and transient control for improving the LVRT capability of grid-connected DFIG-based wind farm," *IEEE Transactions on Applied Superconductivity*, vol. 29, no. 2, 2019.

[103] M. S. Guney and Y. Tepe, "Classification and assessment of energy storage systems," *Renewable and Sustainable Energy Reviews*, vol. 75, pp. 1187 – 1197, 2017.

[104] H. Zhao, Q. Wu, S. Hu, H. Xu, and C. N. Rasmussen, "Review of energy storage system for wind power integration support," *Applied Energy*, vol. 137, pp. 545 – 553, 2015.

[105] M. Świerczyński, R. Teodorescu, C. N. Rasmussen, P. Rodriguez, and H. Vikelgaard, "Overview of the energy storage systems for wind power integration enhancement," in *2010 IEEE International Symposium on Industrial Electronics*, 07 2010, pp. 3749–3756.

[106] M. Rahimi and M. Parniani, "Coordinated control approaches for low-voltage ride-through enhancement in wind turbines with doubly fed induction generators," *IEEE Transactions on Energy Conversion*, vol. 25, no. 3, pp. 873–883, 09 2010.

[107] E. Gatavi, A. Hellany, M. Nagrial, and J. Rizk, "Improved low voltage ride-through capability of DFIG-based wind turbine with breaking resistor and converter control," in *2018 IEEE 12th International Conference on Compatibility, Power Electronics and Power Engineering (CPE-POWERENG 2018)*, 04 2018, pp. 1–6.

[108] Z. Linyuan, L. Jinjun, and L. Fangcheng, "Low voltage ride-through of wind farms using STATCOM combined with series dynamic breaking resistor," in *The 2nd International Symposium on Power Electronics for Distributed Generation Systems*, 06 2010, pp. 841–845.

[109] W. Sanusi, M. Al Hosani, and M. S. E. Moursi, "A novel dc fault ride-through scheme for MTDC networks connecting large-scale wind parks," *IEEE Transactions on Sustainable Energy*, vol. 8, no. 3, pp. 1086–1095, 07 2017.

[110] M. H. Ali and S. D. Alnajjar, "Fault ride through capability enhancement of grid-connected fuel cell system by SDBR," in *2018 IEEE Power Energy Society General Meeting (PESGM)*, 08 2018, pp. 1–5.

[111] P. Huang, M. S. El Moursi, W. Xiao, and J. L. Kirtley Jr, "Novel fault ride-through configuration and transient management scheme for doubly fed

induction generator," *IEEE Transactions on Energy Conversion*, vol. 28, no. 1, pp. 86–94, 03 2013.

[112] T. Ji, X. He, X. Li, K. Liu, and M. Zhang, "Performance analysis and research on LVRT of PMSG wind power systems with SDBR," in *Proceedings of the 33rd Chinese Control Conference*, 07 2014, pp. 6953–6958.

[113] K. E. Okedu, "Optimal position and best switching signal of sdbr in DFIG wind turbine low voltage ride through low voltage ride through capability of doubly fed induction generators," in *2017 IEEE International Electric Machines and Drives Conference (IEMDC)*, 05 2017, pp. 1–6.

[114] Y. Wei, L. Hong, Q. Jiang, and Z. Wang, "A new dynamic strategy for improved ride-through capability of wind turbine generator," in *2011 IEEE Power and Energy Society General Meeting*, 07 2011, pp. 1–6.

[115] M. A. H. Soliman, H. Soliman, and P. K. Soori, "Analysis of the dynamic behavior and LVRT capability of a DFIG using SDBR during grid disturbances," in *2013 7th IEEE GCC Conference and Exhibition (GCC)*, 11 2013, pp. 436–439.

[116] H. A. Mohammadpour, A. Ghaderi, H. Mohammadpour, and M. H. Ali, "Low voltage ride-through enhancement of fixed-speed wind farms using series FACTS controllers," *Sustainable Energy Technologies and Assessments*, vol. 9, pp. 12 – 21, 2015.

[117] L. Zhou, J. Liu, and F. Liu, "Design and implementation of STATCOM combined with series dynamic breaking resistor for low voltage ride-through of wind farms," in *2010 IEEE Energy Conversion Congress and Exposition*, 09 2010, pp. 2501–2506.

[118] T. L. Van, T. H. Truong, M. T. Cao, P. C. Nguyen, and H. Nguyen, "Improved control scheme for low voltage ride-through of PMSG-based wind energy conversion systems," in *2018 4th International Conference on Green Technology and Sustainable Development (GTSD)*, 11 2018, pp. 169–164.

[119] G. Pannell, B. Zahawi, D. J. Atkinson, and P. Missailidis, "Evaluation of the performance of a dc-link brake chopper as a DFIG low-voltage fault-ride-through device," *IEEE Transactions on Energy Conversion*, vol. 28, no. 3, pp. 535–542, 09 2013.

[120] J. F. Conroy and R. Watson, "Low-voltage ride-through of a full converter wind turbine with permanent magnet generator," *IET Renewable Power Generation*, vol. 1, no. 3, pp. 182–189, 09 2007.

[121] S. Galvani, M. T. Hagh, M. B. B. Sharifian, and B. Mohammadi-ivatloo, "Multi-Objective Predictability Based Optimal Placement and Parameters Setting of UPFC in Wind Power Included Power Systems," *IEEE Transactions on Industrial Informatics*, pp. 1–1, 2018.

[122] C. Li, J. Deng, and X. Zhang, "Coordinated design and application of robust damping controllers for shunt FACTS devices to enhance small-signal stability of large-scale power systems," *CSEE Journal of Power and Energy Systems*, vol. 3, no. 4, pp. 399–407, 12 2017.

[123] L. H. Hassan, M. Moghavvemi, H. A. F. Almurib, and K. M. Muttaqi, "A Coordinated Design of PSSs and UPFC-based Stabilizer Using Genetic Algorithm," *IEEE Transactions on Industry Applications*, vol. 50, no. 5, pp. 2957–2966, 09 2014.

[124] N. Yorino, E. E. El-Araby, H. Sasaki, and S. Harada, "A new formulation for FACTS allocation for security enhancement against voltage collapse," *IEEE Transactions on Power Systems*, vol. 18, no. 1, pp. 3–10, 02 2003.

[125] R. Manuela Monteiro Pereira, C. Manuel Machado Ferreira, and F. Maciel Barbosa, "Comparative study of STATCOM and SVC performance on dynamic voltage collapse of an electric power system with wind generation," *IEEE Latin America Transactions*, vol. 12, no. 2, pp. 138–145, 03 2014.

[126] S. Yu, T. K. Chau, T. Fernando, A. V. Savkin, and H. H. Iu, "Novel quasi-decentralized smc-based frequency and voltage stability enhancement strategies using valve position control and FACTS device," *IEEE Access*, vol. 5, pp. 946–955, 2017.

[127] D. Thukaram and G. Yesuratnam, "Optimal reactive power dispatch in a large power system with AC-DC and FACTS controllers," *IET Generation, Transmission Distribution*, vol. 2, no. 1, pp. 71–81, 01 2008.

[128] R. S. Wibowo, N. Yorino, M. Eghbal, Y. Zoka, and Y. Sasaki, "FACTS devices allocation with control coordination considering congestion relief and voltage stability," *IEEE Transactions on Power Systems*, vol. 26, no. 4, pp. 2302–2310, 11 2011.

[129] X. Wei, J. H. Chow, B. Fardanesh, and A. A. Edris, "A dispatch strategy for a unified power-flow controller to maximize voltage-stability-limited power transfer," *IEEE Transactions on Power Delivery*, vol. 20, no. 3, pp. 2022–2029, 07 2005.

[130] H. Wang, "A unified model for the analysis of FACTS devices in damping power system oscillations. III. unified power flow controller," *IEEE Transactions on Power Delivery*, vol. 15, no. 3, pp. 978–983, 07 2000.

[131] E. Gholipour and S. Saadate, "Improving of transient stability of power systems using UPFC," *IEEE Transactions on Power Delivery*, vol. 20, no. 2, pp. 1677–1682, 04 2005.

[132] M. M. Eladany, A. A. Eldesouky, and A. A. Sallam, "Power system transient stability: An algorithm for assessment and enhancement based on catastrophe theory and FACTS devices," *IEEE Access*, vol. 6, pp. 26 424–26 437, 2018.

[133] Y. L. Tan and Y. Wang, "Effects of FACTS controller line compensation on power system stability," *IEEE Power Engineering Review*, vol. 18, no. 8, pp. 55–56, 08 1998.

[134] Y. Wang, R. R. Mohler, R. Spee, and W. Mittelstadt, "Variable-structure FACTS controllers for power system transient stability," *IEEE Transactions on Power Systems*, vol. 7, no. 1, pp. 307–313, 02 1992.

[135] D. Chatterjee and A. Ghosh, "Transient stability assessment of power systems containing series and shunt compensators," *IEEE Transactions on Power Systems*, vol. 22, no. 3, pp. 1210–1220, 08 2007.

[136] M. H. Haque, "Improvement of first swing stability limit by utilizing full benefit of shunt FACTS devices," *IEEE Transactions on Power Systems*, vol. 19, no. 4, pp. 1894–1902, 11 2004.

[137] A. Vahidnia, G. Ledwich, and E. W. Palmer, "Transient stability improvement through wide-area controlled SVCs," *IEEE Transactions on Power Systems*, vol. 31, no. 4, pp. 3082–3089, 07 2016.

[138] J. M. Ramirez, R. J. Davalos, and V. Valenzuela, "Coordination of FACTS-based stabilizers for damping oscillations," *IEEE Power Engineering Review*, vol. 20, no. 12, pp. 46–49, 12 2000.

[139] S. M. Sadeghzadeh, M. Ehsan, N. H. Said, and R. Feuillet, "Improvement of transient stability limit in power system transmission lines using fuzzy control of FACTS devices," *IEEE Transactions on Power Systems*, vol. 13, no. 3, pp. 917–922, 08 1998.

[140] Y. L. Tan, "Analysis of line compensation by shunt-connected FACTS controllers: a comparison between SVC and STATCOM," *IEEE Power Engineering Review*, vol. 19, no. 8, pp. 57–58, 08 1999.

[141] S. Tiwari, R. Naresh, and R. Jha, "Neural network predictive control of UPFC for improving transient stability performance of power system," *Applied Soft Computing*, vol. 11, no. 8, pp. 4581 – 4590, 2011.

[142] B. V. Kumar and N. Srikanth, "A hybrid approach for optimal location and capacity of UPFC to improve the dynamic stability of the power system," *Applied Soft Computing*, vol. 52, pp. 974 – 986, 2017.

[143] M. Nayeripour, M. R. Narimani, T. Niknam, and S. Jam, "Design of sliding mode controller for UPFC to improve power oscillation damping," *Applied Soft Computing*, vol. 11, no. 8, pp. 4766 – 4772, 2011.

[144] M. M. Farsangi, Y. H. Song, and K. Y. Lee, "Choice of FACTS device control inputs for damping interarea oscillations," *IEEE Transactions on Power Systems*, vol. 19, no. 2, pp. 1135–1143, 05 2004.

[145] M. Pereira and L. C. Zanetta, "A current based model for load flow studies with UPFC," *IEEE Transactions on Power Systems*, vol. 28, no. 2, pp. 677–682, 05 2013.

[146] P. Song, Z. Xu, and H. Dong, "UPFC-based line overload control for power system security enhancement," *IET Generation, Transmission Distribution*, vol. 11, no. 13, pp. 3310–3317, 2017.

[147] A. Rajabi-Ghahnavieh, M. Fotuhi-Firuzabad, M. Shahidehpour, and R. Feuillet, "UPFC for Enhancing Power System Reliability," *IEEE Transactions on Power Delivery*, vol. 25, no. 4, pp. 2881–2890, 10 2010.

[148] S. Golshannavaz, F. Aminifar, and D. Nazarpour, "Application of UPFC to Enhancing Oscillatory Response of Series-Compensated Wind Farm Integrations," *IEEE Transactions on Smart Grid*, vol. 5, no. 4, pp. 1961–1968, 07 2014.

[149] M. Molinas, J. Suul, and T. Undeland, "Low voltage ride through of wind farms with cage generators: STATCOM versus SVC," *IEEE Transactions on Power Electronics*, vol. 23, no. 3, pp. 1104–1117, 2008.

[150] M. J. Hossain, H. R. Pota, V. A. Ugrinovskii, and R. A. Ramos, "Simultaneous STATCOM and pitch angle control for improved LVRT capability of fixed-speed wind turbines," *IEEE Transactions on Sustainable Energy*, vol. 1, no. 3, pp. 142–151, 10 2010.

[151] C. Wessels, F. Gebhardt, and F. W. Fuchs, "Fault Ride-Through of a DFIG Wind Turbine Using a Dynamic Voltage Restorer During Symmetrical and Asymmetrical Grid Faults," *IEEE Transactions on Power Electronics*, vol. 26, no. 3, pp. 807–815, 03 2011.

[152] A. O. Ibrahim, T. H. Nguyen, D. C. Lee, and S. C. Kim, "A Fault Ride-Through Technique of DFIG Wind Turbine Systems Using Dynamic Voltage Restorers," *IEEE Transactions on Energy Conversion*, vol. 26, no. 3, pp. 871–882, 09 2011.

[153] D. Ramirez, S. Martinez, C. A. Platero, F. Blazquez, and R. M. de Castro, "Low-Voltage Ride-Through Capability for Wind Generators Based on Dynamic Voltage Restorers," *IEEE Transactions on Energy Conversion*, vol. 26, no. 1, pp. 195–203, 03 2011.

[154] H. Zhou, H. Wei, X. Qiu, J. Xu, X. Wei, and S. Wang, "Improvement of transient voltage stability of the wind farm using SVC and TCSC," in *2011 Asia-Pacific Power and Energy Engineering Conference*, 03 2011, pp. 1–4.

[155] M. J. Hossain, H. R. Pota, and R. A. Ramos, "Improved low-voltage-ride-through capability of fixed speed wind turbines using decentralised control of STATCOM with energy storage system," *IET Generation, Transmission Distribution*, vol. 6, no. 8, pp. 719–730, 08 2012.

[156] T. D. Vrionis, X. I. Koutiva, and N. A. Vovos, "A Genetic Algorithm-Based Low Voltage Ride-Through Control Strategy for Grid Connected Doubly Fed Induction Wind Generators," *IEEE Transactions on Power Systems*, vol. 29, no. 3, pp. 1325–1334, 05 2014.

[157] P. Varaiya and F. F. W. and, "Direct methods for transient stability analysis of power systems: Recent results," *Proceedings of the IEEE*, vol. 73, no. 12, pp. 1703–1715, 12 1985.

[158] P. Kundur, J. Paserba, V. Ajjarapu, G. Andersson, A. Bose, C. Canizares, N. Hatziargyriou, D. Hill, A. Stankovic, C. Taylor, T. Van Cutsem, and V. Vittal, "Definition and classification of power system stability IEEE/CIGRE joint task force on stability terms and definitions," *IEEE Transactions on Power Systems*, vol. 19, no. 3, pp. 1387–1401, 08 2004.

[159] M. Pai, *Energy function analysis for power system stability.* Kluwer Academic Publishers, 1989.

[160] X. P. Zhang, C. Rehtanz, and B. Pal, *Flexible AC Transmission Systems: Modelling and Control.* Springer Science & Business Media, 2012.

[161] Y. Y. Hsu and C. Y. Hsu, "Design of a proportional-integral power system stabilizer." 1985.

[162] D. K. Reitan and N. RamaRao, "A method of improving transient stability by bang-bang control of tie-line reactance," *IEEE Transactions on Power Apparatus and Systems*, vol. PAS-93, no. 1, pp. 303–311, 01 1974.

[163] R. Benayache, W. Bahloul, L. Chrifi-Alaoui, P. Bussy, and M. B. A. Kamoun, "Transient stability of power systems using robust nonlinear second order sliding mode controller," in *Proceedings of the 2010 American Control Conference*, 06 2010, pp. 3311–3316.

[164] S. Cheng, O. P. Malik, and G. S. Hope, "Self-tuning stabiliser for a multimachine power system," *IEE Proceedings C - Generation, Transmission and Distribution*, vol. 133, no. 4, pp. 176–185, 05 1986.

[165] S. Salkuti, "Transient stability enhancement using thyristor controlled series compensator," *International Journal of Electrical and Computer Engineering*, vol. 9, no. 2, pp. 884–893, 2019.

[166] M. Dubey, "Design of genetic algorithm based fuzzy logic power system stabilizers in multimachine power system," in *2008 Joint International Conference on Power System Technology and IEEE Power India Conference*, 10 2008, pp. 1–6.

[167] H. R. Berenji, "Fuzzy Q-learning: a new approach for fuzzy dynamic programming," in *Proceedings of 1994 IEEE 3rd International Fuzzy Systems Conference*, 06 1994, pp. 486–491 vol.1.

[168] P. Y. Glorennec, "Fuzzy Q-learning and dynamical fuzzy Q-learning," in *Proceedings of 1994 IEEE 3rd International Fuzzy Systems Conference*, 06 1994, pp. 474–479 vol.1.

[169] T. Athay, R. Podmore, and S. Virmani, "A practical method for the direct analysis of transient stability," *IEEE Transactions on Power Apparatus and Systems*, vol. PAS-98, no. 2, pp. 573–584, 03 1979.

[170] P. W. Sauer and M. A. Pai, *Power System Dynamics and Stability.* Prentice Hall, Upper Saddle River, New Jersey, 1998.

[171] S. Adam, L. Busoniu, and R. Babuska, "Experience replay for real-time reinforcement learning control," *IEEE Transactions on Systems, Man, and Cybernetics, Part C (Applications and Reviews)*, vol. 42, no. 2, pp. 201–212, 03 2012.

[172] R. S. Sutton and A. G. Barto, *Reinforcement Learning: An Introduction.* The MIT Press, 1999.

[173] D. H. Lee and J. J. Lee, "Incremental receptive field weighted actor-critic," *IEEE Transactions on Industrial Informatics*, vol. 9, no. 1, pp. 62–71, 02 2013.

[174] J. Kennedy and R. Eberhart, "Particle swarm optimization," in *Neural Networks, 1995. Proceedings., IEEE International Conference on*, vol. 4, 11 1995, pp. 1942–1948 vol.4.

[175] Y. Shi and R. Eberhart, "A modified particle swarm optimizer," in *1998 IEEE International Conference on Evolutionary Computation Proceedings. IEEE World Congress on Computational Intelligence (Cat. No.98TH8360)*, 05 1998, pp. 69–73.

[176] R. Mahalakshmi, J. Viknesh, R. M. G, V. M. R., and K. C. S. Thampatty, "Fuzzy logic based rotor side converter for constant power control of grid connected DFIG," in *2016 IEEE International Conference on Power Electronics, Drives and Energy Systems (PEDES)*, 12 2016, pp. 1–6.

[177] Z. Miao and L. Fan, "The art of modeling and simulation of induction generator in wind generation applications using high-order model," *Simulation Modelling Practice and Theory*, vol. 16, no. 9, pp. 1239 – 1253, 2008.

[178] Z. Q. Tang, "Control of wind energy conversion," Master's thesis, The University of Auckland, Auckland, New Zealand, 2009.

[179] H.-S. Ko, G.-G. Yoon, N.-H. Kyung, and W.-P. Hong, "Modeling and control of DFIG-based variable-speed wind-turbine," *Electric Power Systems Research*, vol. 78, no. 11, pp. 1841 – 1849, 2008.

[180] L. Zhou, A. Swain, P. K. Naik, and N. K. C. Nair, "A dynamic fuzzy Q-learning controller to improve power system transient stability," in *2016 IEEE International Conference on Power System Technology (POWERCON)*, 09 2016, pp. 1–6.

[181] B. Yang, L. Jiang, L. Wang, W. Yao, and Q. H. Wu, "Nonlinear maximum power point tracking control and modal analysis of DFIG based wind turbine," *International Journal of Electrical Power & Energy Systems*, vol. 74, pp. 429 – 436, 2016.

[182] J. G. Slootweg, S. W. H. de Haan, H. Polinder, and W. L. Kling, "General model for representing variable speed wind turbines in power system dynamics simulations," *IEEE Transactions on Power Systems*, vol. 18, no. 1, pp. 144–151, 02 2003.

[183] F. Mei and B. Pal, "Modal analysis of grid-connected doubly fed induction generators," *IEEE Transactions on Energy Conversion*, vol. 22, no. 3, pp. 728–736, 09 2007.

[184] D. Almakhles, A. Swain, and N. Patel, "Stability and performance analysis of bit-stream-based feedback control systems." *IEEE Transactions on Industrial Electronics*, vol. 62, no. 7, pp. 4319–4327, 2015.

[185] N. D. Patel, S. K. Nguang, and G. G. Coghill, "Neural network implementation using bit streams," *IEEE Transactions on Neural Networks*, vol. 18, no. 5, pp. 1488–1504, 09 2007.

[186] N. D. Patel, S. Nguang, G. G. Coghill, and A. K. Swain, "Online implementation of servo controllers using bit-streams," in *TENCON 2005 - 2005 IEEE Region 10 Conference*, 11 2005, pp. 1–6.

[187] N. Patel and U. Madawala, "A bit-stream based scalar control of an induction motor," in *2008 34th Annual Conference of IEEE Industrial Electronics*, Nov 2008, pp. 1071–1076.

[188] D. Al-Makhles, A. Swain, and N. Patel, "Delta-sigma based bit-stream controller for a d.c. motor," in *TENCON 2012 IEEE Region 10 Conference*, Nov 2012, pp. 1–5.

[189] N. D. Patel, S. Nguang, G. G. Coghill, and A. K. Swain, "Online implementation of servo controllers using bit-streams," in *TENCON 2005 - 2005 IEEE Region 10 Conference*, Nov 2005, pp. 1–6.

[190] V. I. Utkin, *Sliding Modes in Control and Optimization.* Springer Berlin Heildelberg, 1992.

[191] J.-J. E. Slotine and W. Li, *Applied Nonlinear Control.* Prentice-Hall, 1991.

[192] D. J. Almakhles, A. K. Swain, and A. Nasiri, "The dynamic behaviour of data-driven $\Delta - M$ and $\Delta\Sigma - M$ in sliding mode control," *International Journal of Control*, 2017.

[193] D. Almakhles, A. K. Swain, A. Nasiri, and N. Patel, "An adaptive two-level quantizer for networked control systems," *IEEE Transactions on Control Systems Technology*, vol. 25, no. 3, pp. 1084–1091, 05 2017.

[194] D. Al-Makhles, A. K. Swain, and N. Patel, "Adaptive quantizer for networked control system," in *2014 European Control Conference (ECC)*, 06 2014, pp. 1404–1409.

[195] D. Al-Makhles, N. Patel, and A. Swain, "A two-loop linear control utilizing $\delta\sigma$ modulator," in *2013 Proceedings of the 11th Workshop on Intelligent Solutions in Embedded Systems (WISES)*, 09 2013, pp. 1–6.

[196] D. Al-Makhles, A. Swain, and N. Patel, "Delta-sigma based bit-stream controller for a d.c. motor," in *TENCON 2012 IEEE Region 10 Conference*, 11 2012, pp. 1–5.

[197] D. Al-Makhles, N. Patel, and A. Swain, "Bit-stream control system: Stability and experimental application," in *2013 International Conference on Applied Electronics*, 09 2013, pp. 1–6.

[198] D. Almakhles, "Two-level quantised control systems: sliding-mode approach," *International Journal of Control*, pp. 1–9, 2018.

[199] D. Al-Makhles, N. Patel, and A. Swain, "Conventional and hybrid bitstream in real-time system," in *2013 Proceedings of the 11th Workshop on Intelligent Solutions in Embedded Systems (WISES)*, 09 2013, pp. 1–6.

[200] D. Almakhles, N. Pyle, H. Mehrabi, A. Swain, and A. P. Hu, "Single-bit modulator based controller for capacitive power transfer system," in *2016 IEEE 2nd Annual Southern Power Electronics Conference (SPEC)*, 12 2016, pp. 1–6.

[201] L. Huchel, M. S. E. Moursi, and H. H. Zeineldin, "A Parallel Capacitor Control Strategy for Enhanced FRT Capability of DFIG," *IEEE Transactions on Sustainable Energy*, vol. 6, no. 2, pp. 303–312, 04 2015.

[202] K. E. Okedu, S. M. Muyeen, R. Takahashi, and J. Tamura, "Wind Farms Fault Ride Through Using DFIG With New Protection Scheme," *IEEE Transactions on Sustainable Energy*, vol. 3, no. 2, pp. 242–254, 04 2012.

[203] Y. M. Alharbi, A. M. S. Yunus, and A. A. Siada, "Application of UPFC to improve the LVRT capability of wind turbine generator," in *2012 22nd Australasian Universities Power Engineering Conference (AUPEC)*, 09 2012, pp. 1–4.

[204] H. M. Yassin, H. H. Hanafy, and M. M. Hallouda, "Enhancement low-voltage ride through capability of permanent magnet synchronous generator-based wind turbines using interval type-2 fuzzy control," *IET Renewable Power Generation*, vol. 10, no. 3, pp. 339–348, 2016.

[205] M. J. Hossain, H. R. Pota, V. A. Ugrinovskii, and R. A. Ramos, "Simultaneous STATCOM and Pitch Angle Control for Improved LVRT Capability of Fixed-Speed Wind Turbines," *IEEE Transactions on Sustainable Energy*, vol. 1, no. 3, pp. 142–151, 10 2010.

[206] M. Molinas, J. A. Suul, and T. Undeland, "Low Voltage Ride Through of Wind Farms With Cage Generators: STATCOM versus SVC," *IEEE Transactions on Power Electronics*, vol. 23, no. 3, pp. 1104–1117, 05 2008.

[207] Y. M. Alharbi and A. Abu-Siada, "Application of UPFC to improve the low-voltage-ride-through capability of DFIG," in *2015 IEEE 24th International Symposium on Industrial Electronics (ISIE)*, 06 2015, pp. 665–668.

[208] M. Ferdosian, H. Abdi, and A. Bazaei, "Improving the wind energy conversion system dynamics during fault ride through: UPFC versus STATCOM," in *2015 IEEE International Conference on Industrial Technology (ICIT)*, 03 2015, pp. 2721–2726.

[209] F. Pourpanah, C. J. Tan, C. P. Lim, and J. Mohamad-Saleh, "A Q-learning-based multi-agent system for data classification," *Applied Soft Computing*, vol. 52, pp. 519 – 531, 2017.

[210] M. R. Alimoradi and A. H. Kashan, "A league championship algorithm equipped with network structure and backward Q-learning for extracting stock trading rules," *Applied Soft Computing*, vol. 68, pp. 478 – 493, 2018.

[211] K.R.Padiyar, *FACTS controllers in power transmission and distribution.* New Age International publishers, 2015.

[212] I. Erlich and U. Bachmann, "Grid code requirements concerning connection and operation of wind turbines in Germany," in *IEEE Power Engineering Society General Meeting, 2005*, 06 2005, pp. 1253–1257 Vol. 2.

[213] C. E. Langlois, M. Asmine, M. Fischer, and S. Adloff, "On-site Under Voltage Ride Through performance tests — Assessment of ENERCON Wind Energy converters based on Hydro-Québec Transénergie requirements," in *2012 IEEE Power and Energy Society General Meeting*, 07 2012, pp. 1–8.

[214] E. A. of New Zealand, "Electricity Industry Participation Code 2010: Part 8-Common quality," 10. 2017.

[215] F. Iov, D. Anca, P. Sorensen, and N. Cutululis, "Mapping of Grid Faults and Grid Codes," 01 2007.

[216] M. Mohseni and S. M. Islam, "Review of international grid codes for wind power integration: Diversity, technology and a case for global standard," *Renewable and Sustainable Energy Reviews*, vol. 16, no. 6, pp. 3876 – 3890, 2012.

[217] S. Arabi, H. Hamadanizadeh, and B. B. Fardanesh, "Convertible static compensator performance studies on the NY state transmission system," *IEEE Transactions on Power Systems*, vol. 17, no. 3, pp. 701–706, 08 2002.

[218] G. Isazadeh, A. Khodabakhshian, and E. Gholipour, "Optimal design of convertible static compensator supplementary damping controller to avoid wide area uncontrolled islanding," *IET Generation, Transmission Distribution*, vol. 10, no. 10, pp. 2336–2350, 2016.

[219] X. Jiang, J. H. Chow, A. Edris, B. Fardanesh, and E. Uzunovic, "Transfer path stability enhancement by voltage-sourced converter-based FACTS controllers," *IEEE Transactions on Power Delivery*, vol. 25, no. 2, pp. 1019–1025, 04 2010.

[220] R. S. Sutton, A. G. Barto, and R. J. Williams, "Reinforcement learning is direct adaptive optimal control," *IEEE Control Systems Magazine*, vol. 12, no. 2, pp. 19–22, 04 1992.

[221] M. A. Soliman, H. Hasanien, H. Z. Azazi, E. E. El-kholy, and S. A. Mahmoud, "An adaptive fuzzy logic control strategy for performance enhancement of a grid-connected PMSG-based wind turbine," *IEEE Transactions on Industrial Informatics*, pp. 1–1, 2018.